

Dissertation zur Erlangung des Doktorgrades
der Fakultät für Chemie und Pharmazie
der Ludwig-Maximilians-Universität München

Development of Novel Vaccine Carriers:

Physicochemical and Biological
Characterization of Hexosomes

Letícia Rodrigues Neibecker

(geb. Pires Rodrigues)

aus

Montes Claros - MG, Brasilien

2018

Erklärung

Diese Dissertation wurde im Sinne von §7 der Promotionsordnung vom 28. November 2011 von Herrn Prof. Dr. Gerhard Winter betreut.

Eidesstattliche Versicherung

Diese Dissertation wurde eigenständig und ohne unerlaubte Hilfe erarbeitet.

Den Haag, NL 09/02/2019

Leticia Rodrigues Neibecker
(geb. Pires Rodrigues)

Dissertation eingereicht am: 05/06/2018

1. Gutachter: Prof. Dr. Gerhard Winter
2. Gutachter: Prof. Dr. Wolfgang Frieß

Mündliche Prüfung am: 18/07/2018

Department of Pharmacy - Pharmaceutical Technology and Biopharmaceutics
LUDWIG-MAXIMILIANS-UNIVERSITÄT MÜNCHEN

**DEVELOPMENT OF NOVEL VACCINE CARRIERS:
PHYSICOCHEMICAL AND BIOLOGICAL
CHARACTERIZATION OF HEXOSOMES**

Letícia Rodrigues Neibecker, M.Sc.

To Pascal

Acknowledgements

This work would not have been possible without the support of my advisors, collaboration partners, colleagues, and friends. Here, I would like to express my sincere gratitude and appreciation to all of them.

First, I would like to thank Prof. Gerhard Winter for welcoming me in his research group, for offering me the opportunity to work in such an interesting and challenging project, for his trust, and professional and dedicated supervision during the last years. I am also grateful for his personal and scientific advices, which contributed to my development in both fronts. I also would like to thank Dr. Madlen Hubert for designing this ambitious and international project, for her supervision, patience and guidance during the execution of this work. I am also incredibly thankful for her strong commitment, support and enthusiasm during the research stay in Umeå, SE.

I am highly indebted to Prof. Christine Papadakis and the Soft Matter Physics group of the Technical University of Munich (TUM), whose help with small angle X-ray scattering (SAXS) was essential for the success of this project. It was always a pleasure to work with them. I am grateful for the assistance given by Konstantinos Kyriakos, who introduced me to the world of SAXS measurements, gave me access to the SAXS-lab, and offered great support with the first analyses. I am also very thankful to Konstantinos Raftopoulos, who intensively helped me to keep my project in the schedule when the results were more than unexpected. Further, I want to thank the whole group for the opportunity to join a SANS beam-time at the (Forschungsreaktor München II) FRM II. Also the constant assistance of Sabine Kiermeier (Strahlenschutz, LMU) with safety issues is gratefully acknowledged.

I would like to express my very great appreciation to the assistance and immense knowledge on immunology and vaccination provided by Prof. Camilla Foged and Prof. Anders Elm Pedersen of the University of Copenhagen and Dr. Dennis Christensen of the Statens Serum Institut (SSI). I also want to thank them for hosting me in their groups for three months in Copenhagen and extend my gratitude to my labmates during this research stay: Rie, Mie, Sylvia, Eva, Kaushik, Feng Wan, and Suzana. Especially, I want to thank Renske Wiegertjes for her great help in the lab (at PANUM) and for teaching me how to

perform the isolation of peripheral blood mononuclear cells (PBMCs). I am also very thankful to Signe Tandrup Schmidt, who invested a lot of time in my project and offered great support with the animal studies at the SSI. In addition, nothing we have accomplished would have been possible, especially in such a short period of time, without the great help, input, knowledge, lessons, and advices of the technicians: Fabrice Rose, Karina Juul Vissing and Elisabeth Veyhe Andersen. My time in Copenhagen would have been so much harder and less productive without them. I also would like to thank Liselotte Rothmann Norup for teaching me how to use the flow cytometer and being available for questions and troubleshooting even in unconventional work-hours. My grateful thanks also to Maria Diana Læssøe Pedersen for her valuable and professional advices about sensitive cell cultures. Further, I would like to thank Natascha, Kalpana, and Sebastian for their friendship and funny moments in Copenhagen outside the laboratory.

I also wish to acknowledge Prof. Anan Yaghmur, for the insightful conversations, introduction to the field of lyotropic liquid crystals, and the possibility of joining his team in the synchrotron source at the MAX-Lab in Luleå, SE. I am grateful for the help of Prof. Henrik Franzyk, who provided all the MMG-1 used in this work. I also want to thank Prof. Thomas Rades for his creative ideas and enthusiasm about this project.

A very important part of this project was performed at the Umeå University, SE, in the group of Prof. Richard Lundmark. I am grateful for the possibility given to join his group and for all the knowledge gained. I also would like to thank for his inspiring enthusiasm about science. Furthermore, I want to express my gratitude to Irene Martinez Carrasco for her outstanding expertise and constant support in all microscopy experiments. I am also very thankful for her guidance with image analysis, quantification and presentation. I want to thank Ellin Larsson and Lars Nygård Skalman for their help in the lab, time, patience, good mood, interesting conversations, input and knowledge. I also would like to thank Saowaluck for the pleasant conversations in the very early hours of the day in the lab.

I would like to acknowledge Prof. Hendrik Dietz for enabling the collaboration to perform cryo-TEM, and Fabian Schneider for his time, great commitment and dedication to carry out valuable cryo-TEM measurements.

Prof. Stefan Zahler (Pharmaceutical Biology, LMU) and Dr. David Chiasson (Genetics, LMU) are kindly acknowledged for their help with experiments involving giant unilamellar vesicles (GUVs).

I would like to offer my special thanks to my friends and colleagues of AK Winter, AK Frieß and AK Merkel for the excellent work atmosphere and for the unforgettable time we spent together. Especially, I want to thank my labmate, Katharina Geh for her friendship, and encouragement. Many thanks also to Sabine Kohler, Gabriele Hartl, Alice Hirschmann, Regine Bahr, Imke Leitner, and Ayla Tekbudak for providing constant support behind the scenes to make our work possible.

Finally, I would like to express my gratitude to my husband, Pascal for being my greatest supporter and reminding me of the things that really matter in life.

Publications arising from this thesis

- I **Rodrigues L**, Kyriakos K, Schneider F, Dietz H, Winter G, Papadakis CM, et al. Characterization of Lipid-Based Hexosomes as Versatile Vaccine Carriers. *Molecular Pharmaceutics*. 2016;13:3945-54.
- II **Rodrigues L**, Raftopoulos N K, Tandrup Schmidt S, Schneider F, Dietz H, Rades T, Franzyk H, Elm Pedersen A, Papadakis CM, Christensen D, Foged C, Winter G, Hubert M. Adjuvants based on a monomycoloyl glycerol analogue in hexosomes and liposomes induce different immune responses after vaccination with the *Chlamydia trachomatis* major outer membrane protein. (*Manuscript submitted*)
- III **Rodrigues L**, Schneider F, Zhang X, Papadakis CM, Dietz H, Larsson E, Winter G, Lundmark R, Hubert M. Hexosomes have unusual cellular internalization mechanism. (*Manuscript ready for submission*)

Table of Contents

Acknowledgements.....	I
Publications arising from this thesis.....	V
Table of Contents.....	VII
List of Abbreviations.....	XIII
CHAPTER I General Introduction.....	1
1 Background.....	1
1.1. Challenges in Vaccine Development.....	1
1.2. Vaccine Adjuvants.....	4
1.2.1. Aluminium Salts.....	5
1.2.2. Emulsions.....	5
1.2.3. Immunopotentiators.....	6
1.2.4. Particulate Vaccine Delivery Systems.....	8
1.3. Lyotropic Liquid Crystalline Phases.....	12
1.3.1. Structural Assembly.....	13
1.3.2. Structure Characterization.....	15
1.3.3. Inverse non-lamellar Phases: Current Status.....	20
1.4. Cellular Internalization of Nanocarriers.....	22
1.4.1. Overview of the Main Endocytic Pathways.....	22
1.4.2. Relevance of the Internalization Route for Vaccine Carriers.....	26
2 Aim and outline of the thesis.....	27
CHAPTER II Characterization of Hexosomes as Versatile Vaccine Carriers.....	29

1 Abstract	30
2 Introduction.....	31
3 Materials and methods	32
3.1. Materials	32
3.2. Preparation of Bulk Phases.....	33
3.3. Preparation of Particles.....	33
3.4. Polarization Microscopy	33
3.5. Small-Angle X-ray Scattering (SAXS)	34
3.6. Dynamic Light Scattering (DLS).....	35
3.7. Protein Load Determination	35
3.8. Tryptophan Accessibility Assay	35
3.9. Cryogenic Transmission Electron Microscopy (Cryo-TEM)	36
4 Results and Discussion.....	36
4.1. Characterization of Bulk Phases.....	36
4.2. Particle Preparation.....	40
4.3. Particle Size Optimization	43
4.4. Particle Customization.....	45
4.5. Expanding the Customization Tool Box of Hexosomes.....	50
4.6. Particle Loading	52
5 Conclusion and Outlook	55
CHAPTER III Cellular Internalization of Hexosomes.....	57
1 Abstract	58
2 Introduction.....	58
3 Materials and methods	61

3.1. Materials	61
3.2. Antibodies.....	61
3.3. Preparation of Liposomes.....	62
3.4. Preparation of Hexosomes	62
3.5. Small-Angle X-ray Scattering (SAXS)	62
3.6. Dynamic Light Scattering (DLS).....	63
3.7. Cell Cultures, Cell Lines and Transfections.....	63
3.8. MTT cell proliferation assay.....	64
3.9. High-Throughput Quantification of Particle Uptake	64
3.10. Immunofluorescence microscopy	65
3.11. Particle Uptake Assay Using Live Cell Microscopy	65
3.12. Image Analysis and Quantification	66
3.13. Lipid Monolayer Experiments.....	66
3.14. Calcein Leakage Assay	67
3.15. Giant Unilamellar Vesicles (GUV) Preparation and Imaging	67
3.16. Cryogenic Transmission Electron Microscopy (Cryo-TEM)	68
3.17. Statistical Analysis.....	68
4 Results and Discussion.....	69
4.1. Development and physico-chemical characterization of fluorescently labeled nanoparticles	69
4.2. Phy/MaMo hexosomes have a higher uptake rate in cells than DOPC/DOPE liposomes	70

4.3. Phy/MaMo hexosomes are not internalized via any of the major endocytic pathways.....	73
4.4. Internalization of Phy/MaMo hexosomes is not affected by cytochalasin D, but is drastically lowered after hypotonic cell swelling	76
4.5. Phy/MaMo hexosomes directly interact with models of the plasma membrane	79
5 Conclusion and Outlook	86
CHAPTER IV The Supramolecular Structure of Nano-Self-Assemblies Influences the Adjuvant Efficacy of a Synthetic Mycobacterial Monomycoloyl Glycerol Analogue	87
1 Abstract	88
2 Introduction.....	89
3 Materials and methods	91
3.1. Materials	91
3.2. Synthesis of Mycobacterial Monomycoloyl Glycerol Analogue 1 (MMG-1)	92
3.3. Preparation of Liposomes.....	92
3.4. Preparation of Hexosomes	92
3.5. Small-Angle X-ray Scattering (SAXS)	93
3.6. Cryogenic Transmission Electron Microscopy (Cryo-TEM)	93
3.7. Dynamic Light Scattering (DLS).....	94
3.8. <i>In vitro</i> Experiments:	95
3.8.1. Preparation of Primary Dendritic Cells (DCs) Derived from Peripheral Blood Mononuclear Cells (PBMCs).....	95
3.8.2. Viability Assay	95
3.8.3. Uptake Experiments.....	96
3.8.4. Stimulation of DCs and Evaluation of Surface Marker Expression	96
3.9. Animal Experiments.....	97

3.9.1. Intracellular Cytokine Staining (ICS).....	97
3.9.2. Evaluation of Cytokine Release.....	98
3.9.3. Evaluation of Antibody Responses in Serum.....	99
3.10. Statistical analyses.....	99
4 Results and Discussion.....	99
4.1. Systems composed of MMG-1 and phytantriol self-assemble into an inverse hexagonal phase.....	100
4.2. MMG-1-based hexosomes do not induce DC maturation, whereas CAF04 liposomes stimulate up-regulation of CCR7.	103
4.3. MMG-1-based hexosomes and CAF04 liposomes induce antigen-specific CD4 ⁺ T-cell responses characterized by different cytokine profiles.....	105
4.4. MOMP adjuvanted with CAF04 liposomes induces higher CMI responses than MOMP adjuvanted with MMG-1-based hexosomes.....	108
4.5. MMG-1-based hexosomes and CAF04 liposomes induce different immunostimulation.....	112
4.6. MMG-1-based hexosomes induce stronger humoral responses than CAF04 liposomes.	113
5 Conclusions and Outlook.....	115
CHAPTER V General Conclusions and Outlook.....	117
SUMMARY.....	123

List of Abbreviations

1D	One-dimensional
2D	Two-dimensional
APC	Antigen-Presenting-Cells
Arf6	ADP Ribosylation Factor 6
BCG	Bacillus Calmette Guérin
BSA	Bovine Serum Albumin
CAF	Cationic Adjuvant Formulation
CAM	Cell Adhesion Molecule
Cav1	Caveolin-1
CCD	Charge-Couple Device
CLIC	Clathrin Independent Carriers
CLRs	C-type Lectins Receptors
CLR Mincle	Macrophage-inducible C-type Lectin Receptor
CME	Clathrin-Mediated Endocytosis
CMI	Cell-Mediated Immune
Con A	Concanavalin A
CPP	Critical Packing Parameter
CPPs	Cell Penetrating Peptides
Cryo-TEM	Cryogenic Transmission Electron Microscopy
CTL	Cytotoxic T Lymphocyte
CvME	Caveolae-Mediated Endocytosis
d.nm	Diameter in nanometers
DC	Dendritic Cell
DDA	Dimethyldioctadecylammonium

DENV	Dengue Virus
DLS	Dynamic Light Scattering
DOPC	1,2-dioleoyl-sn-glycero-3-phosphocholine
DOPE	1,2-dioleoyl-sn-glycero-3-phosphoethanolamine
DPPC	1,2-Dipalmitoyl-sn-glycero-3-phosphocholine
DPPG	1,2-Dipalmitoyl-sn-glycero-3-phosphoglycerol sodium salt
FCA	Freund's Complete Adjuvant
FFT	Fast Fourier Transformation
FIA	Freund's Incomplete Adjuvant
FRET	Förster Resonance Energy Transfer
FRM II	Forschungsreaktor München II
GEEC	GPI-Anchored Protein Enriched Early Endosomal Compartment
GFP	Green Fluorescent Protein
GPI	Glycosylphosphatidylinositol
GTPase	Guanosine triphosphatase
GUVs	Giant Unilamellar Vesicles
HAV	Hepatitis A Virus
HBV	Hepatitis B Virus
HC	Heavy Chain
HCV	Hepatitis C Virus
HIV	Human Immunodeficiency Virus
HPV	Human Papillomavirus
ICS	Intracellular Cytokine Staining
IFN- γ	Interferon- γ
Ig	Immunoglobulin
IL	Interleukin

IL2R β	Interleukin-2 Receptor β
ISCOM	Immunostimulating Complex
LC	Liquid Crystal
LDL	Cholesterol Low Density Lipoprotein
LPS	Lipopolysaccharide
LYS	Lysozyme from chicken egg white
MaMo	Mannide Monooleate
MHC	Major Histocompatibility Complex
MMG	Monomycoloyl Glycerol
MMR	Measles, Mumps and Rubella
MOMP	Major Outer Membrane Protein
MPL	Monophosphoril Lipid A
NLR	NOD-like Receptors
NOD	Nucleotide-binding Oligomerization Domain
o/w	Oil-in-Water
OG	Octyl- β -D-glucopyranoside
OVA	Albumin from chicken egg white
PAMP	Pathogen-Associated Molecular Pattern
PBMCs	Peripheral Blood Mononuclear Cells
PBS	Phosphate Buffer Saline
PDI	Polydispersity Index
PEG	Polyethylene Glycol
Phy	Phytantriol
PLA	Poly(lactic acid)
PLGA	Poly(lactic- <i>co</i> -glycolic acid)
PMA	Phorbol-12-Myristate-13-Acetate

POPC	1-Palmitoyl-2-oleoyl-sn-glycero-3-phosphocholine
R18	Octadecyl rhodamine b chloride
rLE	Relative Loading Efficiency
RLR	RIG-I-like Receptor
RSV	Respiratory Syncytial Virus
rt	Room Temperature
SANS	Small Angle Neutron Scattering
SAXS	Small Angle X-ray Scattering
SD	Standard Deviation
siRNA	Small interfering ribonucleic acid
SPECT/CT	Single Photon Emission Computed Tomography combined with Computed Tomography
SSI	Statens Serum Institut
TDB	Trehalose-6,6-Dibehenate
TDM	Trehalose-6,6-Dimycolate
Tf-Fe	Iron-Laden Transferring
Th	T helper cell
TLR	Toll-like Receptors
T _m	Transition Temperature
TMB	3,3',5,5'-Tetramethylbenzidine
TNF- α	Tumor Necrosis Factor- α
TR-SAXS	Time-Resolved Small Angle X-ray Scattering
VLPs	Virus-Like Particles
w/o	Water-in-Oil
wt	Weight
γ -PGA	Poly(γ -glutamic acid)

CHAPTER I

General Introduction

1 BACKGROUND

1.1. Challenges in Vaccine Development

Vaccines have been remarkably effective in promoting global health through the reduction of mortality and morbidity caused by infectious diseases.^{1, 2} Especially considering conditions for which effective therapies do not exist, prophylactic vaccines represent a decisive tool to advance public health.³ For instance, the eradication of smallpox, and the drastic reduction of incidences of polio, diphtheria, tetanus, pertussis, and measles represent direct successes of immunization programs worldwide.^{1, 2} Despite this, and the increasing knowledge on immunization, the development of new vaccines is much slower than the growing necessity for new therapeutic and prophylactic alternatives.⁴ Widespread life-threatening pathogens which could potentially be prevented through vaccination are for example, the human immunodeficiency virus (HIV), leishmanias, chlamydia, *Helicobacter pylori*, schistosomes, hepatitis C virus (HCV), respiratory syncytial virus (RSV), cytomegalovirus, *Staphylococcus aureus*, *Pseudomonas aeruginosa*, *Plasmodium falciparum* (malaria), dengue viruses (DENV-1, 2, 3 and 4), and *Mycobacterium tuberculosis*.^{1, 4} However,

efficacious vaccines against these infections are not yet available. Significant obstacles reside in both scientific and financial areas.⁴

A factor that considerably contributes to the difficult and lengthy development of vaccines is the complexity of pathogens.⁵ For instance, the genetic diversity of pathogens is a substantial barrier in this process. Vaccines against multi-strain pathogens and pathogens exhibiting high mutation rates demand the incorporation of a broader range of antigens. In these cases, multivalent vaccines are established in order to better cover the antigen variability.⁶ However, some cases require additional strategies to compensate the modifications of the pathogens. As an example, multivalent vaccines against seasonal influenza are annually reformulated to enhance the antigen coverage.¹ Yet, this approach is not adequate to overcome extremely high antigen variability. HIV and HCV for instance, rapidly undergo mutations even during the infection process.¹ This generates changes in the target antigenic epitopes and consequently diminishes the functionality of antibodies.⁵ Therefore, the concomitant induction of cellular responses is of utmost importance against this kind of pathogens.¹ In contrast, strong antibody responses are the main biomarkers of protection for several licensed vaccines (*e.g.* smallpox, pertussis, tetanus, diphtheria, rubella, measles, and yellow fever).^{7,8} This shows that the correlates of immunity vary according to the characteristics of the pathogen. Although difficult, their identification constitutes an important and strategic stage of rational vaccine design.^{3,8}

In a simplistic way, vaccines are formulated to mimic natural infections in a tolerable way and ultimately induce immunity. This relies on the premise that the host naturally becomes immune to a re-infection after overcoming the disease. Unfortunately, this is not true for many pathogens (*e.g.* malaria and RSV).¹ In such circumstances, the vaccine must be able to activate immunological pathways that go beyond the scenario encountered in a natural infection to eventually induce protection. Similar challenges are also present in the development of vaccines against pathogens that provoke chronic infections (*e.g.* HIV, HCV and *S. aureus*).¹ Therefore, it is fundamental to thoroughly understand the pathophysiology and the mechanisms of protection against the pathogen concerned not only in humans, but also in the specific animal model used in the research. In this context, the absence of good animal models that closely resemble the human organism considerably intensifies the challenges in vaccine development. For instance, despite considerable differences between

the immunological responses of rodents and humans, mouse models have been a frequent tool in the development of vaccines.⁹ Even nonhuman primate models show significant discrepancies to the human immune system with respect to immunogenetics, microbiome and specificity of viral vectors.⁴ Inadequate preclinical data is frequently generated and hampers the identification of predictive markers of protection, leads to failure in clinical trials, retards the development process, and increases research costs.¹⁻³ For example, several vaccine candidates against *S. aureus* were tested in clinical trials, but today an effective vaccine against this pathogen is still not available. In animal studies, independent reports indicated opsonophagocytic activity as the main predictive marker of protection against *S. aureus*. Unfortunately, this biomarker did not seem to be a correlate of protection in humans.¹⁰

Traditionally, vaccines have been developed for pediatric patients, who are especially susceptible to threats of infectious diseases. With this strategy, protection can be provided to individuals as early as possible. However, there is an urgent need to expand the benefits of vaccination to other groups of the population, e.g. elderly and immune-compromised individuals that are highly vulnerable to infections.¹¹ Needless to say, due to the particular immunological situation and risk of pathogen exposure, vaccine development strategies have to be adjusted. Suitable vaccine candidates must be highly tolerable (ideally, by all groups of the population) and at the same time, potent enough to overcome the low responsiveness of the immune system.¹² Pregnant women constitute another delicate population group that would substantially benefit from additional vaccines. Maternal immunization provides protection to both, mother and infant. For this reason, this is a valuable strategy for health promotion.¹³ Despite the success of maternal vaccination against tetanus, pertussis and influenza, safety concerns are still the main barriers to advance in this field.¹³

Overall, the key impasse in vaccine formulation is the necessity to combine safety and tolerability with potent and persistent immune responses.¹⁴ The so-called traditional approaches of vaccine formulation use live attenuated [e.g. Bacillus Calmette Guérin (BCG) against tuberculosis, and MMR against measles, mumps and rubella] or whole inactivated microorganisms (e.g. hepatitis A vaccine Epaxal®).¹⁵ Here, concerns regarding the reactogenicity of these vaccines and the safety of the patients exposed to them are the prime

limitations.¹⁶ In this context, subunit vaccine technology brought a notorious improvement. These vaccines are based on highly purified and well-defined antigenic motifs (*e.g.* peptides, proteins or polysaccharides) of the target pathogen.^{14, 15} In this way, specific immune responses can be induced, excluding the risk of pathogen replication and drastically reducing the occurrence of unwanted host reactions. Therefore, this technique allows for higher tolerability in comparison to whole-pathogen preparations.^{14, 15} However, subunit vaccines are frequently inefficient, because they do not promote the same level of immunogenicity demonstrated by the traditional ones.^{17, 18} To circumvent this, adjuvants are co-administered to improve the magnitude and type of the immune response.^{17, 18}

1.2. Vaccine Adjuvants

Adjuvants are defined as additives able to enhance specific immune responses against a determined pathogen.¹⁹ In addition to the decisive role of adjuvants in the efficacy of low-immunogenic antigens, they allow significant vaccine dose sparing, which is of utmost importance in the context of global supply.¹⁹ Adjuvants may be either immunopotentiating compounds (section 1.2.3.), particulate delivery systems (section 1.2.4.), or a combination of both.²⁰ The incorporation of antigens into particles provides the possibility of mimicking size, geometry, and kinetics of viruses and bacteria.²¹ Moreover, the particle design encloses a range of possibilities to tune the interaction between the antigen and immune cells, and even eliminate the necessity of multiple dose regimens.²¹ Therefore, the combination of these approaches (particles and immunopotentiators) has been frequently investigated to take advantage of synergistic effects, revealing promising perspectives.²²⁻²⁴ Accordingly, adjuvants represent a broad and heterogeneous group. In the context of subunit vaccines, the incorporation of adjuvants into the formulation is performed considering the immune responses desired, without neglecting safety.¹⁹ Here, diverse aspects must be taken into account. For instance, the route of administration, and the interactions between adjuvant and antigen can modify the biological performance of the formulation. This not only affects the immunological output and effectiveness of the vaccine, but also changes its toxicity profile.^{14, 19} In the next sections, some of the most important adjuvant systems are described.

1.2.1. Aluminium Salts

Aluminum adjuvants (aluminum hydroxide, aluminum phosphate, and potassium alum), collectively referred to as "alum", are the most common adjuvants and were for many years the only approved adjuvants in the USA.²⁵ Aluminum hydroxide is the form of alum most commonly employed as adjuvant.²⁶ Alum is certainly the most employed adjuvant in human vaccines and its safety profile is very well characterized.¹⁸ Despite this, its mechanism of action is less well understood than that of other adjuvants. Alum is formed by charged crystalline aggregates that normally enable the adsorption of antigens.¹⁹ Upon injection, an inflammatory focus is formed, triggering series of events that increase antigen uptake by dendritic cells (DCs), stimulate cell-recruitment and activate immune cells via inflammasome.^{19, 27} The main limitation of aluminum adjuvants is the overall Th2-biased immune response. This makes these adjuvants inappropriate for vaccine formulations against cancer or intracellular pathogens, because in these cases, the induction of Th1 or cytotoxic T lymphocyte (cell-mediated responses) plays a central role.^{14, 27}

1.2.2. Emulsions

Similarly to the aluminum adjuvants, emulsions also have an extensive record of applications in the field of vaccines. The study of emulsions as vaccine adjuvants started with the Freund's Complete Adjuvant (FCA). FCA is a water-in-oil (w/o) emulsion and contains mineral oil, mannide monooleate and killed *Mycobacteria tuberculosis*. This emulsion was found to have a high immunostimulatory profile, but revealed strong adverse effects making it unsuitable for clinical applications.²⁸ The Freund's Incomplete Adjuvant (FIA) was prepared without the mycobacterial component. Despite its lower toxicity compared to FCA, FIA still presented high reactogenicity and its clinical use was limited.^{29, 30} Intense research in this field led to the development of alternative w/o emulsions such as, Montanide ISATM51 and Montanide ISATM720. The first is composed of a mineral oil with 50% water and the latter is formed by squalene oil plus 30% water. Both preparations are stabilized with surfactants from the mannide monooleate family (esters of oleic acid and mannitol).^{29, 31} Their mechanism of action is based on the formation of a depot at the injection site and slow antigen release, culminating with enhanced antibody levels and cytotoxic T lymphocyte (CTL) responses.^{29, 31} These adjuvants have been evaluated in

clinical trials in immunotherapeutics against HIV, malaria, cancer, and autoimmune diseases.^{29, 31} In spite of the successes obtained with w/o emulsions, the development of oil-in-water (o/w) formulations has been preferred due to the better tolerability and lower viscosity, which allows for better injectability and more accurate dosage.³⁰ Another factor that improved tolerability was the substitution of non-degradable mineral oils by metabolizable oils.^{29, 30} The application of these concepts resulted in the development of MF59 and AS03, both present in several licensed human vaccines.³⁰

MF59 and AS03 are squalene-based o/w emulsions licensed in several countries for pandemic influenza vaccines.²⁹ MF59 is composed of nonimmunogenic molecules, namely squalene, Tween 80, and Span 85.^{29, 32} Therefore, its activity originates from the resulting emulsion. Differently, AS03 contains squalene, Tween 80 and the immunopotentiator α -tocopherol.²⁹ Two of the most interesting contributions of MF59 and AS03 to influenza vaccines are the induction of cross-reactivity against multiple strains of the virus and the considerable reduction of the amount of antigen needed (dose sparing).^{32, 33} Their mechanism of action differs from that of alum in a way that these emulsions do not create a depot-effect and the association between antigen and oil droplets is not important for the adjuvancity.³⁰ When compared to alum, MF59 and AS03 generally induce higher antibody and mixed Th1/Th2 responses.^{19, 32} A limitation in the use of emulsions in vaccines is the challenging characterization of antigen molecules in these systems. Therefore, the establishment of suitable separation protocols is required to enable reliable analytics for the monitoring of quality and stability.³²

1.2.3. Immunopotentiators

The adjuvant class of immunopotentiators is represented by ligands able to directly activate receptors of the innate immune system, such as toll-like receptors (TLRs), nucleotide-binding oligomerization domain proteins (NODs), NOD-like receptors (NLRs), C-type lectins receptors (CLRs), and RIG-I-like receptors (RLRs).¹⁵

Monophosphoril lipid A (MPL[®]) is a prominent example of this category. It is a TLR4 agonist derived from lipopolysaccharide (LPS), which is found in the cell wall of Gram-negative bacteria and is able to induce Th1-biased immune responses.^{15, 19} It was the first TLR ligand included in a licensed human vaccine (hepatitis B vaccine, Fendrix[™]). MPL[®] is a

natural product and today many TLR4 agonists are being developed synthetically.³⁴ Unmethylated CpG motifs constitute another example of TLR ligand applied as adjuvant. These sequences are present in bacterial DNA, but in the vertebrate genome they are suppressed and methylated.^{35, 36} Thus, through TLR9 recognition, immune cells are activated and defense mechanisms are induced towards Th1 cell responses.^{17, 18} Vaccine candidates against hepatitis B, containing unmethylated CpGs as adjuvant system, reached phase III clinical trials with promising results.^{19, 36} Likewise, several other pathogen-associated molecular patterns (PAMPs) are identified through TLRs and constitute the basis of a variety of adjuvant molecules [*e.g.* bacterial flagellin (detection through TLR5 induces Th1/Th2 responses), and dsRNA analogues (detection through TLR3 induces Th1 responses)].^{15, 19} Besides TLR ligands, trehalose-6,6-dibehenate (TDB), which is a synthetic analog of the mycobacterial cord factor trehalose-6,6-dimycolate (TDM), has received much attention due to its capacity of inducing strong cellular responses.^{19, 37} The adjuvancity of this glycolipid results from the activation of CLR mincle (macrophage-inducible C-type lectin receptor), which is also known to bind certain fungal species and *S. pneumoniae*.^{37, 38} Synthetic analogues of muramyl dipeptide (MDP), which is originally encountered in the bacterial cell wall, are NOD2 ligands and were also reported to show promising adjuvant activity.^{39, 40} For instance, in a study with dogs, a vaccine candidate containing MDP induced Th1-biased responses and protection against leishmaniasis.⁴¹ The saponin-derived QS21 also represents an important immunostimulatory molecule. This potent adjuvant is a purified fraction of Quil-A[®] and shows lower toxicity in comparison to other saponins.³⁵ Its mechanism of action is yet to be elucidated. However, it was suggested that Quil-A[®] acts through a NLR protein 3-dependent mechanism based on the secretion of the pro-inflammatory interleukin (IL)-1 β following inflammasome activation.⁴² Nevertheless, several combination systems containing QS21 have been tested in clinical phase III studies.¹⁹ Alternatively to the use of these molecules to stimulate the immune system, the direct application of cytokines [*e.g.* IL-1, IL-2, IL-12, interferon (IFN)- γ] as adjuvants has also been studied.³⁵ However, due to considerable instability issues, efforts are still necessary to establish this strategy.³⁵

These examples represent only a small portion of the adjuvant molecules available and highlight the wide range of possibilities regarding mechanisms of action and consequent immunological outputs.

1.2.4. Particulate Vaccine Delivery Systems

Antigen delivery using nanoparticles has several interesting advantages in vaccination. Firstly, the encapsulation into particles enables antigen protection and so avoids its rapid enzymatic degradation.⁴³ Secondly, it is speculated that particulate carriers simulate the antigen presentation naturally performed by the pathogen. Thus, the resulting immune response against the vaccine would be similar, but associated with lower risks.^{21, 43} Other promising attributes are targeted delivery, prolonged antigen release, and the combination of more than one immunogenic agent in the same delivery system to create a multivalent vaccine.⁴³ The limitations regarding the use of nanoparticles as vaccine delivery systems are frequently related to potential unknown toxic effects and intracellular accumulation.⁴³ In addition to this, there are also several obstacles concerning the potential scale-up of their production.⁴³

Among several particulate delivery systems, the most relevant ones for vaccination are virus-like particles (VLPs), immunostimulating complexes (ISCOMs), polymeric nanoparticles, inorganic nanoparticles and lipid-based formulations (liposomes, virosomes, transferosomes, ethosomes, cubosomes).^{44, 45}

1.2.4.1. Virus-like Particles

VLPs are formed by viral capsid proteins that self-assemble into stable particles in a size range of 20-150 nm. Depending on the viral source, the particles display different geometries and shapes, such as spherical, icosahedral, or rod-like.^{21, 43, 46} These systems are attractive adjuvants, because they combine high density of epitopes with nanocarrier properties, which results in improved immunostimulation.^{21, 43} VLPs mimic virus morphology and cell tropism, and have great safety profile, because they lack genomic material and cannot replicate or promote infections.⁴⁷ These advantages are reflected in the increasing number of approved VLP vaccines, such as Engerix[®] (GlaxoSmithKline) and Recombivax[®] (Merck & Co.) against hepatitis B virus (HBV), Cervarix[®] (GlaxoSmithKline) and Gardasil[®] (Merck & Co.) against human papillomavirus (HPV), Inflexal V[®] (Crucell) against influenza, and Epaxal[®] (Crucell) against hepatitis A virus (HAV).^{43, 46} It is important to mention that VLP-based formulations, including commercially available ones, commonly include additional adjuvants to achieve the desired quality and magnitude of immune responses.⁴⁸ A crucial

limitation of this carrier system is the small antigen load that can be incorporated within the particles. This makes the presentation of large antigens like HIV envelope or influenza haemagglutinin proteins difficult.⁴⁹ In addition, in comparison to other particulate systems, the production and purification of VLPs is more challenging, especially at an industrial scale.⁴⁶

1.2.4.2. Immunestimulating Complexes (ISCOMs)

ISCOMs are micellar colloidal systems of approximately 40 nm, formed by well-defined ratios of cholesterol, phospholipid (phosphatidylethanolamine or phosphatidylcholine) and saponine (Quil-A[®] extracted from *Quillaia saponaria*).⁵⁰ The components are mixed in the presence of a surfactant and the removal of the latter through dialysis or centrifugation results in a pentagonal dodecahedron arrangement of micelles (cage-like structure) containing saponins and lipids.⁴⁸ Similar to VLPs, ISCOMs are self-assemblies featuring peculiar geometry and surface structure,⁵⁰ and also have limited antigen loading capacity.²³ However, it has already been shown that the simple mixture of ISCOMs with the antigens, without incorporation (ISCOMs matrices), elicits potent immune responses, which are comparable with the encapsulated system.²³ In pre-clinical studies with small animal models and non-human primates, ISCOMs induced remarkable levels of cytotoxic T lymphocyte (CTL) responses. However, these results were not reproducible in clinical trials.⁴⁸ Many veterinary vaccines include ISCOMs, e.g. ISCOM-EVI vaccine against equine influenza.⁵¹ In spite of this, concerns about severe toxic effects (local reactions, granulomas, and hemolysis) of this saponin-based adjuvant have hindered its establishment for human use.^{43, 52}

1.2.4.3. Polymeric Particles

Adjuvant effects can also be achieved by incorporating the antigen into polymeric particles.⁵³ Depending on their composition, these systems present a diverse range of characteristics regarding size, surface charge, hydrophobicity, targeting, toxicity, and antigen release. These properties may determine their performance in a biological environment and enable immune response optimization. Several materials have been evaluated for the production of biodegradable vaccine carriers such as poly(lactic-co-glycolic acid) [PLGA], poly(lactic acid) [PLA], and poly(γ -glutamic acid) [γ -PGA].^{43, 54} The interest in

PLA/PLGA particles for antigen delivery started in the late 70s due to the well-known safety of these materials and the possibility to control antigen release. However, it was reported that the pH reduction inside the particles, arising from the polymer degradation, promotes damage in a large fraction of the antigen.²⁸ This is an important limiting factor considering that the antigen delivered must be in its antigenically active form to induce proper immune reactions.²⁸ Natural polymers have also been investigated for the preparation of biodegradable vaccine delivery systems. For instance, the polysaccharides pullulan, alginate, inulin (Advax™), and chitosan have been extensively studied.⁵²

1.2.4.4. Inorganic Particles

Inorganic particles are also being developed for vaccine delivery purposes. Here, gold, carbon and silica are the most studied materials.⁴³ For instance, novel porous carbon nanoparticles, loaded with bovine serum albumin (BSA), were able to induce humoral, cellular and mucosal responses *in vivo* after oral immunization. Similarly, in an animal experiment, mesoporous silica nanoparticles, loaded with ovalbumin (OVA), were able to provoke cellular and humoral responses in levels comparable to the Quil-A®-adjuvanted control.⁵⁵ Successful antigen delivery and immunostimulation were also demonstrated for gold nanoparticles.^{56, 57} In addition, changes in size and shape of these carriers were shown to be suitable tools to tailor the immunological output.⁵⁸

Overall, these materials allow for rigid structures and controlled and well-reproducible preparation. However, they are mostly non-degradable and can accumulate within the cells. Therefore, especially in continuous or prolonged periods of exposure, this can become a toxicity issue.^{43, 52}

1.2.4.5. Liposomes

Liposomes are one of the most studied lipid-based drug carriers and are currently applied in several licensed formulations (Doxil®, AmBisome®, Myocet®). Liposomes are vesicles composed of one or more concentric lipid bilayers enclosing an aqueous inner compartment.^{59, 60} They can be prepared using different methods (*e.g.* ethanol injection, film hydration, reverse phase evaporation, and microfluidic) and lipid compositions, resulting in formulations with different physicochemical properties (particle size, size distribution,

lamellarity, polarity, zeta potential, stability, encapsulation volume etc.). These characteristics highly impact their *in vivo* performance.⁵⁹⁻⁶¹

The growing number of studies applying liposomes in vaccines is improving the understanding of their biological performance and helping to clarify what determines their activity.⁴⁸ By exploiting possible customization, liposomes can be tailored to achieve the protective responses needed against a specific pathogen. For instance, it is known that cationic and anionic vesicles are more effective in inducing immune responses than neutral vesicles.⁶¹ This is mainly attributed to the ability of charged particles to interact with the cell membrane, and to release the antigen.^{61, 62} In addition, the comparison between the immune responses elicited by non-PEGylated and PEGylated cationic liposomes [*i.e.* liposomes without and with polyethylene glycol (PEG) coating, respectively] revealed a change from Th1 responses to mainly Th2 responses, respectively.⁶³ This might have been a consequence of the changes in the biodistribution of the liposomes *in vivo*. PEGylation avoids aggregation and inhibits the formation of a depot in the site of injection, which improves the drainage to lymph nodes and results in a different immunological output.⁶³ It was also found that rigid liposomes, formed by lipids with high transition temperatures (T_m), are in general more effective as adjuvant systems.^{62, 64}

A complementary strategy used to improve the levels of immunogenicity of liposome-based vaccines is the incorporation of immunopotentiators in the formulations. For example, the adjuvant AS01 formed by the combination of liposomes, MPL[®] and QS21 is included in a vaccine candidate against malaria, which reached phase 3 in clinical studies.¹⁹ Another important example is the cationic adjuvant formulation (CAF) 01 constituted by liposomes formed by dimethyldioctadecylammonium (DDA) and TDB. CAF01 typically elicits Th1/Th17 biased responses and is in clinical trials phase 1 in a vaccine against tuberculosis.^{19, 65} Similarly, the adjuvant CAF04 is based on the combination of DDA and a synthetic analogue of monomycoloyl glycerol (MMG-1), which is known to stimulate dendritic cells.^{66, 67} CAF04 induces strong Th1/Th17 responses and has shown promising adjuvancity in vaccine candidates against tuberculosis⁶⁸ and chlamydia.⁶⁹

Due to the ability to transport a wide range of molecules, the incorporation of additives in liposomal formulations is often relatively simple. Hydrophilic compounds can be

encapsulated into the aqueous core and hydrophobic compounds can be intercalated into the lipid bilayer.^{23, 70, 71} In theory, this enables the incorporation of antigens and adjuvants of all classes into liposomal formulations. However, the lipid bilayer capacity can become a limiting factor for the inclusion of hydrophobic molecules.⁷² The lipid bilayer may not provide enough hydrophobic environment for the incorporation of a feasible antigen payload. Another important limitation of liposomes is their poor stability and short shelf-life.⁷³ The need of stable particulate systems with higher solubilization capacity for hydrophobic and hydrophilic components increased the research interest in non-lamellar lyotropic liquid crystalline phases including the cubic and hexagonal phases.

1.3. Lyotropic Liquid Crystalline Phases

Liquid crystals (LCs) are thermodynamic phases found between the crystalline solid and simple liquid states. They are also called "mesophases", which originates from the Greek *meso* meaning "in between". Physical properties of LCs combine characteristics of crystals (*e.g.* orientation and order) and liquids (capacity to flow).⁷⁴ LCs formed by organic materials can be divided into two main groups: thermotropic and lyotropic. Thermotropic LCs undergo phase transitions upon changes in the temperature, whereas lyotropic LCs are formed in the presence of a suitable solvent and phase transitions occur as a result of both, temperature and concentration changes.⁷⁵ Lyotropic liquid crystalline phases are spontaneously formed in the presence of water by the self-assembly of amphiphilic lipid molecules. Amphiphilic lipids comprise a hydrophilic headgroup and a hydrophobic hydrocarbon chain region.⁷⁶ Examples of this class of lipids are monoglycerides (*e.g.* monoolein), phospholipids [*e.g.* 1,2-dioleoyl-sn-glycero-3-phosphoethanolamine (DOPE)], urea-based lipids (*e.g.* oleylurea), and glycolipids (*e.g.* 1-*o*-phytanyl-beta-D-xyloside) as shown in Figure 1.^{76,77}

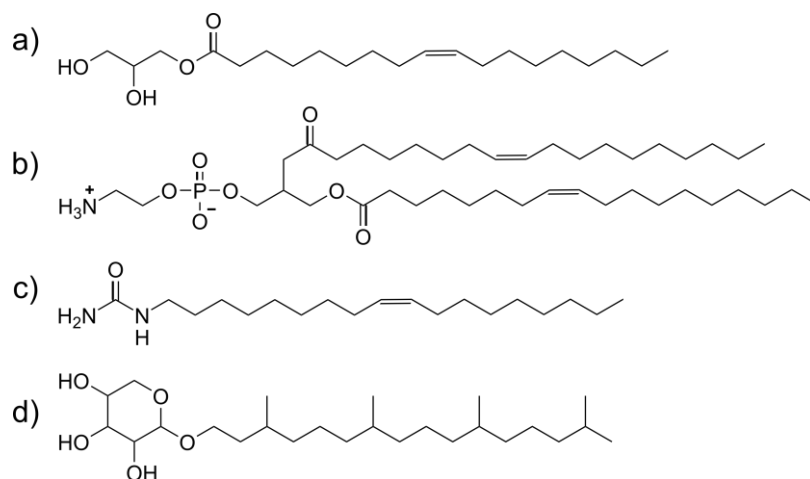


Figure 1: Molecular structures of different amphiphilic lipid molecules: (a) monoolein; (b) DOPE; (c) oleylurea; (d) 1-o-phytanyl-beta-D-xyloside.

The driving force for the lipid self-assembly is the hydrophobic effect, which triggers a reorganization of the amphiphilic molecules to minimize oil-water interactions between the hydrophobic chains and the aqueous environment.⁷⁸ The bulk phases formed can be highly viscous and difficult to handle. In addition, the contact with epithelial tissues may promote irritation. For these reasons, their application in the pharmaceutical and medical fields is limited.⁷⁷ However, there is a growing application potential for the particulate dispersions of these bulk phases.⁷⁹ Using an emulsifier or a steric stabilizer, stable nanoparticles with the same internal organization as found in the parent bulk phase can be generated.^{77,79} This nanostructured particle class has been collectively called “isasomes”, which means: internally self-assembled particles or “somes”.⁸⁰

1.3.1. Structural Assembly

The structure of lyotropic liquid crystalline assemblies depends on the molecular shape of the amphiphiles involved. Here, the evaluation of the critical packing parameter (CPP), also known as dimensionless shape parameter, can be used as a tool to better understand and sometimes to support predictions regarding the phase topology of the formulation.⁷⁹ The CPP can be estimated according to the equation below:

$$CPP = \frac{v}{a_0 \times l_c}$$

where v is the molecular volume of the hydrophobic chain, a_0 is the headgroup area and l_c is the critical chain length.⁸¹ As displayed in Figure 2, inverse structures (also known as Type II) are built by wedge-shaped molecules ($CPP > 1$), cylindrical-shaped lipids ($0.5 < CPP < 1$) form lamellar phase, and normal structures (called Type I) are generated by cone-shaped lipids ($CPP < 1$).⁸¹ The CPP is not constant and will vary according to the environment of the molecule. For instance, variations in temperature, pressure, pH and ionic strength can affect the headgroup hydration, inter-headgroup interactions, and the volume occupied by the hydrophobic chains.⁷² These modifications will in turn culminate with structural rearrangements of the amphiphilic molecules.⁷² In complex formulations, with more than one lipid component and further additives, the structure is a result of the interactions between all formulation components and the manner in which they exist in the given conditions.

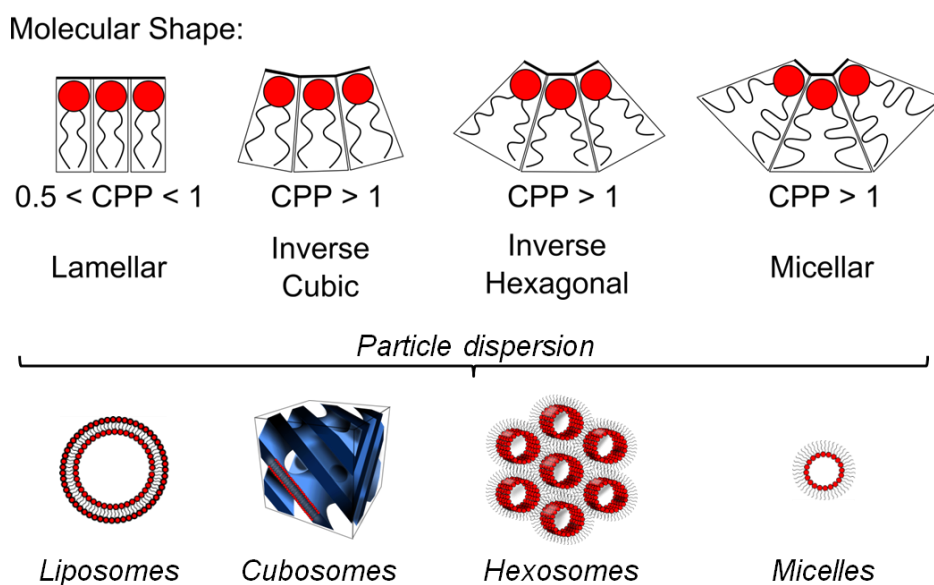


Figure 2: Self-assembly structures and corresponding CPPs.⁷⁹

The dispersion of a lamellar bulk phase ($L\alpha$), in excess of aqueous medium, yields liposomes (Figure 2). These are well studied vesicles composed of one or more concentric lipid bilayers enclosing an inner aqueous compartment.⁵⁹ As highlighted in section 1.2.4.5, liposomes have been successfully employed in the clinic as drug delivery systems.^{79, 82} With an increasing CPP and negative curvature, the inverse cubic phase (QII) is formed (Figure 2). This topology includes three different internal arrangements or space groups: gyroid (G or

Ia3d), double diamond (D or Pn3m), and primitive (P or Im3m).⁷⁶ Despite the particular geometries, the three arrangements are all constructed by a single continuous highly twisted bilayer, which forms a complex 3-D cubic network separating the space into two independent and non-intersecting water channels.^{22, 44, 76, 83} In general, the dispersion of inverse cubic phases yields internally structured particles called cubosomes, which are not necessarily cube-like. They can be spherical and even relatively flat.⁸⁴ The inverse hexagonal phase (HII) has an even higher CPP and a stronger negative interfacial curvature (Figure 2). In particulate form, the HII phase is called hexosome. Hexosomes are internally structured particles, whose repeating unit consists of rod-like arrangements of micelles hexagonally packed with closed water channels.^{76, 85}

1.3.2. Structure Characterization

A major part of the development of nanoparticles internally structured with non-lamellar lyotropic liquid crystalline phases is screening and optimization of the formulation to ensure the generation of the desired structure. In this process, small-angle X-ray scattering (SAXS) is an essential characterization tool. It is the most accepted method for identifying the structure of particles in dispersion.⁸⁶ Time-resolved SAXS (TR-SAXS) further expanded the application of this technique and allowed the kinetic monitoring of phase transitions as well as the identification of intermediary phases. However, TR-SAXS requires the use of synchrotron sources of X-rays.⁸⁷ Laboratory-based SAXS instruments have a relative low photon flux and the measurements take from minutes to hours. In addition, to obtain suitable scattering signal from dispersions, highly concentrated samples are needed.⁸⁸ In the present work concentrations of roughly 10 wt% (total lipid) were used for measurements in laboratory-based SAXS. If performed correctly, this method is non-destructive and the samples can be recollected for further use.⁸⁹ In comparison, data acquisition with synchrotron sources is much more efficient and can be performed in milliseconds in relatively low concentrated samples.⁸⁷

SAXS analyses are based on the fundamentals of light diffraction. Radiation is deviated from its trajectory when it enters a non-uniform medium and the analysis of this scattered radiation can be used to obtain information about the scattering material.⁸⁹ Normally, the scattered light is diffuse and does not provide much information on the scattering object. To

obtain structural information on the scattering element, the detected scattered radiation must have specular (mirror-like) properties. This means that the radiation coming from a single incoming direction is scattered in a single outgoing orientation.^{89, 90} In this way, the pattern of the scattered radiation is angle-dependent and can be associated with the periodicity of well-ordered scattering objects.⁸⁶ Wavelengths (λ) larger than the scattering element produce Rayleigh scattering, which is angle-independent and cannot provide full understanding of the element structure.⁹⁰ To obtain specular scattered light of lyotropic liquid crystalline dispersions, the wavelength of the incident radiation must be in conformity with the nanostructure dimensions.⁹⁰ In addition to this, the radiation used should not damage or modify the object and must be able to penetrate into the material. For these reasons, X-ray (λ in the range of 10 to 0.01 nm) is commonly used in the structural analysis of cubosomes and hexosomes.⁸⁶

As shown in Figure 3, during a SAXS measurement, the sample is irradiated with a well-collimated (minimum spreading, zero-angle position) X-ray beam with a defined wavelength (typically $\lambda = 0.154 - 0.08$ nm) under vacuum (lower background scattering).⁸⁹ Electron density variations in the sample promote scattering of part of the X-rays from the primary beam. The unscattered radiation is blocked by a "beam stop" to protect the detector from the high intensities of the direct beam and improve the observation of weak signals.⁸⁹ The scattered waves reach the detector generating bright or dark spots for constructive (in-phase) or destructive (out of phase) interferences, respectively.⁸⁹ The radiation intensity is recorded in a specific range of angles, generating a 2D scattering pattern of intensities distributed on a plane. This 2D representation can be radially integrated in order to create a 1D plot of intensity measured in function of the scattering angle 2θ .^{17, 19} Alternatively, the 1D representation can be shown in function of the momentum transfer (q), which can be calculated according to the equation below:⁹⁰

$$q = \frac{4\pi \sin\theta/2}{\lambda}$$

The patterns of rings (2D plot) or peaks (1D plot) obtained is characteristic of the internal structure of the sample. These patterns are formed by the strong signals originated from constructive interferences of the scattered radiation. In this context, the Bragg's law describes the conditions for the occurrence of constructive interferences.⁹¹ Figure 3B shows

two schematic parallel lattice planes of a hypothetical crystalline system. The incident radiation number "1" hits the first plane and the incident radiation number "2" hits the second lattice plane. The waves "1" and "2" come from the same source with the same wavelength (λ) and with peaks and valleys aligned (in-phase). A constructive interference happens if the scattered radiation remains in-phase.^{90, 91} However, due to the interaction with the sample, "2" has a longer path length than "1". Therefore, the condition for keeping alignment is that the path length difference is an integer multiple (n) of the wavelength (λ).⁸⁹⁻⁹¹ The path length difference between "1" and "2" is the sum of AB and BC (shown in red), which is equal to $2AB$. $2AB$ can be geometrically calculated as demonstrated (increased detail Figure 3B), resulting in $2d\sin\theta$, where d is the distance between the parallel lattice planes and θ is the scattering angle. In this way, the Bragg's law ($n\lambda = 2d\sin\theta$)⁹² describes the condition for the occurrence of constructive interferences, which result in peaks of high intensity called "Bragg peaks".⁹⁰

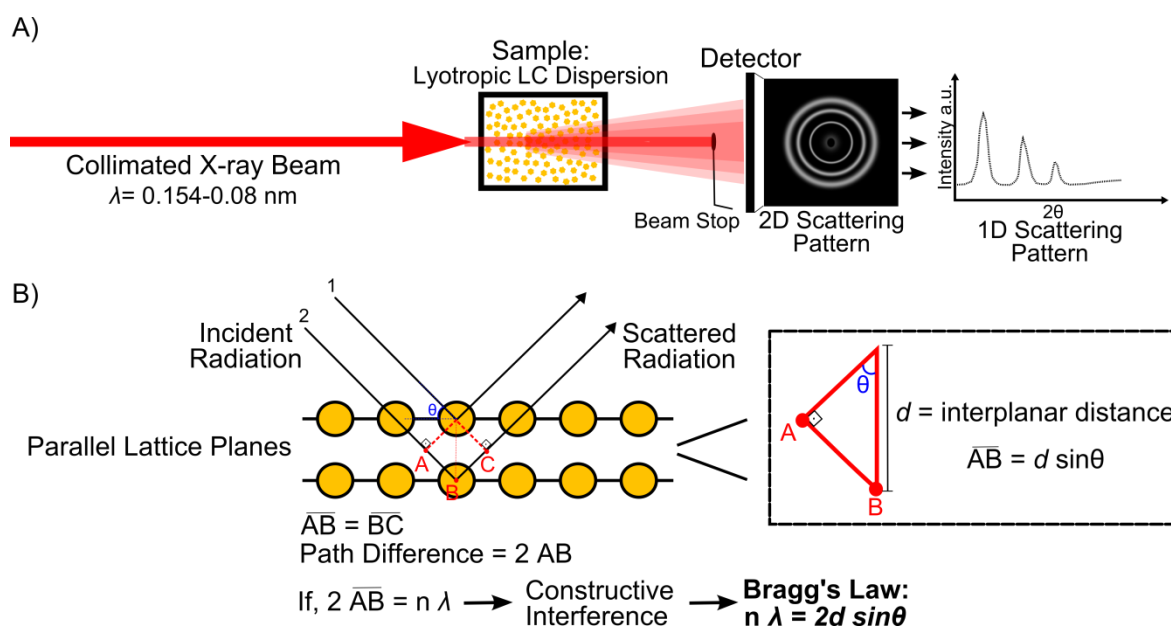


Figure 3: Principles of SAXS measurement (A) and the Bragg's law (B).^{89, 91}

The identification of structural features of a material is based on the analysis of the relative q -positions of the Bragg peaks (q -position of peak x / q -position of peak 1), which can also be identified with Miller indices. Table 1 displays the typical Bragg Peaks (with the

correspondent Miller indices) observed for the different types of mesophase commonly assembled by lipids.^{93, 94}

Table 1: Bragg peaks and corresponding Miller indices of lyotropic liquid crystal phases.^{93, 94}

Mesophase	Bragg Peaks								Miller indices
	1	$\sqrt{2}$	$\sqrt{3}$	$\sqrt{4}$	$\sqrt{6}$	$\sqrt{7}$	$\sqrt{8}$	$\sqrt{9}$	
QII Pn3m	---	110	111	200	211	---	220	221	
QII Im3m	---	110	---	200	211	---	220	---	
QII Ia3d	---	---	---	---	211	---	220	---	
L α	110	---	---	220	---	---	---	300	
HII	10	---	11	20	---	21	---	30	

Different from the patterns shown in Table 1, the typical scattering profile of micellar phases (L2) is composed by only one broad peak.⁸⁸

In comparison to solid crystals, the Bragg peaks measured from lyotropic LCs formed by lipids occur at much lower q -positions.⁷⁹ This indicates lower scattering angles (θ) and consequently larger dimensions. As indicated by the Bragg's Law (Figure 3B), the scattering angle is inversely proportional to the interplanar distances (d).

The coexistence of multiple phases in the same sample may produce SAXS data, which is difficult to interpret. This happens because the contribution of different structures to the scattering pattern cannot be separated. To understand the structural properties of such systems, other complementary characterization methods are necessary, such as cryogenic transmission electron microscopy (cryo-TEM).⁹⁵

In cryo-TEM, the sample is vitrified in liquid ethane prior to analysis, being imaged in the frozen-hydrated state. In this way, the structures are better preserved and maintain a higher fidelity with their native state in dispersion.⁹⁶ The visualization of dried samples may yield discrepant micrographs and lead to misinterpretations. Therefore, vitrification is highly important when studying lyotropic LC systems, whose morphology depends on the hydration level.⁷²

Due to its resolution of 2 to 3 nm, cryo-TEM allows for a detailed morphological analysis of single particles. The combination of tilting experiments (modification of observation axis) and Fast Fourier Transformation (FFT) enables not just the differentiation between QII and

HII phases, but also precise identification of the particular space group of QII structures. This makes cryo-TEM especially advantageous for the analysis of complex systems.^{72, 95, 97}

The application of SAXS and cryo-TEM as complementary techniques for the characterization of lyotropic liquid crystalline dispersions allows for a reliable and substantial understanding of the structural properties of the particles.⁷⁹ However, both methods are expensive and not easily accessible. In this context, optical polarization microscopy showed to be a reliable method for a preliminary mesophase characterization and formulation screening.⁹⁸ This technique is affordable, rapid, and typically available in most laboratories.⁷² Furthermore, microscopes equipped with a temperature controlled stage enlarged the scope of the analyses, enabling the additional investigation of phase behavior upon temperature variations.⁷² It is important to consider that this method does not enable conclusive identification of the mesophase, but provides critical information on the material. In addition, it is only feasible for the evaluation of bulks. Assuming that the dispersed nanostructured particles retain the internal organization of the original bulk mesophase,^{99, 100} polarization microscopy is an important tool for the screening of formulations for nanoparticle dispersions.

The analysis is mainly based on the determination of the optical isotropy or anisotropy of the mesophase. Crossed polarizing filters do not allow the transmission of light. However, if a sample placed between these polars is anisotropic, the light is rotated and some light transmission is observed.⁹⁸ Regarding lyotropic liquid mesophases, lamellar ($L\alpha$) and inverse hexagonal (HII) phases show birefringence (both are anisotropic). Differently, inverse cubic (QII) and micellar (L2) phases are isotropic. $L\alpha$ can be distinguished from HII based on their "optical texture".^{98, 101} Characteristic textures of $L\alpha$ phases are for instance, long and thin cords, mosaic-like structures, or circular formations containing the "Maltese-cross". The typical texture of HII phases is the so-called "fan texture".^{98, 101} Knowledge of "optical textures" can be useful to support this preliminary identification of a mesophase. However, this is a very challenging task, which can lead to fragile conclusions. In addition, it is crucial to consider that unusual textures can occur. QII and L2 phases do not show birefringence under polarized light, but can be differentiated from each other based on their apparent viscosity. QII phases are highly viscous, for this reason the samples normally have

structured interfaces. L2 phases in contrast, have low viscosity and therefore display smooth interfaces.⁷²

Overall, optical polarization microscopy is a very useful technique to obtain insights about the sample and monitor the initial formulation developing process. In order to precisely identify the structure of the material, it is absolutely necessary to confirm the results with more powerful techniques (*e.g.* SAXS and cryo-TEM).

1.3.3. Inverse non-lamellar Phases: Current Status

Cubosomes and hexosomes are the most prominent examples of particles internally structured with inversed non-lamellar phases. They show advantageous physical-chemical properties, which make them promising drug carriers. For instance, these formulations have good stability in excess water, their intricate structure, network of water channels, high amount of lipid per particle, and large internal interface area allow for high loading efficiencies of a wide range of compounds (*e.g.* hydrophobic, hydrophilic and amphiphilic molecules). Therefore, these systems have great potential to overcome encapsulation constraints encountered in other nanoparticles.^{76, 100, 102} In the context of vaccine development, an important limitation of other kind of particles is the small antigen load that can be incorporated within the particles (VLPs, ISCOMs, liposomes). Moreover, it has been reported that non-lamellar structures show fusogenic properties.^{103, 104} Considering this, it is hypothesized that cubosomes and hexosomes also have this property, which could enable cargo delivery directly to the cytosol. This characteristic could be of great advantage for vaccination. The delivery of antigen to the cytosol of antigen presenting cells (APCs) may further enhance the stimulation of cytotoxic T lymphocyte (CTL) immune responses.¹⁰⁵ In addition, it has been demonstrated that the induction of transitions between the different structures can be used as an efficient tool to modify and control the release profile of entrapped active molecules.^{85, 106, 107}

In spite of the growing interest in non-lamellar lyotropic liquid crystalline phases and their great potential for application in the pharmaceutical context, this research field is still very much in its infancy.⁷⁹ The main challenges arise from the intrinsic multidisciplinary nature of this subject, low availability of the principal characterization tools and from the lack of predictability regarding the structure and its behavior in complex formulations and

environments. A key issue with much of the literature on non-lamellar phases, is that it comprises mainly physico-chemical analyses. There is a lack of comprehensive studies and concrete evidences, and an excess of conjectures regarding the performance of these systems in the biological environment. This is especially critical with respect to hexosomes. To date there are no studies demonstrating the application of hexosomes as vaccine carriers and only surprisingly few reporting their general evaluation in a biological context. This status hinders interlaboratory comparisons and analysis regarding reproducibility. Nevertheless, it was demonstrated for instance, that hexosomes loaded with progesterone improve oromucosal delivery and storage stability.¹⁰⁸ In addition, hexosomes were reported to greatly enhance the topical delivery of cyclosporine A.¹⁰⁹ In another study, hexosomes were successfully radiolabeled and their theranostic potential was investigated in mice through single photon emission computed tomography combined with computed tomography (SPECT/CT).¹¹⁰ Besides this, hexosomes loaded with docetaxel showed 20-fold higher cytotoxicity against HeLa cells than the free antineoplastic drug.¹¹¹ Overall, these nanoparticles have been less well studied than cubosomes and not much is known about their feasibility as delivery systems. In contrast, studies reporting the application of cubosomes as vaccine delivery systems have already been reported showing promising results. It was demonstrated in an animal model that cubosomes were more efficient in inducing antigen-specific cellular responses than liposomes.¹¹² In addition, in a study on needle-free transcutaneous immunization using lipid carriers, cubosomes showed superior skin penetration and retention in comparison to liposomes and transferosomes.⁴⁴ Furthermore, cubosomes also revealed promising perspectives when applied as an ocular delivery system for flurbiprofen, showing suitable tolerability and enhanced transcorneal penetration.¹¹³

Overall, there is little known about the performance of particles internally structured with inversed non-lamellar phases *in vivo*. Consequently, the potential application of these formulations remains speculative. The present study aims to fill this gap in knowledge and provides a comprehensive investigation on hexosomes from formulation development, interaction with the cell membrane and internalization mechanism, to their application as adjuvant and vaccine delivery system *in vivo*.

1.4. Cellular Internalization of Nanocarriers

1.4.1. Overview of the Main Endocytic Pathways

It is well known today that nanoparticle-based formulations have the potential to improve the biological performance of drugs with poor solubility, non-specific cytotoxicity, low bioavailability, and/or inappropriate pharmacokinetics and pharmacodynamics.¹¹⁴ However, the favorable performance of a nanoparticle-based formulation depends largely on their interactions with the cells, especially when the drug target is localized intracellularly.¹¹⁵ The therapeutic outcome is determined by efficient cellular uptake, appropriate post-internalization traffic and intracellular fate. Considering that the mechanism of cellular internalization generally determines the uptake rate and the subsequent series of intracellular events, it is of utmost importance to evaluate and optimize this aspect.¹¹⁵ It is well known that the physicochemical properties of the nanocarriers (*e.g.* size, shape, surface features) play a central role in this matter. However, reliable tools and patterns, that help to predict via which pathway drug delivery vehicles may enter cells, have yet to be established.¹¹⁶

The main internalization pathways can be divided into phagocytosis and pinocytosis (Figure 4). Phagocytosis is performed primarily by specialized cells, called phagocytes (*e.g.* macrophages, monocytes, neutrophils, and dendritic cells). It is involved in several physiological processes, for example, in tissue remodeling, clearance of dying cells, and host defense against pathogens and non-self elements.¹¹⁶ In a simplified way, this internalization pathway occurs in three steps. First, the nanocarriers are opsonized through the interaction with immunoglobulins (IgG, IgM), complement components (C3, C4, C5), and serum proteins (laminin, fibronectin, type I collagen, C-reactive protein).¹¹⁶ Then, the opsonized particles adhere onto the phagocyte through specific interactions between the opsonins and receptors of the cell surface (*e.g.* Fc receptors, complement receptors, mannose receptors).¹¹⁶ This initiates a signaling cascade that induces actin rearrangement and pseudopodia projection around the particle, culminating with its engulfment. After ingestion, the vesicle formed acidifies, ultimately forming a phagolysosome with enzymatic content (esterases, cathepsins) to induce degradation of the internalized material.¹¹⁶

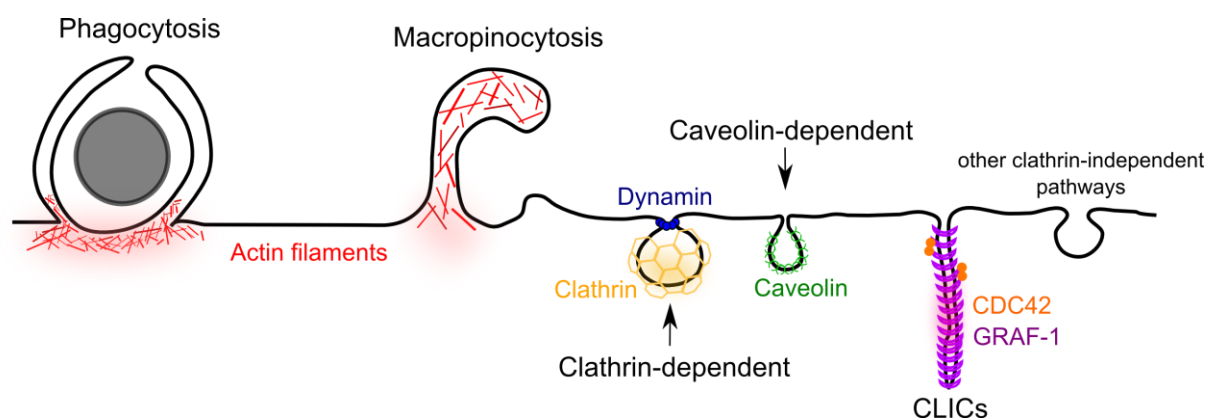


Figure 4: Principal endocytic mechanisms of nanocarrier internalization and some of their main regulatory proteins. CLIC (clathrin-independent carriers). ¹¹⁷

Due to the importance of particle opsonization for the phagocytosis, particle surface characteristics ¹¹⁸⁻¹²⁰ play a decisive role in this internalization pathway. It is known that the adsorption of proteins is fostered by surface hydrophobicity and charge. ^{118, 119} Thus, surface coating with the hydrophilic PEG, poloxamer, or poloxamine polymers impedes protein binding and decreases interaction with phagocytes, yielding long-circulating stealth® particles. ^{121, 122} A recent report further highlights the effect of particle shape, whereby elongated PLGA nanoparticles were less efficiently taken up by macrophages than their spherical counterparts. ¹²³ The same study demonstrated a synergistic effect of PEGylation and particle elongation to inhibit phagocytosis. ¹²³ Besides these factors, larger particles generally show a higher uptake via phagocytosis. ^{116, 124}

Pinocytosis is a non-phagocytic process and refers to the internalization of the bulk extracellular fluid (“cell-drinking”). ¹¹⁵ It can be subdivided in macropinocytosis, clathrin-mediated endocytosis (CME), caveolae-mediated endocytosis (CvME), and clathrin- and caveolae-independent pathways, which are less well characterized (Figure 4). Macropinocytosis occurs in diverse cell types, including macrophages. Similarly to phagocytosis, it is actin-dependent and involves the formation of long membrane protrusions. However, while during phagocytosis these protrusions are projected around the opsonized particle and close the vesicles (“zipper-up”), during macropinocytosis a pseudopodium surrounds the particle, collapses, and fuses with the membrane (Figure 4). ¹²⁵

Another contrast is that macropinocytosis seems to be unspecific and it does not involve any kind of receptor-ligand interaction.¹¹⁵

CME takes place in all mammalian cells and it plays an important role in the internalization of essential nutrients [e.g. cholesterol low density lipoprotein (LDL), iron-laden transferring (Tf-Fe)] and in the intercellular communication. CME can be triggered through specific receptor-ligand interactions, but it can also occur in a receptor-independent manner.^{125, 126}

Clathrin is a three-legged protein (triskelion), which assembles in basket-like structures with polyhedral lattice and supports membrane budding. Thus, clathrin-coated pits are formed on the plasma membrane and at late invagination stages the guanosine triphosphatase (GTPase) dynamin aids their fission, releasing clathrin-coated vesicles (Figure 4).^{126, 127}

CvME occurs through flask-shaped structures called calveolae (Latin for “little caves”) (Figure 4)¹²⁸, which are formed by caveolin and cavin family proteins. Caveolin-1 (Cav1) is the main structural component.¹²⁵ Caveolae are present in diverse extents among the different mammalian cell types. For instance, while they are extremely abundant in endothelial cells, smooth muscle cells, adipocytes, and fibroblasts, their presence is insignificant in kidney cells.¹²⁹ Considering that the physiological functions of caveolae are not fully understood, this heterogeneous distribution could suggest their implication in specialized cellular processes.¹²⁹ For example, in endothelial cells, it is suggested that CvME is involved in the transcytosis of serum proteins from the bloodstream into tissues.^{125, 126} Regarding the role of CvME in the uptake of drug delivery vehicles, it is proposed that the particles interact with the cell surface moving along to caveolae, where they get trapped and subsequently internalized.¹²⁶ Similarly to clathrin-coated pits, scission of caveolae from plasma membrane is thought to be driven by dynamin.^{125, 126}

In general, nanoparticles internalized through the mechanisms above described are transported primarily to endosomes.¹¹⁴ Early endosomes, also referred to as sorting endosomes, have a pH~6. Further acidification by ATP-dependent proton pumps, results in late endosomes (pH~5). Posterior fusion with lysosomes exposes the cargo to a digestive hydrolytic environment.¹¹⁴ Interestingly, for many years, it was believed that the contents internalized by the CvME pathway were transported to independent organelles of neutral pH and rich in caveolin, called caveosome.¹³⁰ For this reason, CvME was considered a

suitable internalization route to deliver sensitive molecules (*e.g.* peptides, proteins, nucleic acids) and circumvent lysosomal degradation.¹¹⁶ However, subsequent work classified caveosomes as aberrant formations of late endosomes and multivesicular bodies resulting from the overexpression of Cav1.¹³¹ Thus, it is still unclear whether CvME indeed constitutes an alternative pathway to avoid degradative fate of the internalized cargo.¹³²

Besides these classical endocytic routes, several clathrin- and caveolae-independent pathways have already been identified. For instance, cell adhesion molecule (CAM)-mediated endocytosis, flotillin-1-dependent endocytosis, ADP ribosylation factor 6 (Arf6)-dependent endocytosis, interleukin-2 receptor β (IL2R β)-mediated endocytosis, and the clathrin independent carriers (CLICs)/GPI-anchored protein enriched early endosomal compartment (GEEC) pathway were described.¹¹⁵ The CLICs pathways (Figure 4) have been reported to be involved in the internalization of bacterial exotoxins, glycosylphosphatidylinositol (GPI)-linked proteins, and fluid.¹³³ In addition, CLICs have been suggested to play a fundamental role in membrane repair and remodeling, homeostasis, and cell migration.¹³⁴ Interestingly, Howes et al. found that CLICs constitutes the major pathway for fluid internalization in fibroblasts, accounting for up to 70% of total fluid internalization.¹³⁴ This pathway occurs through pleiomorphic tubovesicular structures of several micrometers, originated directly from the cell membrane, and without rigid coat (Figure 4).¹³⁴⁻¹³⁶ Cdc42 activity is essential to form these structures,¹³⁴ and the protein GTPase regulator associated with focal adhesion kinase-1 (GRAF-1) governs this internalization route.¹³³ CLICs mature into GEECs and subsequently fuse with early endosomes.¹³⁴ The relevance of CLIC/GEEC and other clathrin- and caveolae-independent pathways in the context of drug delivery has yet to be established.¹²⁶

The identification of clear patterns that link physico-chemical properties of nanocarriers to a preferred internalization route is challenging.¹¹⁶ In contrast to phagocytosis, pinocytic mechanisms occur essentially in all kinds of cells.¹¹⁶ Unfortunately, experiments performed with different cell types often show considerable disparity.¹¹⁶ In addition, more than one internalization pathway may take place simultaneously, which increases the complexity of data analysis and comparison.¹¹⁶ For this reason, the impacts of determined particle characteristics on the uptake must be carefully interpreted, without extrapolation. For example, size-dependence has been demonstrated for polystyrene beads in B16 cell line

(murine melanoma). In this study, the authors observed predominantly CME for particles smaller than 200 d.nm (diameter in nm) and a shift to CvME for larger particles.¹³⁷ In another study using HeLa cells, polystyrene particles larger than 45 d.nm were internalized through CME and particles smaller than 25 d.nm seemed to undergo a clathrin-independent pathway and to by-pass lysosomal degradation.¹³⁸ Regarding particle surface charge, several studies reported higher uptake for positively charged particles in comparison to their negative counterparts.¹¹⁶ Considering that the cell membrane is negatively charged, the positive charge of particles may facilitate interactions and consequently improve internalization efficiency.¹¹⁶ Different from the phagocytosis evasion observed for stealth® particles discussed above, it was demonstrated that PEGylation of polymeric particles impacted the protein corona and improved uptake efficiency.^{139,140}

It should be highlighted that studying particle uptake is challenging and must be carefully performed in order to obtain useful results. Important control aspects are often neglected in this type of study, which limits interpretation of the findings. For example, it should be considered, that widely used pharmacological inhibitors generally have unspecific effects on endocytosis, and impact cell physiology as a whole.¹¹⁵ For this reason, the depletion of specific proteins has become the method of choice to achieve better selectivity.¹¹⁵ Furthermore, it is crucial to take into account that the suppression of an internalization route might induce the stimulation of other pathways.¹¹⁵ Another important aspect is, when using the expression of fluorescently tagged proteins as structural markers [for example Cav1-green fluorescent protein (GFP) as a marker for caveolae], the expression should be similar to that of the endogenous protein to avoid artifacts caused by overexpression.¹²⁹ In addition, the experimental conditions of *in vitro* assays (*e.g.* cell density, phase of growth, and confluence) have to be kept consistent, since they might interfere in the endocytic behavior.¹¹⁵

1.4.2. Relevance of the Internalization Route for Vaccine Carriers

The innate response involves the activity of the phagocytic and complement system.¹⁴¹ This first line of defense plays an elemental role in recognizing vaccines and adjuvants, and starting protective reactions that will culminate in pathogen destruction and enhancement of adaptive responses.¹⁴² The adaptive system is the second line of defense with highly specific

responses against the pathogenic agent.¹⁴¹ It was originally proposed that pathogens or vaccines in the extracellular medium are engulfed by antigen-presenting cells (APCs), processed, and displayed on major histocompatibility complex (MHC) class II on the cell surface. Then, these molecules are recognized by CD4⁺ T cells, which mature to become T helper cells 1 or 2 (Th1 or Th2). In contrast, antigens being produced within infected cells (intracellular pathogens) are presented on MHC class I and activate CD8⁺ T cells, which differentiate to cytotoxic T lymphocytes (CTLs).¹⁴³ However, posterior investigation revealed a process called cross-presentation, in which antigens from the extracellular environment are presented through MHC class I and induce CTL responses.¹⁴⁴ Due to the pivotal role of CTL responses against challenging vaccination targets, such as HIV and cancer,⁷³ there is a growing interest in exploring cross-presentation in vaccine development.¹⁴⁴ For this purpose, optimal interactions between immune cells and antigen delivery systems are necessary. It has already been reported that the mechanism of antigen internalization combined with its subsequent intracellular trafficking are decisive to allow cross-presentation. For instance, it was demonstrated that when APCs internalize soluble ovalbumin (OVA) via mannose receptor-mediated endocytosis, the antigen is processed and presented through MHC class I (cross presentation). However, if the mannose receptor is suppressed, the antigen presentation occurs through MHC class II.⁷³ Therefore, the importance of the internalization route of vaccine carriers goes beyond issues with antigen degradation in the lysosomes. The uptake pathway is directly involved in the series of events that determine the immunological output and the vaccine efficacy.

2 AIM AND OUTLINE OF THE THESIS

This project was conceived to increase the understanding in vaccine delivery and generate new tools to address challenges involved in modern vaccine development. The aim of this work was to develop and characterize new self-adjuvanting vaccine carriers to help bridge the gap between tolerability and induction of potent and persistent immune responses. The strategy was to use lipids, with proven immunostimulatory properties, to produce nanoparticles internally structured with lyotropic liquid crystalline phases, and develop new adjuvant formulations with improved performance. Thus, this work summarizes the

development of novel formulations and their physicochemical characterization, their interactions with cell membrane, and their biological performance *in vitro* and *in vivo*. Thesis outline:

Chapter I: This chapter gives a comprehensive overview of the scientific literature and background knowledge used to support the studies shown in the following chapters. A thorough introduction to modern vaccine formulations, lyotropic liquid crystalline phases, and cellular internalization mechanisms is provided.

Chapter II: This chapter shows the rational formulation development of hexosomes based on phytantriol and mannide monooleate (Phy/MaMo). It presents different preparation methods, structural characterization, loading and controlled customization of the systems based on changes in size, surface charge and internal structure.

Chapter III: This chapter describes the studies elucidating the internalization mechanism of hexosomes by cells. Here, different methods were applied to understand the uptake pathway for Phy/MaMo hexosomes in comparison to a conventional DOPC/DOPE liposomal formulation in HeLa cells. Comprehensive experiments with model cell membranes are also shown.

Chapter IV: This chapter demonstrates the important role of delivery systems in eliciting immune responses. Hexosomes and cationic liposomes, both containing the lipid adjuvant MMG-1, are compared by probing their immunostimulatory activity *in vitro* and in an animal model.

Chapter V: This chapter brings together the main outcomes of this work and constructs a general conclusion about the knowledge gained. Besides this, a critical outlook is presented with comments on the remaining open-questions and possibilities to elucidate them. In addition, hypothesis about the potential and perspectives regarding the application of the novel nanocarriers are given.

CHAPTER II

Characterization of Hexosomes as Versatile Vaccine Carriers

A version of this chapter has been published in Molecular Pharmaceutics:

Rodrigues L., Kyriakos K., Schneider F., Dietz H., Winter G., Papadakis C. M., Hubert M. (2016). „Characterization of lipid-based hexosomes as versatile vaccine carriers.” Molecular pharmaceutics, 13(11), 3945-3954.

This work was conducted in collaboration with the Soft Matter Physics Group and Institute for Advanced Study of the Technische Universität München. The manuscript was written by Rodrigues L. The SAXS measurements were performed by Rodrigues L and Kyriakos K under the supervision of Papadakis C M. Cryo-TEM image acquisition was conducted by Schneider F and supervised by Dietz H. All data analyses and additional experimental work were performed by Rodrigues L and supervised by Winter G and Hubert M.

The section 4.5 “Expanding the Customization Tool Box of Hexosomes” of this chapter and the figures showing molecular structures are not present in the published article.

1 ABSTRACT

Sub-unit vaccines typically show insufficient immunogenicity. To address this issue, we developed a novel self-adjuvanting particulate carrier system based upon the lipids phytantriol (Phy) and mannide monooleate (MaMo). Phy is a lipid known to form non-lamellar phases in fully hydrated systems, whereas MaMo has been found to promote immune responses in emulsion form. A bulk phase composition of Phy/MaMo (14 wt%) showed hexagonal (HII) phase behavior over a practical temperature range (including room and body temperature), and was therefore used for particle development. Hexosomes stabilized with different concentrations of either poloxamer 407, Myrj 59 or Pluronic F108 were successfully prepared. To demonstrate the versatile nature of these systems, the particles were further modified with positively and negatively charged lipids to change the zeta potential, and loaded with model antigens, whilst maintaining the HII structure. In addition, octyl- β -D-glucopyranoside was shown to be a suitable tool to transform hexosomes in cubosomes in a controlled manner. Overall, Phy/MaMo based hexosomes are structurally robust and amenable to customization, rendering them suitable as antigen delivery carriers.

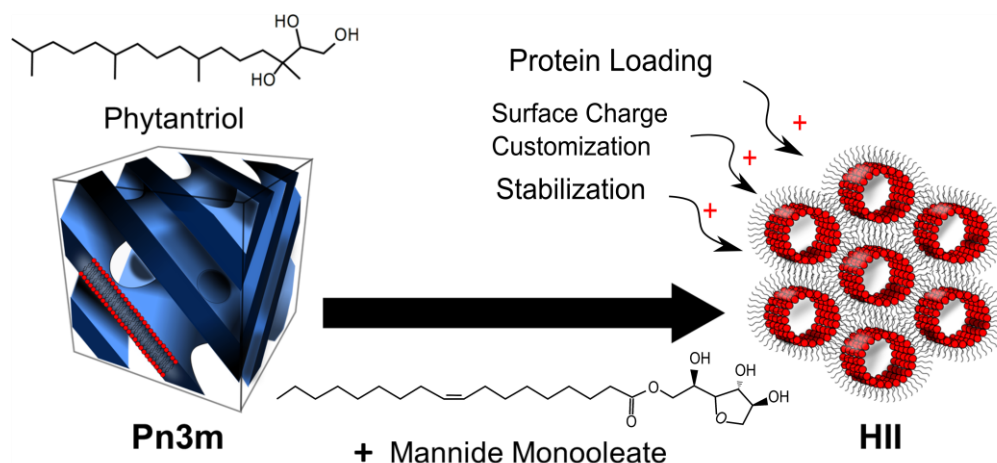


Figure 5: Graphical Abstract - Characterization of Lipid-Based Hexosomes as Versatile Vaccine Carriers.

2 INTRODUCTION

Vaccines are of utmost importance for global health and demonstrate one of the greatest medical successes. Especially vaccines based on highly purified and well-defined antigenic motifs (sub-unit vaccines) improved the safety and tolerability over the traditional whole-pathogen preparations.¹⁴ Nevertheless, sub-unit vaccines are often inefficient, because they are not able to induce the same level of immunogenicity demonstrated by the traditional ones.¹⁴⁵ To circumvent these issues, several strategies have been considered. For instance, potent immunostimulatory compounds (adjuvants) are co-administered with the antigen molecules to improve the strength and type of the immune response.²⁵ The incorporation of antigens into particulate delivery systems can prevent the premature degradation of the antigen *in-vivo* and at the same time allows mimicking the size, geometry, and kinetics of viruses and bacteria.¹⁴⁵ Moreover, the particle design offers a range of possibilities for tuning interactions between antigen molecules and immune cells as well as overcoming multiple dose regimens.¹⁴⁵ Progresses in the field of particulate delivery systems revealed promising potential for lipid-based particles such as cubosomes and hexosomes.^{22, 146} Cubosomes are internally structured with an inverse bicontinuous cubic phase. They are formed by a highly twisted continuous lipid bilayer creating a complex network with 3-D cubic symmetry and two non-intersecting water channels.⁷⁶ Hexosomes are rod-shaped inverse micelles organized in a hexagonal structure with closed water channels.⁷⁶ Due to their high interfacial areas and network of water channels, these particles are known as multi-compartment carriers and have great potential to overcome encapsulation constraints encountered with other particulate systems (liposomes, virus-like particles, and ISCOMs).^{22, 100, 102} Moreover, it has already been reported that non-lamellar structures (like cubic and hexagonal) show fusogenic properties,^{103, 147} which could contribute to the delivery of antigens directly to the cytosol of antigen-presenting cells (APCs), stimulating cytotoxic T lymphocyte (CTL) immune responses.

The present work proposes the development of new self-assembled lipid-based particles with non-lamellar internal structures and immunostimulatory properties for vaccine delivery. For this purpose, the phase behavior of systems containing phytantriol (Phy) and mannide monooleate (MaMo) was investigated (Figure 6).

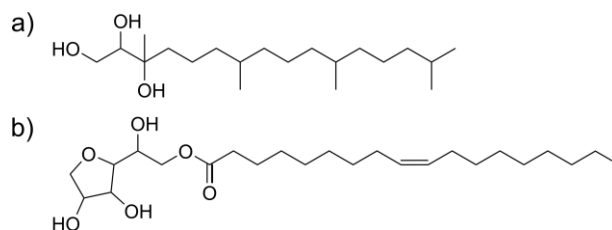


Figure 6: Molecular structures of (a) phytantriol and (b) mannide monooleate.

Phy is a well-characterized lipid able to form non-lamellar phases in fully hydrated systems.¹⁴⁸ MaMo is an emulsifier applied in several adjuvant systems (Montanide ISA 51 and 720, and Freund's adjuvant)¹⁴⁹ and it is known to promote Th1 and Th2 responses in emulsion form.¹⁵⁰ The current approach aimed to synergistically combine the structural properties of Phy with the intrinsic biological activity of MaMo in one unique system to deliver antigens for immunization purposes. Different analytical methods, such as small-angle X-ray scattering (SAXS), cryogenic transmission electron microscopy (cryo-TEM) and polarization microscopy, were applied to characterize these new systems and to systematically develop customized nanostructured particles. The hexosomes could be modified with other charged lipids and model antigens without compromising the internal hexagonal structure. Taken together, the results presented here emphasize the versatility of these systems and demonstrate their great application potential for the delivery of biopharmaceuticals.

3 MATERIALS AND METHODS

3.1. Materials

Phytantriol (Phy) from DSM Nutritional Products Europe Ltd was kindly provided by Nordmann, Rassmann GmbH (Hamburg, Germany). Mannide monooleate from plant (MaMo), dimethyldioctadecyl-ammonium bromide (DDA), poloxamer 407, albumin from chicken egg white (OVA), and lysozyme from chicken egg white (LYS) were purchased from Sigma-Aldrich (Taufkirchen, Germany). Pluronic F108 and Myrj 59 were a gift from Croda (Barcelona, Spain). 1,2-dioleoyloxy-3-trimethylammonium propane chloride (Dotap), and 1,2-distearoyl-sn-glycero-3-phospho-rac-glycerol sodium salt (DSPG) were purchased from

Lipoid GmbH (Ludwigshafen, Germany). CBQCA Protein Quantitation Kit was purchased from Life Technologies GmbH (Darmstadt, Germany). Phosphate buffer saline solution (PBS) was prepared at pH 7.2-7.6 using potassium chloride (Merck KGaA), potassium phosphate monobasic (Merck KGaA), sodium chloride (Merck KGaA), and sodium phosphate dibasic anhydrous (Grüssing GmbH).

3.2. Preparation of Bulk Phases

Appropriate amounts of Phy and MaMo were melted together at 70°C using the Thermomixer comfort (Eppendorf). In order to obtain a homogeneous molten, the samples were frequently vortexed. Highly purified water was added to obtain fully hydrated bulks (final lipid concentration of 50 wt%).

3.3. Preparation of Particles

Phy (86 mg), and MaMo (14 mg) were weighed and homogenized together as described for the bulk phases. To disperse particles from the bulk phase poloxamer 407, Pluronic F108 or Myrj 59 were applied as stabilizers in concentrations ranging from 5 to 30 wt% of the total lipid mass. The stabilizer solution in PBS was added to the Phy/MaMo mixture and followed by intense vortexing to give a final lipid concentration of 10 wt%. The samples were then agitated for 30 min at 3500 rpm in a dual asymmetric centrifuge (SpeedMixer™), followed by 3 cycles of sonication of 1 min with 4 s pulse, 2 s pause, and 20% amplitude (Bandelin Sonopuls HD3200 with sonotrode MS72). To introduce different particle surface charges, Phy and MaMo were homogenized with different amounts of charged lipids (DDA, Dotap, or DSPG). The samples were then processed as described above. In order to prepare protein loaded particles, appropriate amounts of either LYS or OVA were dissolved in the stabilizer solution and added to the lipid molten. Subsequently, the samples were agitated and sonicated as specified above. All samples were stored at room temperature (rt).

3.4. Polarization Microscopy

Polarization microscopy was performed as a preliminary screening method to select the bulk phases for SAXS measurements. The analyses were carried out using the Keyence

microscope BZ-8100E equipped with a heating stage (Thermo Plate from TokaiHit) and polarization filters. A thin layer of sample (fully hydrated bulk) was applied between 2 cover glasses and observed under polarized light at temperatures from 25°C to 50°C. The presence of birefringence is an indication of lamellar ($L\alpha$) or inverse hexagonal (HII) phases. Inverse bicontinuous cubic (QII) and micellar (L2) phases typically show isotropic behavior.¹⁵¹ Liposomes, hexosomes, cubosomes, and micelles can be derived from the dispersion of bulk phases with $L\alpha$, HII, QII, and L2 structures, respectively.¹⁰³

3.5. Small-Angle X-ray Scattering (SAXS)

SAXS analyses were accomplished using a Ganesha 300XL instrument equipped with a GENIX 3D microfocus Cu X-ray source and a 2D Pilatus 300K detector in a fully evacuated sample chamber. The bulk samples were mounted in a Linkam cell between mica windows (thickness 5-7 μm). For the characterization of particles, the dispersions were introduced into glass capillaries (1 mm light path), which were then hermetically sealed and mounted in a heatable/coolable cell. The samples were measured after 10 min of equilibration at the selected temperature. The wavelength was $\lambda=1.54 \text{ \AA}$ and the sample-to-detector distance 401.4 mm (Linkam cell) and 406.2 mm (capillaries). The acquisition time was 30 and 120 min for bulks and particles, respectively. Longer acquisition times were used for the particles in order to increase the statistics and compensate the lower scattering signal. A pin diode was used to measure the transmission of the sample. The 2D images were azimuthally averaged and the background from the mica windows was subtracted, taking the transmission into account.

In order to identify the different liquid crystalline phases, the q -position ($q = 4\pi \sin(\theta/2)/\lambda$ is the momentum transfer) of each Bragg reflection was determined by fitting a Lorentz function. The ratios of the relative peak positions were calculated and compared to patterns described in the literature.^{152, 153} The repeat distance d was calculated using $d = 2\pi/q_1$, where q_1 is the position of the first peak. The mean lattice parameter a was determined according to the scattering law for the respective mesophase, namely $a = \sqrt{2d}$ for Pn3m (cubic double diamond) and $a = 2d/\sqrt{3}$ for HII (inverse hexagonal).¹⁵⁴

3.6. Dynamic Light Scattering (DLS)

Size and zeta potential analyses were performed using the Malvern Zetasizer Nano ZS (Malvern Instruments GmbH). Samples were diluted (1:200) and measured in PMMA cuvettes or DTS1060C capillary cells for the determination of size and zeta potential, respectively. All measurements were performed in triplicate, at 25°C, and in buffering conditions relevant for biological experiments (PBS, pH 7.4).

3.7. Protein Load Determination

In order to separate the free protein, the particles were washed four times with PBS using a centrifugal concentrator (Vivaspin 20 with PES membrane and MWCO 100k). To disrupt the particles and release potentially encapsulated protein molecules, the washed samples were incubated for 30 min at rt with Triton-X 0.5%. After centrifugation (21000 g, 10 min), the protein content was quantified with the CBQCA Kit according to the manufacturer's protocol. Considering possible material loss that may occur during the washing steps, the values obtained after protein quantification were corrected by the dry mass of each sample (determined gravimetrically). The experiments were conducted in triplicates. Relative loading efficiencies were compared using a paired Student's *t*-test performed by SigmaPlot 12.5 (Systat Software Inc., Germany).

3.8. Tryptophan Accessibility Assay

The accessibility of tryptophan residues to the collisional quencher acrylamide was evaluated. The fluorescence of protein molecules in buffered solution, and when loaded in particles, was investigated upon the addition of acrylamide at different concentrations (0.2 to 2 M). The fluorescence was monitored using the Cary Eclipse Fluorimeter at 25°C with excitation 280 nm (slit width 10 nm) and emission 300-400 nm (slit width 5 nm). To compare the fluorescence intensities in different environments, the ratios between unquenched (F_0) and quenched (F) signals were calculated for each sample.

3.9. Cryogenic Transmission Electron Microscopy (Cryo-TEM)

Vitrified specimens of selected formulations at approximately 5 wt% (total lipid) were prepared in a Vitrobot (FEI, The Netherlands) at 22°C and 90% humidity. A volume of 3 μ l of the particle dispersion was applied on 400-mesh Quantifoil R2/1 copper grids (Quantifoil, Germany) that were negatively glow discharged with a Plasma Cleaner (EMS, USA) at 35 mA for 45 s. After 15 s equilibration, the excess of liquid was removed through blotting (3 s, blot force -1) and the grids were automatically vitrified in liquid ethane below -172°C. The samples were imaged using a Tecnai Spirit microscope (FEI, The Netherlands), equipped with an Eagle 4k charge-couple device (CCD) camera and a Cryo-Transfer Holder (Gatan, Inc., USA). The system was operated at an acceleration voltage of 120 kV under low dose conditions (SerialEM acquisition software) with 26'000-, 30'000-, and 40'000-fold magnification. Image analysis was performed using Fiji.

4 RESULTS AND DISCUSSION

The design of novel particulate systems with non-lamellar internal structures and desired characteristics can be challenging, especially in complex formulations. Moreover, as it is very difficult to predict the impact of each additive on the mesophase structure, comprehensive studies are required. In the present work, formulations based on a combination of Phy and MaMo were systematically developed and the effects of various additives on relevant properties such as size, morphology, stability, charge, and loading were evaluated.

4.1. Characterization of Bulk Phases

To investigate the behavior of systems formed by Phy and MaMo, fully hydrated bulk phases of Phy/MaMo were prepared at different ratios in highly purified water and characterized using polarization microscopy and SAXS. Polarization microscopy was used to pre-screen a large number of samples and establish a phase diagram outline (Figure 7A), which enabled the selection of feasible temperature and concentration ranges for the SAXS analyses. The observation of anisotropy under polarized light is an indication of lamellar

(L α), or inverse hexagonal (HII) structures, which, in dispersion, can yield liposomes, or hexosomes, respectively. Isotropy, in turn, is an evidence of inverse bicontinuous cubic (QII), or micellar (L2) structures, which can be dispersed in cubosomes, or micelles, respectively.^{103, 151} This analysis is challenging for liquid samples due to their high mobility, which hampered the visualization of transitions and birefringence. For this reason, the phase diagram outline was restricted to samples containing 0-20 wt% MaMo which were gel-like at rt.

As displayed in Figure 7A, bulks prepared with Phy at 100% appeared isotropic under polarized light at almost all temperatures investigated. This, together with the gel-like consistency, illustrated the typical aspect of inverse bicontinuous cubic phases (QII). Likewise, Dong et al. observed isotropic properties and high viscosity for fully hydrated bulks of Phy.¹⁵⁵ However, they reported a transition to anisotropic behavior at temperatures above 60°C, while in the present work, the formation of birefringent structures occurred already at 50°C (Figure 7A). The phase diagram outline (Figure 7A) revealed that even low concentrations of MaMo had a remarkable impact on the structure of pure Phy. At 2-4 wt%, MaMo induced a transition from iso- to anisotropic behavior with an intermediate region showing characteristics of both phases. This transition can be seen in more detail in Figure 7B, in which the micrographs obtained for a fully hydrated bulk formed by 3.3 wt% MaMo in Phy are displayed. At 25°C, the isotropic and featureless aspect of this bulk was evident. In addition, the high viscosity of the sample was noticeable through its irregular interface, which suggested an inverse cubic structure (QII). At 33°C, the formation of small birefringent areas was observed. This anisotropic aspect is characteristic for both, lamellar (L α), and inverse hexagonal (HII) phases.¹⁵¹ At higher temperatures (34-50°C), the anisotropic properties became gradually more dominant and the addition of more MaMo (Figure 7A) shifted the transition from iso- to anisotropic behavior to temperatures below 25°C.

These findings demonstrated the remarkable ability of MaMo to modify the phase behavior of Phy and indicated the establishment of an anisotropic mesophase at room temperature (Figure 7A). At 15-20 wt% MaMo, the bulk samples underwent a transition from anisotropic to isotropic at higher temperatures (above 35°C). In comparison with the initial isotropic

structure, the second isotropic phase displayed higher fluidity, which may be an indication of a micellar (L2) structure.^{155, 156}

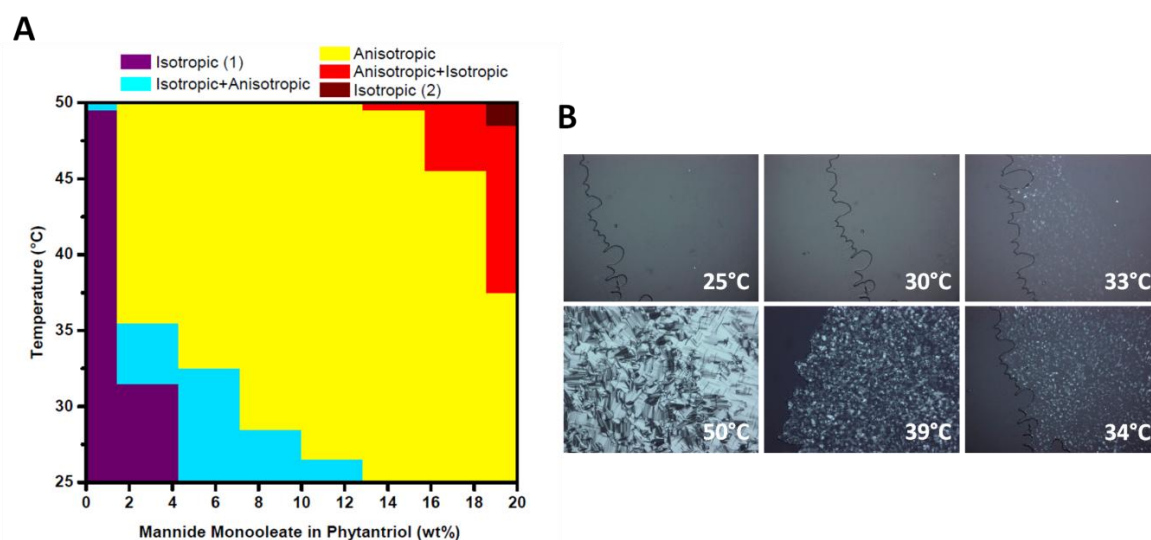


Figure 7: A: Phase diagram outline established through polarization microscopy of fully hydrated bulk phases formed by Phy and MaMo at different weight ratios and temperatures. B: Polarization micrographs of a fully hydrated bulk formed by 3.3 wt% of MaMo in Phy at different temperatures.

In order to fully understand the impact of MaMo on Phy systems and to precisely identify the mesophases along with their internal arrangements in a broader concentration and temperature range, SAXS measurements were performed. As shown in Figure 8A, in pure Phy systems, a phase transition from inverse bicontinuous cubic double diamond (Pn3m) to HII occurred at approximately 50°C. At 60°C, a pure HII topology was identified. Interestingly, this structure did not prevail in a large temperature range, and already at 70°C, the sample displayed an inverse micellar (L2) structure. Similarly, the characterization of Phy bulks reported by other groups^{155, 157} revealed Pn3m structures at room temperature, followed by transitions to HII and subsequently to L2 upon temperature increase. However, the literature is not fully consistent with respect to the phase transition temperatures determined in the present work. Deviations of up to 10°C were identified.¹⁰⁰ It is known that the origin of the substances used plays a decisive role in this matter, i.e. the phase behavior strongly depends on the purity of the Phy used.^{100, 158} This may explain the deviations from reports of other groups.

Higher MaMo ratios facilitated the formation of HII structures (Figure 8A). The phase transition from Pn3m to HII observed in pure Phy systems at 50°C was reduced to values below 25°C. Analogously, the temperature of the phase transition from HII to L2 was progressively decreased as the MaMo content increased (from 60-70°C in 100% Phy to 25-37°C in 28 wt% MaMo in Phy). Samples containing 40-80 wt% MaMo in Phy showed phase separation, while concentrations above 80 wt% resulted in stable and homogeneous samples with L2 structure.

The phase modulation demonstrated by MaMo in Phy bulks is comparable to other lipidic systems, such as Phy/vitamin E acetate,¹⁵⁵ glyceryl monooleate/diolein,¹⁵⁹ and glyceryl monooleate/oleic acid.¹⁶⁰ Analogously, the original inverse cubic structure was successfully transformed to HII with the incorporation of each component in a concentration dependent fashion.^{155, 159, 160}

Among all Phy/MaMo ratios evaluated, Phy bulk phases containing 14 wt% MaMo were found to be the most suitable for this study. At this MaMo content, HII mesophases were formed and maintained over the largest temperature range, including body and room temperature, as indicated by SAXS analysis (Figure 8B). Interestingly, the SAXS results revealed that a temperature increase from 25 to 37°C promoted a reduction of the lattice parameter from 4.85 ± 0.01 to 4.63 ± 0.01 nm. This temperature dependent behavior was seen in all samples and may be explained by the higher conformational disorder and volume expansion in the chain region of the lipid molecules at higher temperatures.¹⁰³ At 50°C, the first and most intense peak became broader, while the intensity of the second and third peak was reduced, indicating a HII-L2 phase transition (Figure 8B). At 60°C and 70°C, the typical scattering profile for L2 structures, featuring only one broad peak, was observed. The presence of HII structures over a large temperature range may be advantageous for the customization of the systems and particle stabilization without sacrificing the non-lamellar profile.

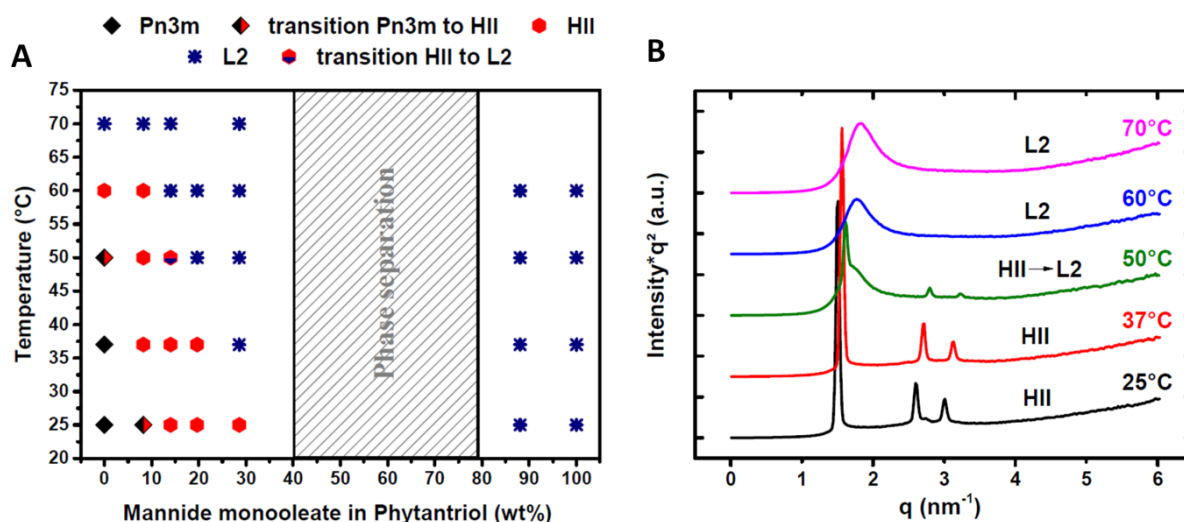


Figure 8: A: Phase diagram obtained by SAXS measurements of fully-hydrated bulk phases formed by Phy and MaMo at different weight ratios and temperatures. B: SAXS curves as a function of temperature of 14 wt% MaMo in Phy (fully hydrated bulk phase); Pn3m (inverse bicontinuous cubic double diamond); HII (inverse hexagonal); L2 (inverse micellar).

4.2. Particle Preparation

The preparation of particles requires the addition of a stabilizing agent, which enables the dispersion of the bulk phase and prevents particle aggregation and/or flocculation.¹⁰⁰ However, depending on the concentration used, this emulsifier can increase the toxicity of the particles and also disturb their internal structure.¹⁶¹ Poloxamer 407 (also known as Pluronic F127) is the most commonly used stabilizing agent in lyotropic liquid dispersions.¹⁰⁰ A recent study identified Pluronic F108 (poloxamer 338) to be even more effective as a stabilizer than Pluronic F127 for dispersed systems composed of Phy or glyceryl monooleate.¹⁶² Similarly, an excellent stabilization capacity of Phy-based cubosomes has also been reported for Myrj 59 (Polyoxyethylene-100-stearate).¹⁶³ The molecular structures of these three stabilizers are displayed in Figure 9.

Based on the reduction of the particle size seen in Figure 10, it may be assumed that at 5 wt% Myrj 59 dispersed the bulk phase more efficiently than the other stabilizers. However, when considering the number of stabilizer molecules necessary to stabilize a specific number of lipid molecules, 5 wt% of Myrj 59, corresponding to 0.37 mol%, can be practically compared to samples stabilized with 15 wt% poloxamer 407 and Pluronic F108, corresponding to 0.41 and 0.35 mol%, respectively, within this data set. This comparison revealed that Myrj 59 is the least potent stabilizing agent and thus contradicts descriptions by Chong et al., in which Myrj 59 was considered a more potent stabilizing agent than Pluronic F127.¹⁶³ Particles dispersed with Pluronic F108 and poloxamer 407 showed comparable size profiles, whereby Pluronic F108 promoted a slightly better size reduction, possibly due to its longer polyoxypropylene chain (Figure 9).¹⁶²

It is important to consider that stabilizers with longer chains may promote a more intensive stealth effect in biological systems, as observed with a standard PEGylation. In this work, the hexosomes are intended to be used for vaccine delivery, and the particle uptake by the immune cells is a desired effect. For this reason, stabilizing agents with shorter molecules, such as poloxamer 407 and Myrj 59, are preferred over Pluronic F108 (Figure 9).

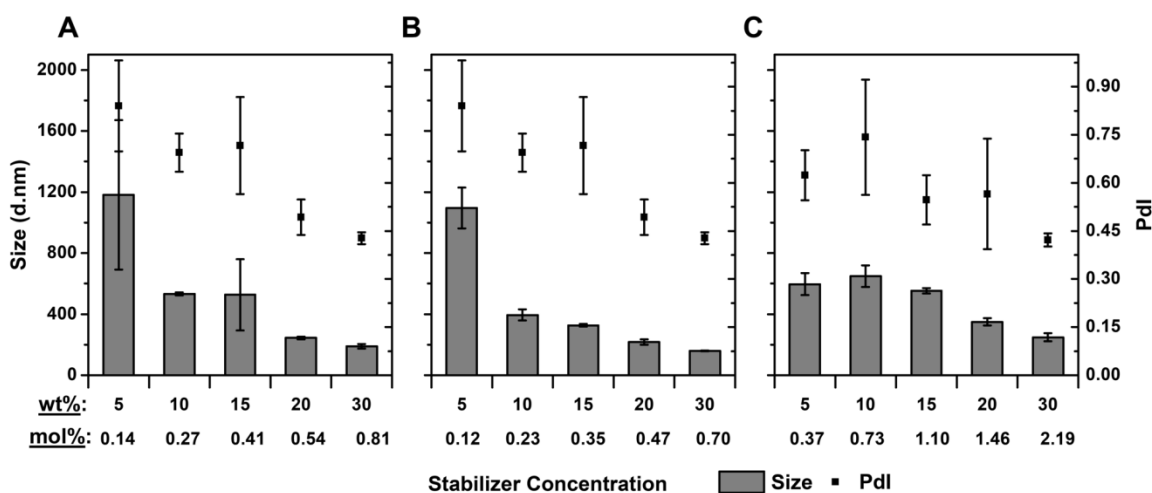


Figure 10: Size characterization by dynamic light scattering of Phy/MaMo (14 wt%) formulations containing poloxamer 407 (A), Pluronic F108 (B), and Myrj 59 (C) at different concentrations. The stabilizer concentrations are given in weight% and in mol% of the total lipid in the formulation. Bars depict mean \pm SD of three independent measurements.

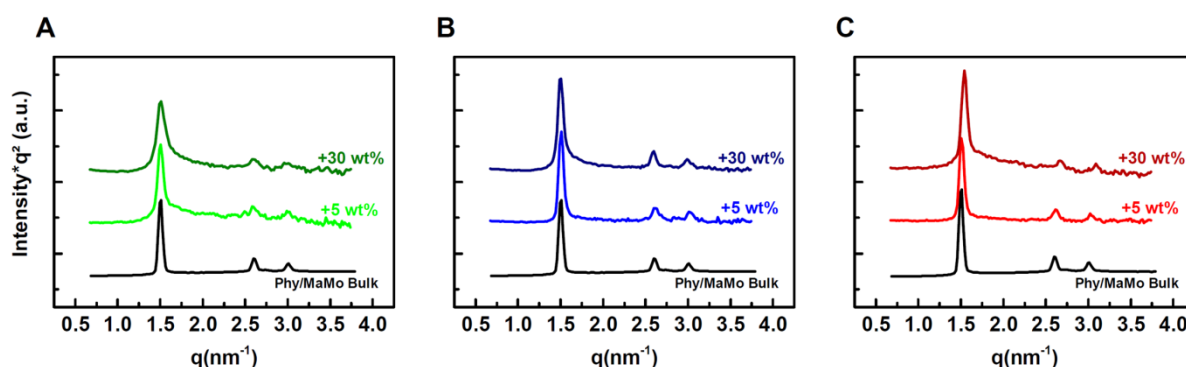


Figure 11: Structure characterization through SAXS of Phy/MaMo (14 wt%) formulations containing poloxamer 407 (A), Pluronic F108 (B), and Myrj 59 (C) at 5 and 30 wt% of total lipid. The black curve represents the non-dispersed bulk phase without stabilizer. Measurements were performed at 25 °C. The curves were vertically shifted for clarity.

4.3. Particle Size Optimization

The formation of non-lamellar structured particles is typically achieved through the dispersion of the bulk phase in the presence of stabilizers.^{151, 164} In order to prepare relatively monodisperse systems with stable particles in the submicron range, the dispersion technique is followed by a post-treatment to further improve the size profile. For instance, heat treatment (125°C for 20 min),¹⁶⁵ autoclaving (121°C for 15 min at 1 bar)⁸³ and high pressure homogenization¹⁶⁶ have been reported as suitable dispersion post-treatment methods to reduce the size distribution of glyceryl monooleate cubosomes stabilized with Pluronic F127. Figure 12 shows strategies applied in the present work to optimize the size profile of Phy/MaMo particles stabilized with 30 wt% Myrj 59. When incubated overnight at 40°C, the particles showed a drastic size reduction in comparison to samples kept at room temperature (Figure 12A). Maintaining constant storage conditions, size and PDI remained constant over 45 days. Interestingly, samples not subjected to this temperature treatment underwent a progressive size reduction over time.

These results suggested that the temperature treatment accelerated an equilibration process of the system, yielding a stable and relatively monodisperse particle dispersion that can be stored at rt for at least 45 days. This phenomenon was observed only in samples stabilized with Myrj 59, and to date, to the best of our knowledge, there are no reports addressing similar findings. Studies on cubosomes stabilized with Pluronic F127 showed that intensive

heat treatment (125°C for 20 min) yielded larger particles with a more narrow size distribution,^{165, 167} while lower temperatures for longer time periods (95°C for two hours) did not induce the same effects.¹⁶⁵ It may be hypothesized that Pluronic F127 and Myrj 59 have different stabilization mechanisms and interact differently with the lipidic structure.

Alternatively, three-fold extrusion of the formulations through a polycarbonate membrane of 400 nm pore size yielded stable particles with a similar size profile (Figure 12B). One major advantage of the temperature treatment over the extrusion is that it maintains the sample integrity, because material loss is not possible. However, depending on the encapsulated content, the temperature treatment may induce instability issues and premature release. SAXS analysis confirmed the conservation of the HII structures after both size optimization strategies (Figure 12) and affirmed that both methods are suitable to improve the size profile of these systems.

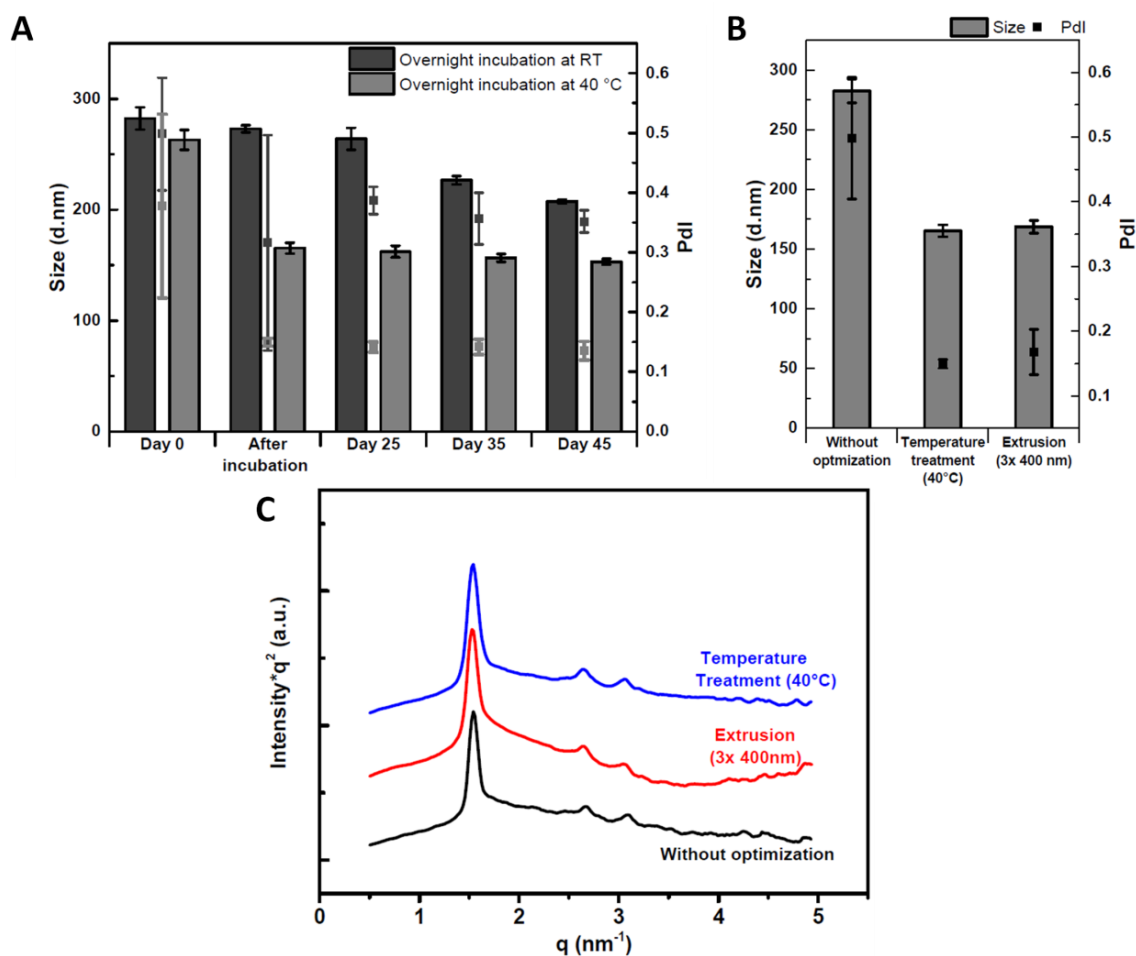


Figure 12: Size optimization strategies shown for Phy/MaMo (14 wt%) hexosomes stabilized with 30 wt% Myrj 59. **A:** Size (columns) and PdI (squares) monitored by DLS of samples stored at room temperature (rt) (dark grey), and samples incubated overnight at 40°C (light grey). **B:** Effect of size optimization using temperature treatment at 40°C and extrusion through a polycarbonate membrane of 400 nm pore size. Data is displayed as mean \pm SD of three independent measurements. **C:** SAXS curves from particles without size optimization (black), subjected to extrusion through a polycarbonate membrane of 400 nm pore size (red), and subjected to temperature treatment overnight at 40°C (blue).

4.4. Particle Customization

Considering the relevance of the overall surface charge of delivery systems in the interactions with cells, hexosomes carrying a positive or negative overall surface charge were developed in the present work. For this purpose, DDA (+), Dotap (+), and DSPG (-) (Figure 13) were added at various concentrations (5-30 wt%) to the standard Phy/MaMo (14

wt%) formulation. The measured zeta potential of each hexosome formulation correlated with the amount of incorporated charged lipid, whereby increased concentrations resulted in higher absolute values (positive/negative) (Figure 14).

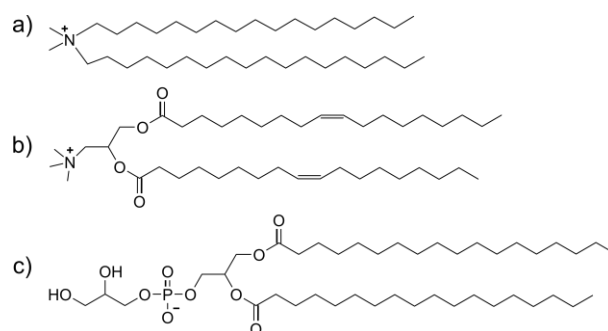


Figure 13: Molecular structures of DDA (a), Dotap (b), and DSPG (c).

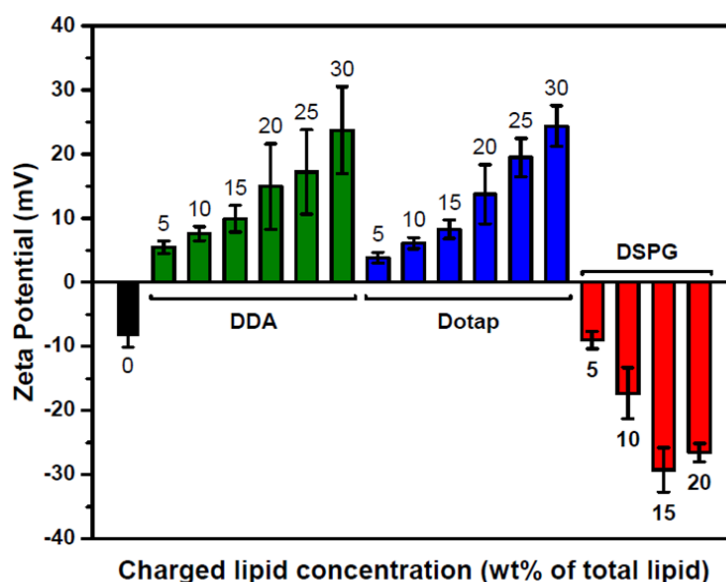


Figure 14: Zeta potential values of Phy/MaMo (14 wt%) hexosomes stabilized with 15 wt% poloxamer 407 containing different amounts of charged lipids, as given in the graph in wt% of the total lipid amount. All measurements were performed at rt, in buffering conditions relevant for biological studies (PBS, pH 7.4). Data shows the average of three independent measurements \pm SD.

The nature of the charged lipid and its concentration are critical for the internal structure of the particles.¹⁰⁰ SAXS was used to verify whether the hexagonal structure in samples containing relatively high concentrations of charged lipids was maintained (Figure 15). The addition of DDA had a considerable impact on the HII mesophase at 25°C (Figure 15). The

first and third peak at 1.217 ± 0.003 and 1.481 ± 0.006 nm^{-1} , respectively, corresponded to the $\sqrt{2}$ and $\sqrt{3}$ reflections and indicated Pn3m structures. This suggested a transition or coexistence of Pn3m and HII phases. Within the lipid domain, the positive charge of DDA increased the repulsion between the headgroups. It was assumed that this imbalance of lateral stresses reduced the negative curvature of the structure, which promoted a transition from a hexagonal to a cubic geometry.^{168, 169} Interestingly, a temperature increase from 25°C to 37°C promoted a recovery of the system, which displayed peaks at 1.381 ± 0.001 , 2.395 ± 0.006 , and 2.752 ± 0.009 nm^{-1} (corresponding to 1, $\sqrt{3}$, and $\sqrt{4}$ reflections in Figure 15) and represented a predominant HII profile. A plausible explanation may be that higher temperature led to greater conformational disorder and splay in the chain region and so compensated the lateral stresses between the headgroups.¹⁰³ The HII structure formed at 37°C showed Bragg reflections at lower q values than the original bulks (black curves) suggesting an enlargement of the cell unit.

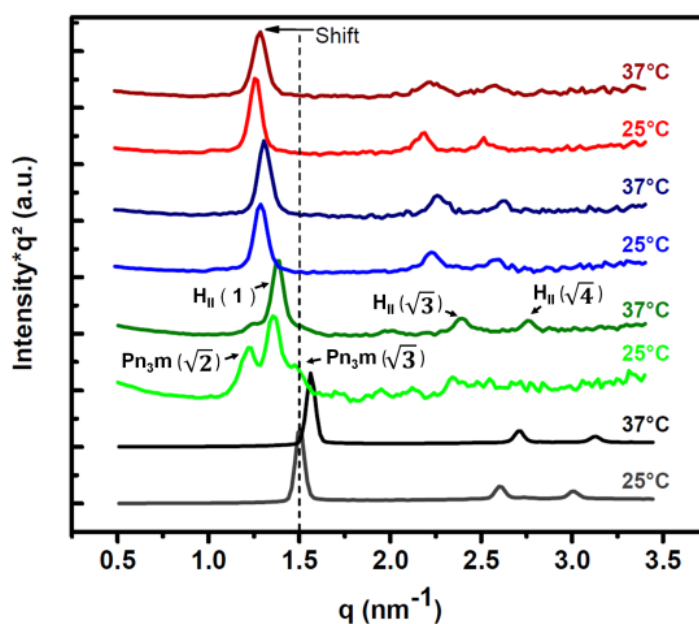


Figure 15: Effect of additional charged lipid on Phy/MaMo (14 wt%) hexosomes stabilized with 15 wt% Poloxamer 407. SAXS patterns are shown for the following samples at 25°C and 37°C: standard Phy/MaMo (14 wt%) bulk phase (black), 30 wt% DDA (green), 25 wt% Dotap (blue), and 15 wt% DSPG (red). The curves were shifted vertically for clarity. The vertical dashed line highlights a shift of the Bragg reflections to lower q values for samples containing charged lipids in comparison with the original Phy/MaMo (14 wt%) bulk.

Formulations containing Dotap (blue curves), and DSPG (red curves) maintained the HII structure at both temperatures and showed an increased lattice parameter from 4.84 ± 0.01 nm (bulk phase) to 5.62 ± 0.01 and 5.75 ± 0.01 nm for Dotap and DSPG, respectively (at 25°C , Table 2). A higher lattice parameter correlates with an enlargement of the water channel diameter.¹⁷⁰ This modulation of the internal structure may be used as potential tool for drug encapsulation. Similarly to the Phy/MaMo bulk phases (Figure 8B), hexosomes containing DSPG and Dotap revealed a reduction of the lattice parameter upon temperature increase (Table 2). However, this behavior was less pronounced, which is most likely due to repulsion between the charged headgroups (Figure 13) and sterical hindrance.¹⁰³

Table 2: Change in lattice parameter upon temperature increase of charged Phy/MaMo (14 wt%) hexosomes stabilized with 10 wt% Poloxamer 407.

Formulation	Lattice Parameter		
	at 25°C (nm)	at 37°C (nm)	Difference** (%)
Bulk*	4.84	4.64	4.08
Hexosomes + 25 wt% Dotap	5.62	5.55	1.28
Hexosomes + 15 wt% DSPG	5.75	5.66	1.61

*Bulks do not contain stabilizers and charged lipids. **Lattice parameter reduction from 25°C to 37°C .

The effect of DDA on the internal structure in comparison to Dotap at similar molar concentrations was surprising (Figure 16). Due to its smaller headgroup and saturated hydrocarbon chains (Figure 13), DDA was expected to show minimal impact on the hexagonal structure. However, it seemed to induce a transition from the hexagonal to the cubic phase, whereas Dotap, which consists of a trimethylammonium headgroup and two unsaturated hydrocarbon chains (Figure 13), only enlarged the lattice parameter. As mentioned earlier, it is believed that due to its molecular structure, DDA generated an imbalance between the hydrophobic chains and headgroup. Even though Dotap is a more voluminous molecule than DDA, the results indicated that the headgroup and hydrocarbon chain regions contributed more equally to the packing parameter^{100, 103} and the HII structure was preserved.

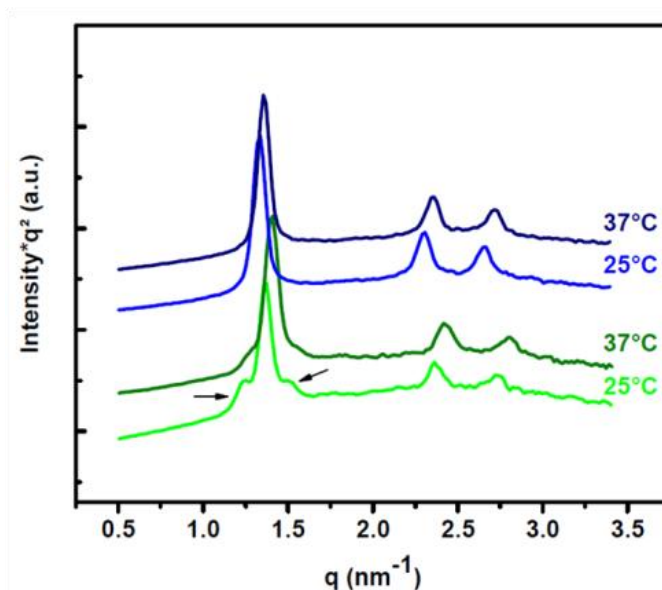


Figure 16: Effect of the headgroup dimension on the internal structure of Phy/MaMo (14 wt%) hexosomes stabilized with 10 wt% poloxamer 407. SAXS data are displayed for hexosomes containing the same molar concentration (ca. 14 mol%) of DDA (green) and Dotap (blue) at 25 and 37 °C. Arrows indicate perturbation of the pure HII peak profile. The curves were vertically shifted for clarity.

The effect of the addition of charged lipids on the structure of Phy/MaMo hexosomes was also observed with Cryo-TEM (Figure 17). The electron micrographs of the standard formulation (without addition of charged lipid), and formulations containing 25 wt% Dotap or 15 wt% DSPG revealed particles with clear parallel lines forming curved striations, and/or hexagonal shape, which are characteristic for hexosomes.⁹⁷ Differently, samples containing 30 wt% DDA displayed a more undefined structural profile. The particles appeared to have a spherical shape and showed internal structures with undulated distorted lines. These observations are in agreement with the SAXS measurements (Figure 17).

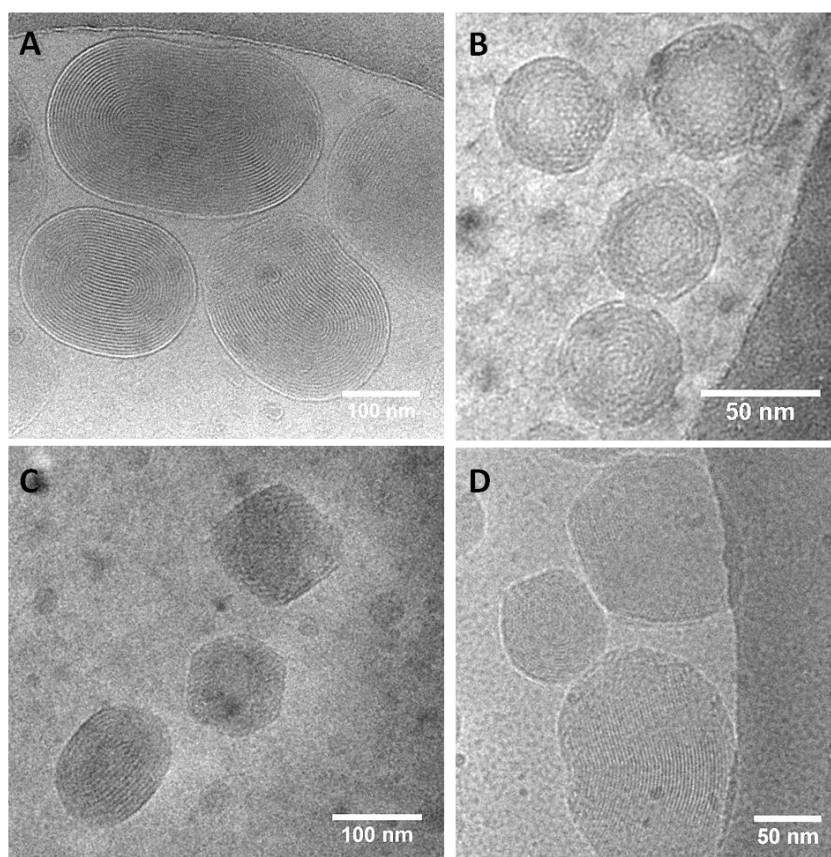


Figure 17: Cryo-TEM images of Phy/MaMo (14 wt%) formulations stabilized with 15 wt% Poloxamer 407. A: without additional charged lipid; B: addition of 30 wt% DDA; C: addition of 25 wt% Dotap; D: addition of 15 wt% DSPG.

4.5. Expanding the Customization Tool Box of Hexosomes

In order to amplify the variety of potential applications of Phy/MaMo dispersions, and prove the versatility of these formulations, octyl- β -D-glucopyranoside (OG) was evaluated as a tool to modify the internal structure of the particles in a controlled manner. This additive has been successfully used to enlarge the water channels of glyceryl monooleate cubosomes.¹⁷¹ A preliminary evaluation of the effect of OG addition in Phy/MaMo systems was performed in the bulk phases using polarization microscopy (Figure 18A). Bulks containing 5 wt% OG showed a considerable reduction of the birefringence, which became limited to very small areas. The anisotropic regions probably constituted conserved HII structure of the original bulk, suggesting the coexistence of two phases in the system. A further concentration increase of OG to 10 wt% promoted a fully conversion of the sample to

an isotropic bulk. The SAXS measurements of Phy/MaMo (14 wt%) dispersions containing OG (Figure 18B and C), confirmed the phase transition observed with polarization microscopy and revealed the formation of Pn3m (cubic double diamond) phases, indicated by the reflections in the relative positions equivalent to $\sqrt{2}$, $\sqrt{3}$, $\sqrt{4}$, $\sqrt{6}$, and $\sqrt{8}$.⁹³ OG might have promoted an increase of the positive curvature of the lipid arrangement, resulting in a shift from HII (lattice parameter 4.8 nm) to Pn3m (lattice parameters 6.8 and 7.2 nm for 5 and 10 wt% OG, respectively). Moreover, the SAXS analysis indicated that samples containing 10 wt% OG seemed to lose the Pn3m structure (black arrows) only at temperatures above 45°C. In contrast, samples with 5 wt% OG already displayed L2 structure at 45°C. In this way, OG demonstrated the capacity to modulate the structure of Phy/MaMo systems, inducing the phase transition from HII to Pn3m in a concentration dependent manner, which gives room for control and further optimization depending on the other formulation additives.

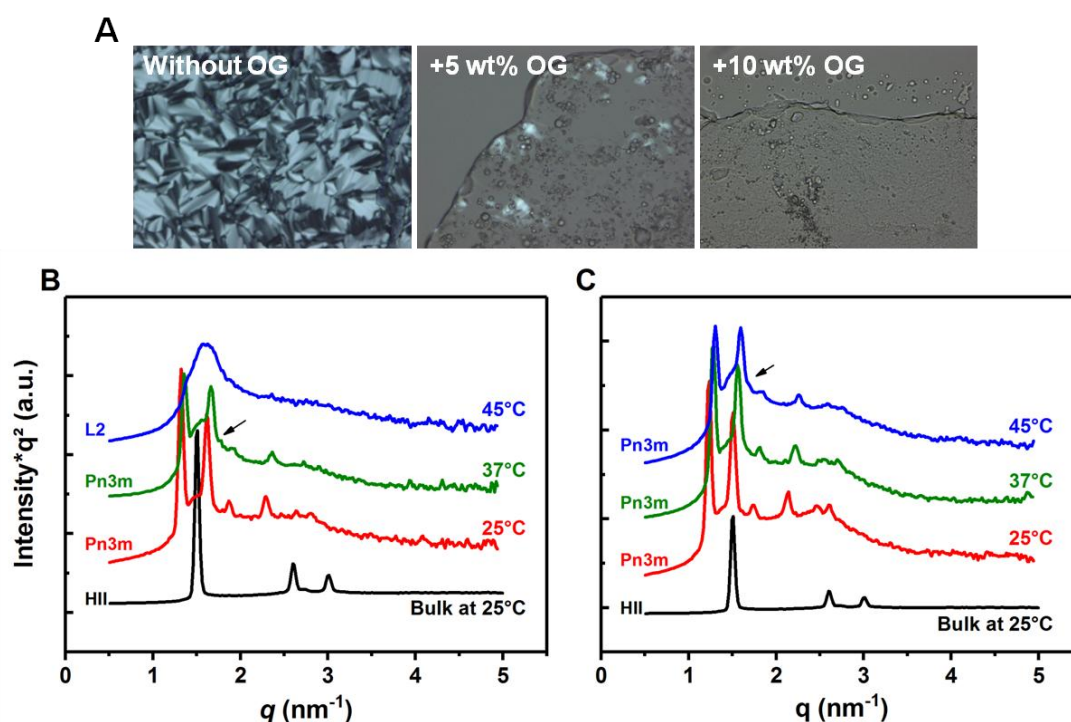


Figure 18: Effect of octyl- β -D-glucopyranoside (OG) on Phy/MaMo (14 wt%) formulations. **A:** Polarization microscopy of Phy/MaMo (14 wt%) fully hydrated bulks containing different concentrations of (OG) at 25°C; **B and C:** SAXS measurements at different temperatures of Phy/MaMo (14 wt%) particles stabilized with 5 wt% poloxamer 407 with addition of 5 wt% (B) and 10 wt% (C) OG. L2 (micellar); Pn3m (cubic double diamond); HII (inverse hexagonal). Black curve represents the bulk phase (without stabilizer, and OG) for comparison. Curves were shifted vertically for clarity.

4.6. Particle Loading

The entrapment of two different model antigens, namely lysozyme (LYS) and ovalbumin (OVA), into the delivery systems and its impact on the HII structure of Phy/MaMo (14 wt%) was investigated. In comparison to OVA, LYS is smaller in size and positively charged at pH 7.4 (Table 3). Due to these characteristics, a simple encapsulation and interactions with the negatively charged Phy/MaMo hexosomes were thought to be facilitated for LYS, which could result in higher loading efficiency in comparison with OVA. The macromolecules were added to the homogenized lipid molten in a buffered solution together with the stabilizer. According to the literature, lipid molecules self-assemble upon contact with aqueous medium containing a model antigen, which is then enclosed within the water channels.^{146, 172} Contrary to the expectations, the relative loading efficiency obtained for OVA was significantly higher compared to LYS (rLE% of 25 vs. 7, $p \leq 0.001$, Table 3).

Table 3: Characteristics of the model proteins used in the loading studies.^{173, 174}

Protein	Dimensions (nm)	pI*	Charge at pH 7.4	rLE% \pm SD**
Lysozyme (14.2 kDa)	2.8 \times 3.2 \times 3.0	11	Positive	7 \pm 3
Ovalbumin (42.7 kDa)	7.0 \times 3.6 \times 3.0	4.5	Negative	25 \pm 3

*pI (Isoelectric point); **rLE% \pm SD (Mean relative loading efficiency \pm standard deviation).

SAXS measurements of hexosomes loaded with either OVA or LYS revealed that the HII topology and lattice parameter were conserved for both proteins (Figure 19A). However, when comparing the dimensions of these proteins (Table 3) and the lattice parameter (distance between the centers of two adjacent cylinders)¹⁷⁵ of 4.8 nm, a simple encapsulation into the water channels without a noticeable impact on the structure is highly unlikely. An alternative loading mechanism suggested by Angelova et al.¹⁷⁶ proposes the association of protein molecules to the interfaces of the domains of cubic arrangement within the cubosomes, creating "pockets of local disorder".¹⁷⁷ This mechanism may explain the considerable rLE%, despite the geometric mismatch between the proteins and water channels, but it does not justify the absence of modifications in the Phy/MaMo HII structure.

To obtain insights into the localization of the loaded protein within the hexosomes, a tryptophan accessibility assay was performed, whereby the fluorescence of tryptophan residues is quenched with acrylamide. Proteins encapsulated within the hexosomes are in a

more isolated environment and thus less exposed to the acrylamide than proteins adsorbed to the particle surface.¹⁷⁸ In contrast to the buffer solution, less quenching of the fluorescence and thus lower quencher efficiencies (F_0/F) was observed for both proteins when loaded into hexosomal formulation (Figure 20). This suggested that OVA and LYS were to some extent integrated into the lipidic structure. However, in direct comparison to OVA, LYS showed a stronger reduction of the quenching efficiency when it was loaded into hexosomes. This indicated that the incorporation into hexosomes shielded LYS from the aqueous environment more efficiently than OVA and thereby, reduced its availability for acrylamide quenching.

The Phy/MaMo (14 wt%) system was further challenged by simultaneously including 30 wt% DDA and either OVA or LYS as a model antigen (Figure 19B). As discussed earlier, the inclusion of DDA led to a combination of cubic and hexagonal phases. Upon protein loading, the intensity of the Pn3m reflections, at approximately 1.22 and 1.48 nm⁻¹, were reduced (indicated by stars in Figure 19B). Additionally, the reflections observed at $q > 2.0$ nm⁻¹ appeared more visible for loaded particles. Overall, the protein addition seemed to drive the systems back to pure HII assemblies. This effect was more profound for samples containing LYS. This ability of both proteins to modify the internal structure suggested a strong association of the protein molecules with the lipid network.

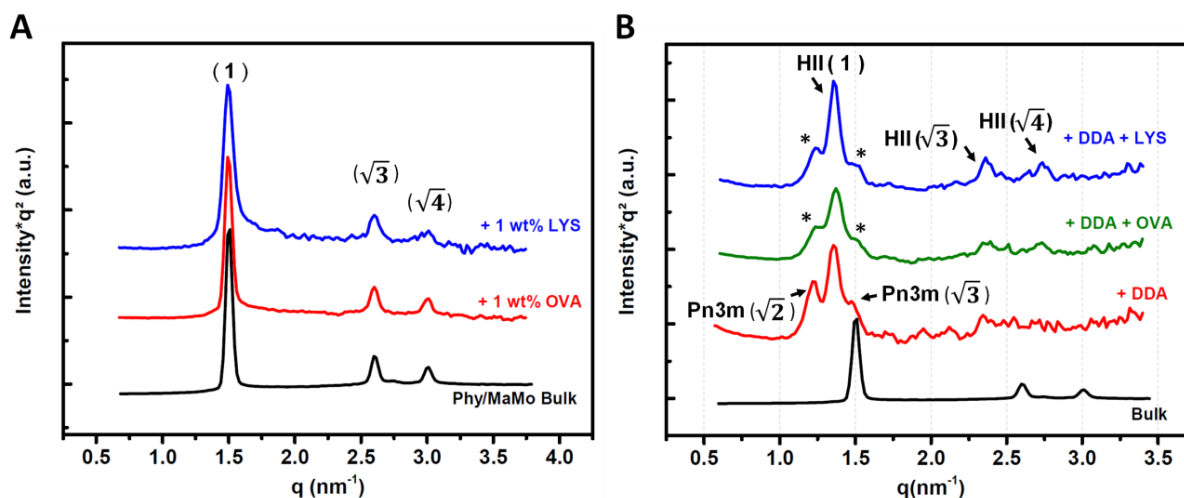


Figure 19: A: SAXS curves of hexosomes formed by Phy/MaMo (14 wt%), stabilized with 5 wt% poloxamer 407 and loaded with either 1 wt% (of total lipid) of LYS (blue) or OVA (red). B: SAXS characterization of hexosomes formed by Phy/MaMo (14 wt%) and 30 wt% DDA, stabilized with 15 wt% poloxamer 407. Plain hexosomes (red), loaded with 1 wt% OVA (green), loaded with 1 wt% LYS (blue). Black curve represents the bulk phase (without stabilizer, DDA, and protein) for comparison. Curves were shifted vertically for clarity. Measurements were performed at 25°C.

A comparable recovery of the HII structure was seen for plain hexosomes containing 30 wt% DDA (Figure 15) upon temperature increase. With rising temperature, the fluidity of the hydrocarbon chains increased, and compensated the lateral stresses introduced by the positive headgroups of DDA. Similarly to the temperature effect, the incorporation of protein molecules may have caused a volume expansion in the hydrophobic chain region, which contributed to the reestablishment of the hexagonal structure. These findings suggested that the proteins mostly interacted with the hydrophobic chains via nonpolar interactions. That this effect was more pronounced for LYS is in agreement with findings from the tryptophan accessibility assay. Considering that both, the lipid assembly and LYS, were positively charged at pH 7.4 (Table 3), it may be hypothesized that the loading mechanism is mainly driven by the hydrophobic forces rather than electrostatic interactions.

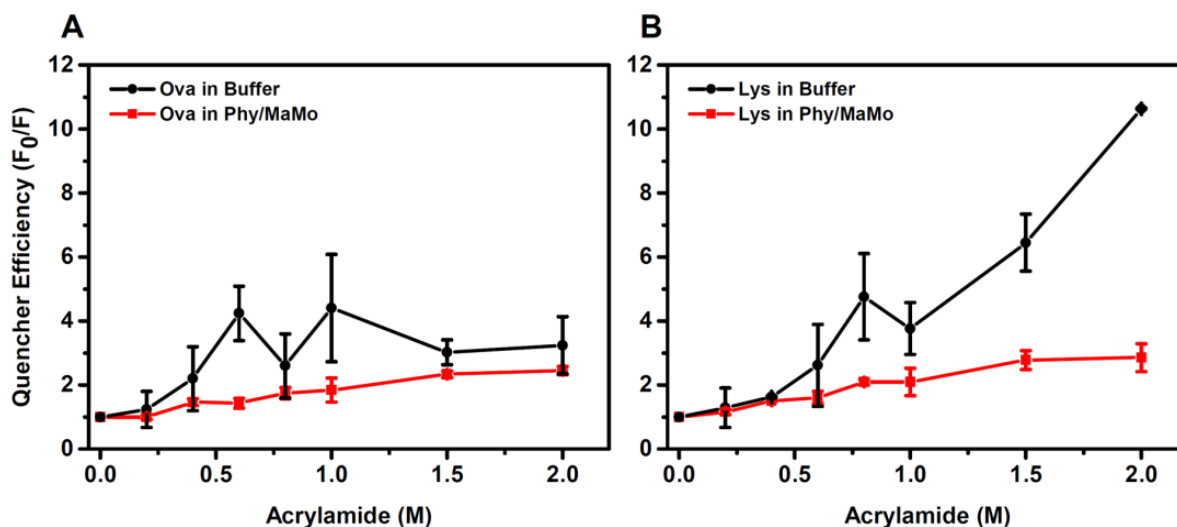


Figure 20: Tryptophan accessibility assay with acrylamide in Phy/MaMo (14 wt%) hexosomes stabilized with 25 wt% poloxamer 407, and loaded with 0.1 wt% (of total lipid) ovalbumin (A) or lysozyme (B). Unquenched protein (F_0); Quenched protein (F). Data is shown as mean \pm SD of two independent experiments performed in triplicate.

5 CONCLUSION AND OUTLOOK

This study demonstrated the rational development of novel vaccine delivery systems based on internally structured particles. Phy/MaMo (14 wt%) hexosomes were successfully dispersed from their bulk phases using either poloxamer 407, Myrj 59, or Pluronic F108. The particle size profiles of the various formulations were a result of the combination of dispersion method, as well as the type and concentration of the stabilizer. Different approaches, such as inclusion of various additives and dispersion post-treatments, were combined in order to obtain systems with desired characteristics. Phy/MaMo (14 wt%) revealed broad margins to tune relevant properties without sacrificing the HII internal arrangement. For example, the incorporation of charged lipids to modify the overall particle charge, as well as the loading of different model proteins could be performed without compromising the HII profile of the particles. This remarkable structural robustness is unusual in lyotropic liquid crystalline dispersions, which are known for their susceptibility to phase transformations without satisfactory predictability.¹⁰³ Nonetheless, the addition of

OG was identified as a suitable tool to transform Phy/MaMo (14 wt%) hexosomes in cubosomes with Pn3m structure in a concentration-dependent and controlled manner. Future efforts are needed to fully understand the role of internally structured particles in living systems. In this context, relevant investigations will be performed to further optimize hexosomes and improve their current status as antigen delivery system.

CHAPTER III

Cellular Internalization of Hexosomes

A version of this chapter is ready for submission:

Rodrigues L., Schneider F., Zhang X., Papadakis C. M., Dietz H., Larsson E., Winter G., Lundmark R., Hubert M. „Hexosomes have unusual cellular internalization mechanism.”

This work was conducted in collaboration with the Soft Matter Physics Group and Institute for Advanced Study of the Technische Universität München, and the department of Medical Biochemistry and Biophysics of the Umeå University. The manuscript was written by Rodrigues L. The SAXS measurements were performed by Rodrigues L and Zhang X under the supervision of Papadakis C M. Cryo-TEM image acquisition was conducted by Schneider F and supervised by Dietz H. Western Blot experiments were performed by Larsson E and Rodrigues L. All data analyses and additional experimental work were performed by Rodrigues L and supervised by Winter G, Lundmark R and Hubert M.

1 ABSTRACT

The growing importance of biotherapeutics increased the interest in the development of innovative delivery systems, able to carry and protect high amounts of the cargo molecules and deliver them to their targets intracellularly. In this context, lipid-based particles internally structured with non-lamellar phases, such as cubosomes and hexosomes gained attention. The research in this field is still in its infancy and little is known about the performance of these nanoparticles in biological environments. An important subject of speculation is whether non-lamellar structured particles have fusogenic properties. This hypothesis arises from the involvement of non-lamellar conformations of lipids in natural processes of the cell membrane such as fusion. This work aims to address this, investigating the cellular internalization mechanism of hexosomes in comparison to liposomes. For this purpose, series of particle uptake experiments in HeLa cells were performed after silencing of important regulatory proteins of the major endocytosis pathways, and modifying the rigidity and tension of the cell membrane. Additionally, the interactions of the nanoparticles with model lipid membranes were studied from a physico-chemical perspective. The results showed that liposomes were internalized by multiple endocytic pathways. Surprisingly, hexosomes showed an uncommon uptake mechanism independent of standard endocytosis and distinct from fusion, or poration of the cell membrane. Hexosomes revealed superior interaction capacity with model lipid membranes and showed the ability to induce distortions that most likely enable their rapid cellular internalization. In addition, our results suggested that the occurrence of these distortions requires some extent of membrane flexibility. Thus, this work reveals hexosomes as potential intracellular delivery systems.

2 INTRODUCTION

Carrier systems for drug delivery have been extensively investigated to enhance the properties of therapeutics and enable their application in the biomedical context.^{179, 180} Naturally occurring nanostructures have been a source of inspiration to develop new particulate delivery systems made of biomolecules. For instance, due to their diverse chemical structure, amphiphilic lipids offer a range of desirable properties to provide a

powerful toolbox for the design of nanocarriers.¹⁸¹ In the presence of aqueous media, these molecules self-assemble into distinct mesophases as a function of their shape features and correspondent critical packing parameter (section 1.3.1).^{79, 100} Besides the typical lamellar phase found in biomembranes, lipids can adopt negatively curved non-lamellar structures such as inverse cubic or hexagonal phases.¹⁸¹⁻¹⁸³ It is proposed that these structures are involved in transitory processes of the cell membrane, such as fusion, fission, and pore formation.¹⁸⁴

Liposomes, the best-known lipid-based drug delivery systems, are vesicles based on one or more lipid bilayers. They are extensively used experimentally to deliver various pharmaceuticals and are commercially available in several licensed preparations, *e.g.* liposomal amphotericin B (AmBisome®), liposomal cytosine arabinoside (DepoCyt®), and liposomal doxorubicin (Myocet®).¹⁷⁹ However, due to key limitations such as low encapsulation efficiency of hydrophobic and voluminous drugs, short shelf life, and high manufacturing costs,^{100, 185, 186} particles with a non-lamellar internal structure have recently gained increasing attention. As an example, hexosomes are internally structured with an inverse hexagonal (HII) phase and are assemblies of rod-shaped inverse micelles, which create cylinders filled with water organized in a hexagonal geometry.⁸⁸ Due to their intricate internal structure of lipids and water channels, these particles have a large lipid-water interface¹⁰⁰ and several studies demonstrated adequate entrapment capacities for diverse molecules (*e.g.* amino acids, peptides, proteins, nucleic acids, small molecules).^{172, 187-191} In addition, liquid formulations of non-lamellar internally structured particles provided good storage stability over 160 days at rt (stability after longer storage periods was not evaluated).¹⁹²

Cellular internalization of liposomes occurs through different endocytic machineries (*e.g.* via clathrin-coated pits).¹⁸¹ Over the last two decades, several strategies have been developed to target certain uptake process and to enhance delivery to the target organelle.⁸² It is widely accepted that the therapeutic effect of proteins, peptides or nucleic acids depends on either a direct delivery to the cytoplasm, or the ability to escape from the early endosomes to avoid enzymatic degradation in the lysosomes.^{179, 193} Facilitating an endosomal escape has long been the focus of gene delivery research. For instance, pH-sensitive PEGylated cationic liposomes are used for siRNA (small interfering ribonucleic acid) delivery.¹⁹⁴ Here, the

PEGylation enhances stability of the positive vesicles in serum and upon slight pH decrease in endosomes, the PEG chains are cleaved, allowing the cationic vesicles to fuse with the endosomal membrane and to release the cargo into the cytoplasm.¹⁹⁴ Another strategy is the incorporation of fusogenic agents, such as cell penetrating peptides (CPPs) into the delivery systems.^{194, 195} Similarly, the use of virusporins, a virus peptide with lytic activity, to induce pore formation in the cell/endosomal membrane has also been reported.^{196, 197} However, all these strategies are frequently associated with toxicity issues, short circulation times, instability of the formulation, and low specificity.^{179, 181, 198} In this context, particles with a non-lamellar internal structure emerged as promising alternatives to liposomes as cytoplasmatic delivery systems. Different studies highlight the superior silencing efficiencies of siRNA when delivered using non-lamellar structured nanoparticles [bicontinuous cubic gyroid (QII_C) and HII] in comparison to liposomes.^{198, 199} The authors explained this outcome with an enhanced endosomal escape provoked by fusion of the nanocarriers with the endosomal membrane.^{198, 199} A similar phenomenon is seen in natural processes of cell membrane fusion,¹⁸⁴ when increasing negative curvature of two apposed bilayers results in the formation of a non-lamellar intermediate conformation (stalk structure) connecting the bilayers.^{181, 200}

Nanoparticles based on non-lamellar structures, such as hexosomes are believed to be able to fuse with cell membranes and are generating considerable interest in terms of their potential for direct cytoplasmic delivery of therapeutics.^{78, 181} Despite this interest, what we know about the interaction of non-lamellar structured nanoparticles with cell membranes is largely based on very limited data. Moreover, the way they enter cells remains highly speculative. The aim of the present work was therefore to comprehensively study the internalization of hexosomes in cells. Previous work of our group described the physico-chemical characterization of a robust hexosomal formulation based on phytantriol (Phy) and mannide monooleate (MaMo).⁸⁸ Due to its remarkable structural stability, this formulation was selected for the present internalization studies. We monitored the uptake of fluorescently labeled hexosomes in HeLa cells by spectrophotometry and quantitative fluorescence imaging in comparison to liposomes. To understand how their uptake is mediated, we silenced regulatory proteins of major endocytic pathways alone and in various combinations. Additionally, the membrane activity was assayed from a physico-chemical perspective using lipid monolayers, giant unilamellar vesicles (GUVs) and cryo-TEM.

The results revealed that the uptake of liposomes was mediated by multiple pathways as suggested earlier. We found that the internalization of hexosomes was independent of any endocytic activity and could only be inhibited by increasing the tension and rigidity of the membrane. This and the data obtained from the interaction studies with model membranes argue against a simple membrane fusion, but suggest that hexosomes have uncommon membrane-destabilizing properties. An implication of this is the possibility that hexosomes induce a distortion of the lipid bilayer that enables their rapid passage through the membrane without the generation of permanent pores.

3 MATERIALS AND METHODS

3.1. Materials

Phytantriol (Phy) from DSM Nutritional Products Europe Ltd was a gift from Nordmann, Rassmann GmbH (Hamburg, DE). Mannide monooleate (MaMo), poloxamer 407 (P407), thiazolyl blue tetrazolium bromide (MTT reagent), cytochalasin D, paraformaldehyde (PFA), goat serum, and saponin from quilaja bark were purchased from Sigma-Aldrich (St. Louis, MO, US). 1,2-Dioleoyl-sn-glycero-3-phosphocholine (DOPC) and 1,2-dioleoyl-sn-glycero-3-phosphoethanolamine (DOPE) were purchased from Avanti Polar Lipids Inc. (Alabaster, AL, US). 1-Palmitoyl-2-oleoyl-sn-glycero-3-phosphocholine (POPC) was purchased from Lipoid GmbH (Ludwigshafen, DE). Octadecyl rhodamine b chloride (R18), Marina Blue 1,2-dihexadecanoyl-sn-glycero-3-phosphoethanolamine (Marina Blue DHPE), high purity calcein and 4',6-diamidino-2-phenylindole dihydrochloride (DAPI) were purchased from Life Technologies (Eugene, OR, US). All other chemicals and reagents were of analytical grade and were purchased from commercial suppliers.

3.2. Antibodies

Purchased primary antibodies were: mouse anti-clathrin heavy chain (1:1000), clone 23 (BD Transduction Laboratories), rabbit anti -caveolin1 (1:5000), clone ab2910 (Abcam), rabbit anti-Cdc42 (1:5000), clone ab109553 (Abcam). Secondary antibodies conjugated to horseradish peroxidase (HRP, Sigma Aldrich and Agrisera) were used for western blot

detection. Immunoprecipitation of GRAF1 was performed using the same siRNA and method as described by Doherty GJ et al.²⁰¹

3.3. Preparation of Liposomes

DOPC/DOPE (1:1 molar ratio) liposomes labeled with 0.05 mol% R18 were prepared according to the film method²⁰². The appropriate amounts of each lipid (DOPC, DOPE, and R18 as stock solutions in chloroform) were added to a mixture of methanol:chloroform (3:7, v/v) and gently vortexed. The lipids were then dried under a stream of nitrogen to give a thin film. To generate vesicles, the lipid film was rehydrated in an appropriate volume of phosphate-buffered saline (PBS, pH 7.4) and incubated for 30 min at room temperature (rt). Glass beads were added to facilitate rehydration. Subsequently, the liposome dispersion was bath sonicated for 15 min (Transsonic T 310, Elma, Singen, DE).

3.4. Preparation of Hexosomes

Phy/MaMo (8:1 molar ratio) hexosomes labeled with 0.05 mol% R18 were prepared as previously reported⁸⁸. Briefly, appropriate amounts of Phy and MaMo were weighed and melted at 70°C using the Thermomixer comfort (Eppendorf, Hamburg, Germany). The sample was agitated for 15 min in a dual asymmetric centrifuge (SpeedMixer™ DAC 150.1 CM41) at 3500 rpm to homogenize the lipid melt. Subsequently, R18 dissolved in DMSO was added to the lipid melt followed by dual asymmetric centrifugation (15 min at 3500 rpm). Then, 1 ml of poloxamer 407 solution in PBS was added to the sample (0.41 mol% of the total lipid content) and the sample was again thoroughly mixed using the dual asymmetric centrifugation (30 min at 3500 rpm). The sample was then probe-type ultrasonicated in three cycles of 1 min with 4 s pulse and 2 s pause at an amplitude of 20% (Bandelin Sonopuls HD3200 with sonotrode MS72).

3.5. Small-Angle X-ray Scattering (SAXS)

In order to improve the scattering signal, highly concentrated samples (100 mg/ml) of R18-labeled DOPC/DOPE liposomes and Phy/MaMo hexosomes were prepared. SAXS measurements were performed using a Ganesha 300XL instrument (SAXSLAB ApS,

Copenhagen, DK) equipped with a GENIX 3D microfocuss Cu X-ray source (XENOX, Sassenage, FR) and a 2D Pilatus 300K detector (Dectris, Baden-Daettwil, CH). The sample chamber and beam path were under vacuum. The samples were loaded into glass capillaries (1 mm light path, SAXSLAB), which were hermetically sealed and mounted in a temperature-controlled cell. The samples were measured after 10 min of equilibration at 25°C, 37°C and 42°C. The wavelength was $\lambda = 1.54 \text{ \AA}$, the sample-to-detector distance was 406.2 mm, and the acquisition time was 60 min. A pin diode was used to measure the transmission of the sample. The 2D images were azimuthally averaged, and the background from the glass capillaries was subtracted, taking the transmission into account.

To identify the different liquid crystalline phases, the q -position [$q = 4\pi \sin(\theta/2)/\lambda$ is the momentum transfer] of each Bragg reflection was determined by fitting a Lorentz function (θ is the scattering angle). The ratios of the relative peak positions were calculated and compared to patterns described in the literature^{93, 152}.

3.6. Dynamic Light Scattering (DLS)

The hydrodynamic diameter (z -average), polydispersity index (PDI) and zeta potential of the particles were measured with a Malvern Zetasizer Nano ZS (Malvern Instruments, Worcestershire, UK). The dispersions were diluted (1:100) and added into PMMA cuvettes (BRAND®) or DTS1060C capillary cells (Malvern Instruments) for the analysis of z -average and zeta potential, respectively. The measurements were not affected by the sample concentration within the range used in this study. The measurements were performed in triplicate at 25°C under buffering conditions relevant for biological experiments (PBS, pH 7.4). The values of PBS were used for viscosity and refractive indexes. The Zetasizer Software version 7.03 (Macromedia Inc.) was used for acquisition and analysis of the data.

3.7. Cell Cultures, Cell Lines and Transfections

HeLa cells (ATCC-CRM-CCL-2) were grown in Dulbecco's Modified Eagle's medium (DMEM, high glucose, L-glutamine, sodium pyruvate, and phenol red) supplemented with 10% (v/v) fetal bovine serum (FBS, both from Life Technologies) at 37°C in 5% CO₂. The Flp-In TRex HeLa cell line expressing caveolin-1-GFP was generated as previously described²⁰³ and maintained in DMEM supplemented with 10% (v/v) FBS, 100 µg/ml hygromycin B,

and 5 µg/ml blasticidin S HCl (InvivoGen, San Diego, CA, USA) for plasmid selection. Low expression of the fluorescently tagged caveolin-1 was induced by incubation with 0.5 ng/ml doxycycline hyclate (Sigma-Aldrich) for 18-24h.

To study the uptake mechanism(s), targeted proteins were silenced with stealth RNAi (siRNA) against either caveolin1 (Cav1HSS141467), dynamin II (DNM2HSS102856), GRAF-1 (ARHGAP26HSS118162), CLTC (CLTCHSS102017, all from Life Technologies), Cdc42 (ON-TARGETplus siRNA human, J-005057-05, Dharmacon, Lafayette, CO, US) or a combination of these. Stealth RNAi siRNA negative control 462001 (Life Technologies) was used as control. Transfections for single and double knockdowns were performed with Lipofectamine 2000 and Opti-MEM (both from Life Technologies) according to the manufacturer's instructions. HeLa cells were transfected twice over a period of 72 h before the uptake experiment. Protein levels were analyzed by SDS-PAGE and immunoblotting.

3.8. MTT cell proliferation assay

HeLa cells were seeded in transparent 96-well plates (Sarstedt, Nümbrecht, DE) at 15×10^3 cells/well and incubated overnight (37°C, 5% CO₂). A range of concentrations from 10 to 150 nmol/ml (total lipid) of either liposomes or hexosomes (both labeled with R18) were added to the cells and incubated for 24 h at 37°C in 5% CO₂. The medium was subsequently replaced with MTT reagent solution in cell culture medium (0.5 mg/ml). Following 3 h of incubation, the supernatant was discarded and DMSO/ethanol (1:1, v/v) was added to dissolve the purple formazan precipitate. The absorption was then measured at 570 nm and corrected with a background measured at the range 630-690 nm.

3.9. High-Throughput Quantification of Particle Uptake

HeLa cells were seeded in black 96-well plates with flat clear bottom (Corning, NY, USA) at 15×10^3 cells/well and incubated at 37°C in 5% CO₂. On the following day the cells were incubated with either liposomes or hexosomes (both labeled with R18) at 30 nmol/ml (total lipid) for different periods of time over 6 h. This experiment was performed at 37°C and 4°C, to distinguish particle internalization from particle attachment on the cell surface (membrane trafficking is blocked at 4°C) ²⁰⁴. After incubation, the cells were washed twice with cold PBS containing 10% FBS, fixed with 4% PFA in PBS, and the nuclei stained with

DAPI. Fluorescence intensities were measured with a Synergy H4 plate reader (BioTek Instruments Inc., VT, USA). The quantification was based on the fluorescence intensity of R18 ($\lambda_{\text{ex}}/\lambda_{\text{em}} = 548/578$ nm) normalized by the fluorescence of DAPI ($\lambda_{\text{ex}}/\lambda_{\text{em}} = 358/461$ nm), which is proportional to the cell density in each well and allows for a signal correction based on the cell number. This experimental setup was also used to investigate the effect of the single knockdown of either caveolin1, clathrin, dynamin, Cdc42, or GRAF-1 on the cellular internalization of liposomes and hexosomes.

3.10. Immunofluorescence microscopy

For immunofluorescence analysis, HeLa cells were seeded on glass coverslips (diameter 12 mm, No. 1.5H, high precision, Paul Marienfeld GmbH & Co. KG, Lauda-Königshofen, DE) in 24-well plates at 50×10^3 cells/well and incubated overnight (37°C, 5% CO₂). Following incubation with either R18-labeled liposomes, or hexosomes at 30 nmol/ml (total lipid) for 1 h and 6 h, the cells were washed twice with cold PBS containing 10% FBS. Cells were fixed with 4% PFA in PBS and then immunostained with primary mouse monoclonal antibody anti-CD44 (Abcam plc, Cambridge, UK) and goat anti-mouse IgG secondary antibody coupled to Alexa Fluor 647 (ThermoFisher Scientific Inc., Waltham, MA, US) as previously described¹³³. Fixed samples were imaged using the Nikon A1R confocal (laser scanning confocal microscope) controlled by Nikon NIS Elements interface with a Nikon Eclipse Ti-E inverted microscope, equipped with a Nikon CFI Plan Apochromat 60x oil (N.A 1.40) DIC objective. Micrographs were prepared using Fiji²⁰⁵ and Adobe Photoshop (CS6).

3.11. Particle Uptake Assay Using Live Cell Microscopy

The day before the uptake experiment, HeLa cells, induced caveolin-1-GFP Flp-In TRex HeLa cells or HeLa cells treated with different siRNA were seeded on glass coverslips (diameter 25 mm, high precision, Paul Marienfeld GmbH & Co. KG, Lauda-Königshofen, DE) in 6-well plates at 3×10^5 cells/well. Live cell experiments were conducted in phenol red-free DMEM supplemented with 15 mM HEPES and 1 mM sodium pyruvate using an Attofluor cell chamber (ThermoFisher Scientific Inc.) at 37 °C in 5% CO₂. R18-labeled liposomes and hexosomes were added to cells at 30 nmol/ml (total lipid). For quantification purposes, z-stacks of at least ten different cells were taken. Images were acquired using the

Zeiss Cell Observer Spinning Disk Confocal controlled by ZEN interface with an Axio Observer.Z1 inverted microscope with a 63× lens, equipped with a CSU-X1A 5000 Spinning Disk Unit and an EMCCD camera iXon Ultra from ANDOR. Micrographs were prepared using Fiji ²⁰⁵ and Adobe Photoshop (CS6). To block actin polymerization, induced caveolin-1-GFP Flp-In TRex HeLa cell were pre-treated with 1 μM cytochalasin D for 30 min prior to incubation with the nanoparticles. After the pre-treatment, the medium was exchanged and the uptake of liposomes and hexosomes [30 nmol/ml (total lipid)] was monitored by live-cell microscopy as described above. To study the role of membrane tension on the particle uptake, the cell membrane rigidity of Flp-Ins expressing caveolin-1-GFP was increased by a hypotonic treatment. The osmolarity of the culture medium was changed by gentle replacement with imaging media:sterile water (1:3, v/v). After an incubation of ca. 10 min, liposomes and hexosomes were added at 30 nmol/ml (total lipid) and the uptake monitored by live cell microscopy as described above.

3.12. Image Analysis and Quantification

After image acquisition, quantification of the particle uptake was performed using the software FIJI (ImageJ 1.51i). Briefly, the maximum intensity projection of each Z-stack was created followed by feature extraction with the Feature J Laplacian tool. Next, a threshold range was adjusted and the fluorescence intensity of the internalized particles was analyzed.

3.13. Lipid Monolayer Experiments

Lipid monolayers were formed at 37°C by spreading a total amount of 39 nmol POPC in chloroform on a PBS subphase in a MicroTrough XL (Kibron Inc., Helsinki, FI). After the solvent had been allowed to evaporate for 10 min, the monolayer was compressed at 5 mm/min to achieve a target surface pressure of 30 mN/m. A volume of 100 μl of either liposomes, hexosomes [both at 15 μmol/ml (total lipid)] or the neat components [Phy, MaMo and P407 (all at the same concentration contained in the hexosomes)] was injected below the monolayer into the subphase. Due to the capacity of Quil-A® to intercalate into cell membranes, ²⁰⁶ this adjuvant was used to enable comparability with a known pharmaceutical relevant example. For this purpose, 0.1 mg/ml QuilA (Invivogen, San Diego, CA, USA) was incorporated to liposomes and hexosomes. These modified

formulations and QuilA in PBS (0.1 mg/ml) were injected into the subphase as described above. The surface pressure (π) was recorded as a function of time using a microbalance equipped with a Dyneprobe (Kibron Inc.) made of a metal alloyed with a hydrophilic oxide. The Filmware Software version 4.0 (Kibron Inc.) was used for data acquisition and Origin 8.1 (Origin Lab Corp.) for analysis of the adsorption curves.

3.14. Calcein Leakage Assay

Using the same procedure as described above, a dry lipid film was prepared from 7.8 μmol POPC in methanol:chloroform (3:7, v/v) and hydrated with an aqueous calcein solution in PBS (500 μl , 46 mM) to form calcein-containing liposomes. The vesicles were probe-type ultrasonicated in three cycles of 1 min with 4 s pulse and 2 s pause at an amplitude of 20% (Bandelin Sonopuls HD3200 with sonotrode MS72). The nontrapped dye molecules were removed by gel filtration using Sephadex G-50 (Sigma-Aldrich) with PBS buffer. The fractions containing POPC vesicles were identified by DLS and pooled. For the leakage assay, calcein loaded vesicles were incubated with either liposomes, hexosomes [both at 15 $\mu\text{mol}/\text{ml}$ (total lipid)] or the neat components [Phy, MaMo and P407 (all at the same concentration contained in the hexosomes)] with a ratio of 5:1 (calcein vesicles:formulations) for 1 h at rt. After incubation, a three-fold dilution with PBS was performed to reduce turbidity and the fluorescence intensities were measured at $\lambda_{\text{ex}}/\lambda_{\text{em}}$ 490/570 nm. Calcein vesicles incubated with PBS were used as a negative control and represented the absence of leakage. Its fluorescence intensity was used to normalize the data collected for the other samples.

3.15. Giant Unilamellar Vesicles (GUV) Preparation and Imaging

GUVs were prepared by electroformation using a Vesicle Prep Pro chamber (Nanion Technologies, Munich, DE) following the manufacturer's protocol. A lipid mixture containing POPC (0.2 μmol) and 0.1 mol% Marina Blue DHPE in chloroform was applied to an indium tin oxide (ITO) coated slide and the solvent was evaporated at rt. Subsequently, an o-ring lubricated with silicone grease was placed around the dried lipid film and aqueous sucrose solution (150 mM, volume of 250 μl) was applied on the lipid film. A second ITO coated slide was placed on top of the o-ring and the slides were mounted in the Vesicle Prep

Pro chamber. Next, an alternating current electric field (3 V, 5 Hz) was applied for 5 h at 36°C. To study the interactions of GUVs with the different lipid-based carriers, R18-labeled hexosomes and liposomes were diluted in 150 mM aqueous glucose solution to a final concentration of 60 nmol/ml of total lipid. These samples were then mixed with an equal volume of GUVs dispersion. After 4 h of incubation at rt, images were acquired using Zeiss Cell Observer Spinning Disk Confocal controlled by ZEN interface with an Axio Observer.Z1 inverted microscope with a 63X lens, equipped with a CSU-X1A 5000 Spinning Disk Unit and an EMCCD camera iXon Ultra from ANDOR. The Marina Blue DHPE and R18-labeled nanoparticles were excited with 405 and 561 nm lasers, respectively.

3.16. Cryogenic Transmission Electron Microscopy (Cryo-TEM)

Vitrified specimens of selected dispersions at approximately 5 % (w/w) of total lipid were prepared using a Vitrobot (FEI, Eindhoven, NL) at 22.0°C and 90% humidity. A volume of 3.5 µl of the particle dispersion was applied on 400-mesh C-Flat CF-2/1-4C copper grids (Protochips, Morrisville, NC, USA) negatively glow discharged with a Plasma Cleaner (EMS, Hatfield, PA, USA) at 45 mA for 45 s. After 45 s equilibration, the excess of liquid was removed by blotting (4 s, “blot force” -1), and the grids were automatically vitrified in liquid ethane below -172°C. The samples were imaged using a Tecnai Spirit microscope (FEI) equipped with a Tietz TemCam-F416 charge-couple device (CCD) camera and a Cryo-Transfer Holder (Gatan, Inc., Pleasanton, CA, USA). The system was operated at an acceleration voltage of 120 kV under low-dose conditions (SerialEM Tecnai v3.5.6 acquisition software) with 26.000-, 30.000-, 42.000- and 52.000-fold magnification.

3.17. Statistical Analysis

All experiments were repeated at least twice with duplicates or triplicates. Statistics were performed by one-way ANOVA using Tukey’s post hoc test for multicomparison between the groups or by Student *t*-test for comparison with the control group. All calculations were carried out using OriginPro 2017 (Northampton, MA, USA).

4 RESULTS AND DISCUSSION

To investigate the cell entry mechanism of hexosomes and to study the role of non-lamellar phases in the interaction with cells, a series of functional studies in HeLa cells was performed. These studies were carried out in parallel with liposomes to allow comparison. To get insight into their cellular uptake, we specifically inhibited major pathways using siRNA silencing. We further interfered with the actin cytoskeleton and membrane rigidity to assess their role in endocytosis. To clarify observations in cells, we employed simplified models of the cell membrane for biophysical studies.

4.1. Development and physico-chemical characterization of fluorescently labeled nanoparticles

To enable comparison between a non-lamellar and a lamellar particulate system, the experiments of this work were performed with Phy/MaMo hexosomes⁸⁸ and a common DOPC/DOPE (1:1 molar ratio) liposomal formulation. For uptake quantification using confocal microscopy, the particles were fluorescently tagged with octadecyl rhodamine B chloride (R18, 0.05 mol%). Due to its lipophilic character, and headgroup-tail structure, this fluorescent molecule is largely employed in labeling of lipid-based nanoparticles.^{207, 208} We performed SAXS measurements to ascertain that the inverse hexagonal (HII) structure of hexosomes and the lamellar (L α) structure of liposomes were not affected by the inclusion of R18.

Labeled Phy/MaMo particles featured a pattern of a typical hexagonal phase, which is characterized by Bragg reflections at the relative positions 1, $\sqrt{3}$, and $\sqrt{4}$, at all temperatures measured (Figure 21A).¹⁵² As seen in earlier studies,⁸⁸ the reflections shifted slightly to higher q -values upon a temperature increase from 25°C to 42°C, indicating a negligible contraction of the repeating cell unit in the HII phase. At 42°C, a broadening of the first peak ($q = 1.583 \pm 0.002 \text{ nm}^{-1}$) was observed. This together with the reduction of the intensities of the second ($q = 2.736 \pm 0.002 \text{ nm}^{-1}$) and the third ($q = 3.181 \pm 0.003 \text{ nm}^{-1}$) peaks suggested the beginning of a phase transition. The q -values of the SAXS reflection peaks measured for DOPC/DOPE liposomes ($1.036 \pm 0.001 \text{ nm}^{-1}$, $2.067 \pm 0.001 \text{ nm}^{-1}$ and $3.111 \pm 0.007 \text{ nm}^{-1}$) align

with the expected relative peak positions for the $L\alpha$ phase 1, 2, and 3 (Figure 21B).¹⁵² The internal structure was neither affected by the presence of R18 nor a change in temperature.

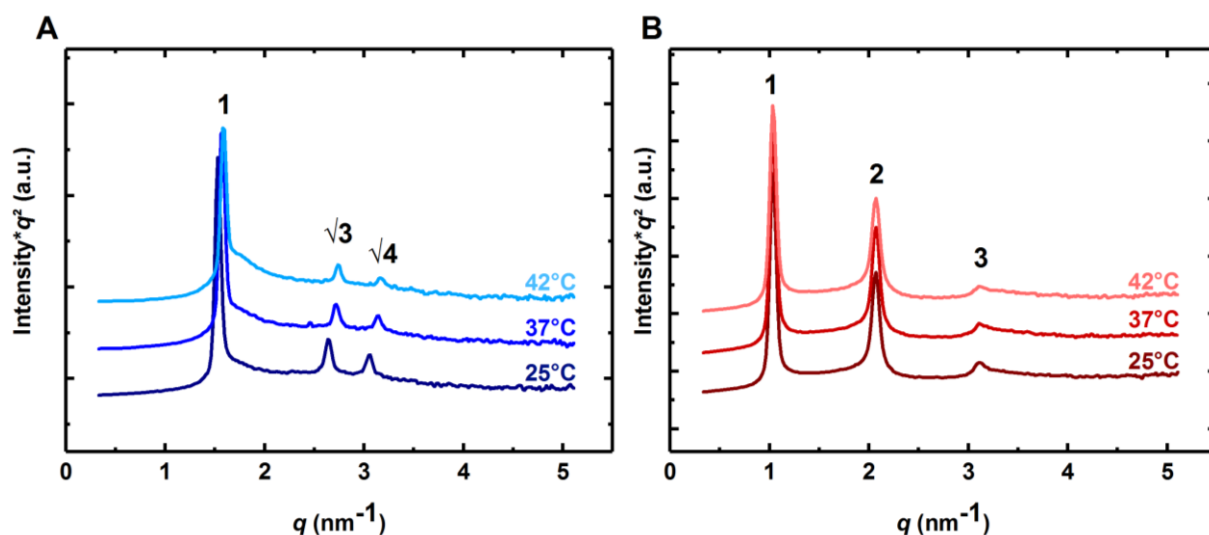


Figure 21: SAXS curves for R18-labeled Phy/MaMo hexosomes (A) and DOPC/DOPE liposomes (B) recorded at indicated temperatures. The curves are shifted vertically for clarity.

Hydrodynamic diameters (*z*-average) of the particles were in a similar range; however, liposomes showed a more heterogeneous size distribution compared to hexosomes (Table 4). Phy/MaMo hexosomes are dispersed from the bulk phase with the help of a steric stabilizer (poloxamer 407), which facilitates homogenization and yields particles of more uniform size. While both systems possess negative surface net charges, DOPC/DOPE liposomes showed a higher absolute zeta-potential in comparison to Phy/MaMo hexosomes (Table 4).

Table 4: *z*-average, PDI, and zeta-potential of R18-labeled Phy/MaMo hexosomes and DOPC/DOPE liposomes dispersed in PBS (mean values \pm SD, $n = 3$)

Nanoparticle	<i>z</i> -Average (d.nm)	PDI	Zeta-potential (mV)
Phy/MaMo hexosomes	210 \pm 5	0.18 \pm 0.01	-5.3 \pm 0.8
DOPC/DOPE liposomes	153 \pm 3	0.34 \pm 0.05	-20.3 \pm 0.6

4.2. Phy/MaMo hexosomes have a higher uptake rate in cells than DOPC/DOPE liposomes

To study the impact of the physico-chemical characteristics of hexosomes and liposomes on their internalization kinetics, the overall uptake was quantified over time regardless of the type of internalization.

The MTT cell proliferation assay was used to identify the effect of nanoparticle concentration on cell viability (Figure 22). HeLa cells were exposed to a range of concentrations for 24 h. A dose-dependent reduction in cell survival was observed for Phy/MaMo hexosomes. Concentrations above 60 nmol/ml (total lipid concentration) drastically decreased the cell viability in comparison to liposomes, which showed minor cytotoxic effects at higher concentrations (Figure 22). Based on the viability results, all subsequent experiments were performed at 30 nmol/ml (total lipid concentration), a concentration at which none of the nanoparticles negatively affected cell viability.

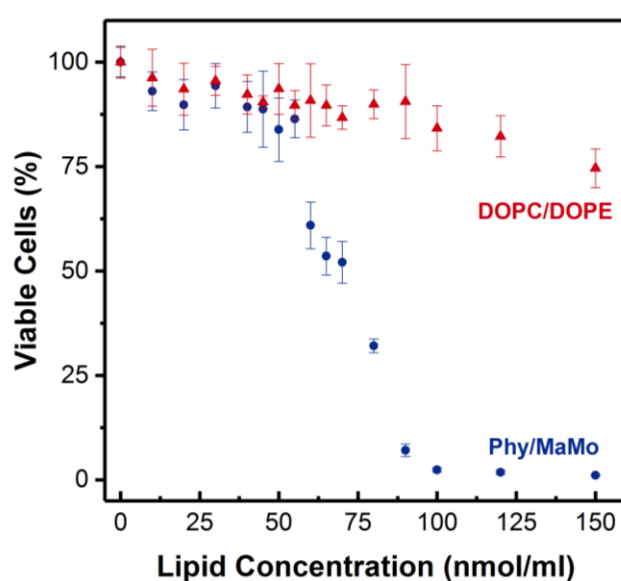


Figure 22: MTT cell proliferation assay of HeLa cells treated for 24 h with various concentrations of R18-labeled Phy/MaMo hexosomes and DOPC/DOPE liposomes. Each data point represents the mean \pm SD ($n = 2$).

The high-throughput quantification of particle uptake revealed a considerably higher internalization of Phy/MaMo hexosomes over time at 37°C in comparison to DOPC/DOPE liposomes (Figure 23). This may explain the striking differences observed in the toxicity profile of these formulations (Figure 22). As a control, this uptake experiment was also performed at 4°C (Figure 23, open symbols) to enable differentiation between internalized and adsorbed particles. At 4°C, energy-dependent pathways are inhibited, and passive diffusion cannot generally take place due to the increased membrane rigidity.²⁰⁹ Neither cells incubated with hexosomes, nor cells incubated with liposomes displayed sensible fluorescence signal at 4°C (Figure 23). This validated that the fluorescence measured after

incubation at 37°C was due to an internalization of particles. The different uptake kinetics, as indicated by the slopes, suggested that liposomes and hexosomes might have distinct cell entry pathways (Figure 23). This is in agreement with the expected impact on cell-particle interactions due to the specific physico-chemical properties of each system.²¹⁰

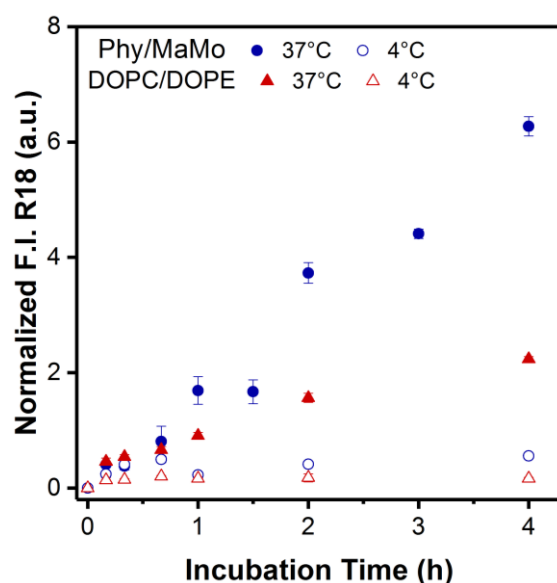


Figure 23: Uptake kinetics of R18-labeled Phy/MaMo hexosomes (blue circles) compared to DOPC/DOPE liposomes (red triangles) by HeLa cells over a period of 4 h measured by fluorescence using the microplate reader. Cells were incubated with nanoparticles at 30 nmol/ml (total lipid), at either 4°C or 37°C. The fluorescence of R18 was normalized by the fluorescence intensity of DAPI (nuclear stain), which corresponds to the cell number. Data points show mean values \pm SEM ($n = 2$).

Cellular uptake of the nanoparticles was further characterized by confocal microscopy to confirm their intracellular localization after 1 hour and 4 hours (Figure 24A and B, respectively). In comparison to liposomes, Phy/MaMo hexosomes are extensively present intracellularly as shown in the orthogonal slices (Figure 24). This is in agreement with the data shown in Figure 23.

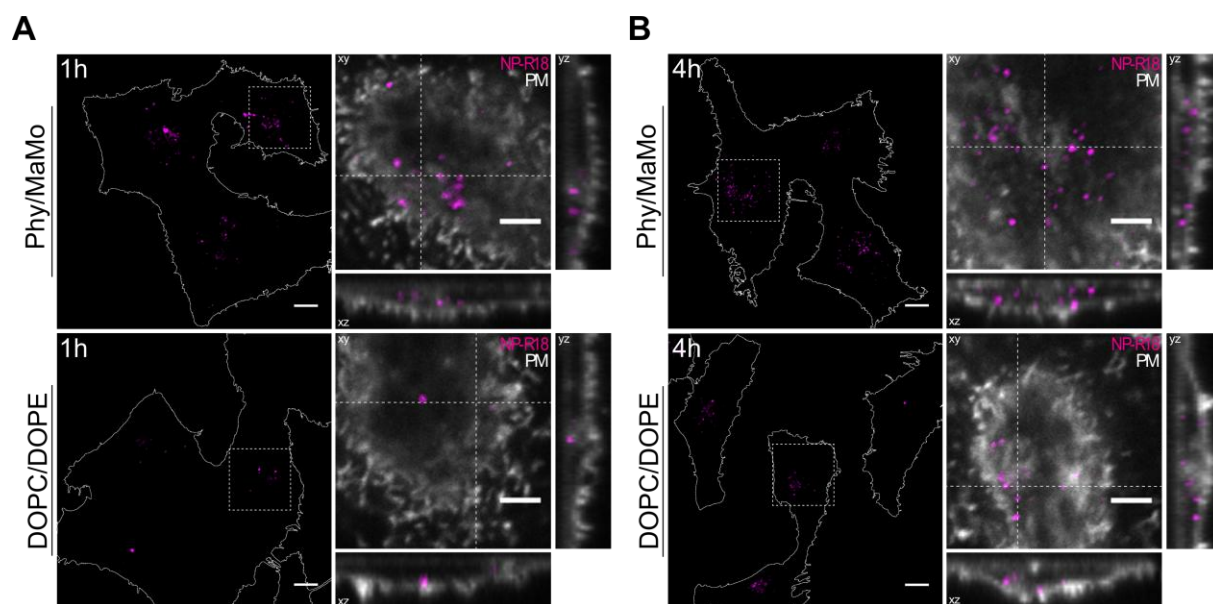


Figure 24: Representative confocal images of R18-labeled Phy/MaMo hexosomes and DOPC/DOPE liposomes incubated for 1 h (A) and 4 h (B) with HeLa cells (NP, nanoparticles shown in magenta). Cells were grown on coverslips, treated and fixed in PFA 4%. The plasma membrane (PM) was visualized by immunofluorescence using anti-CD44 antibody (shown in white). Orthogonal views of a single optical plane (xy, xz, yz) showing the intersection planes at the position of the white cross-hair. Scale bars, 10 μm .

In general, upon interaction with cells, the fluorescent label of fusogenic particles diffuses along the membranes.²¹¹ Interestingly, none of the formulations in this work showed this phenomenon (Figure 24) and R18 was not detected in the cell membrane. Therefore, we did not find visual evidences that support the hypothesis that Phy/MaMo hexosomes have fusogenic properties.

4.3. Phy/MaMo hexosomes are not internalized via any of the major endocytic pathways

The differences in uptake kinetics between hexosomes and liposomes raise the question of which endocytic mechanisms are responsible for the internalization of each type. To address this we downregulated specific target proteins of major endocytic pathways using siRNA (Figure 25).

Clathrin-mediated endocytosis (CME) is the most characterized uptake route and depends on clathrin heavy chain (HC), which forms the main assembly unit of the “coated pits”.¹²⁵

Caveolae are flask-shaped invaginations of the cell membrane and endocytosis via this pathway (caveolae-mediated endocytosis, CvME) requires caveolin-1 (Cav1).¹²⁵ The regulation of the clathrin-independent carriers (CLICs) pathway, a less well known route, is mainly dependent on Cdc42 and GTPase regulator associated with focal adhesion kinase-1 (GRAF1) (Figure 25).¹³³ Dynamin has been reported to be involved in CME, CvME and some clathrin- and caveolae-independent internalization routes.^{125, 212}

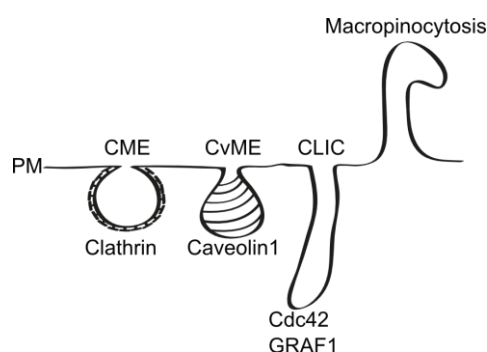


Figure 25: Schematic illustration of different endocytic pathways and their key regulators.

Silencing of clathrin HC, Cav1, dynamin, Cdc42, and GRAF1 did not reduce the internalization of hexosomes after 4 h of incubation (Figure 26A, see Figure 26B for protein levels). Surprisingly, knockdown of GRAF1 seemed to provoke an increase of the uptake (Figure 26A). Similarly, GRAF1 downregulation has already been reported to induce an increase in the internalization of *Helicobacter pylori* vesicles by human gastric adenocarcinoma cell line AGS (ATCC 1739).²¹³ This was attributed to distortions of the membrane promoted by GRAF1 depletion, which is supported by the crucial role of CLICs, in fluid internalization, homeostasis and membrane tension regulation.^{134, 135} Overall, these results suggested a non-endocytic internalization mechanism for Phy/MaMo hexosomes. In contrast, inhibition of any of the proteins reduced the uptake of DOPC/DOPE liposomes to a similar degree after 4 h of incubation (Figure 26A). This indicated that DOPC/DOPE liposomes are unspecifically internalized.

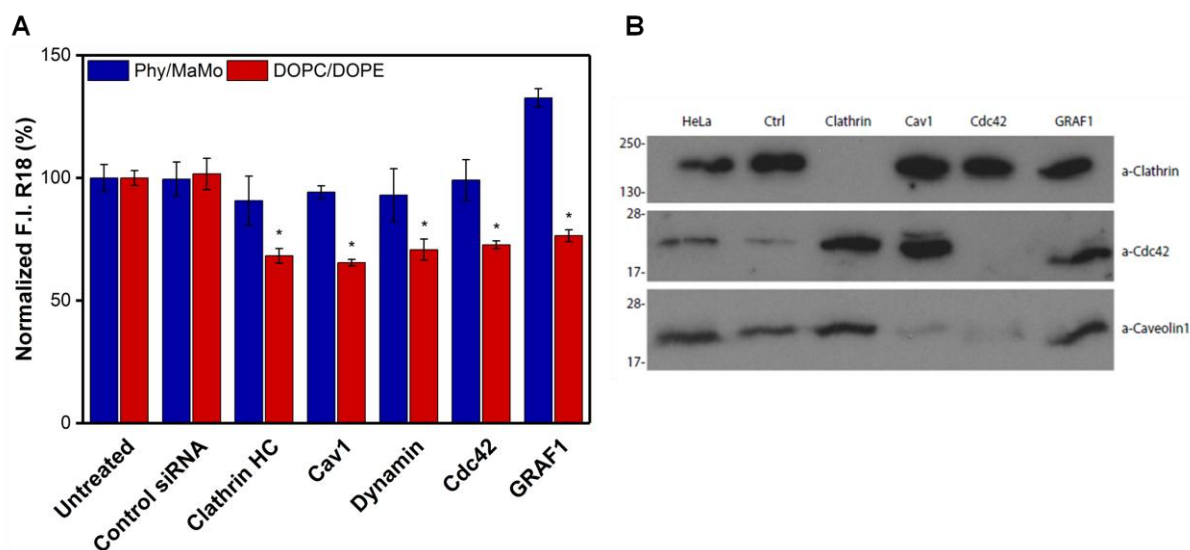


Figure 26: Cellular uptake of R18-labeled Phy/MaMo hexosomes and DOPC/DOPE liposomes following siRNA-mediated depletion of target proteins. HeLa cells were incubated with nanoparticles at 30 nmol/ml (total lipid) for 4 h at 37°C. Uptake was quantified by fluorescence measurements using the microplate reader and the signal was corrected by DAPI fluorescence intensity. The uptake measured for untreated HeLas was set as 100%. Values are presented as mean + SEM ($n = 3$). *, $p \leq 0.05$ compared to untreated (A). Representative Western blot analysis of HeLa cells untreated (HeLa), treated with control siRNA (Ctrl) or siRNA against target proteins (Cav1, Cdc42, Graf1) (B).

It is known that blocking an endocytic route may upregulate other processes.²¹⁴ To verify that the unchanged overall uptake of hexosomes was not due to activation of other pathways, we silenced two pathways simultaneously. The uptake was monitored in live cell using spinning disk microscopy, which enhanced the sensitivity and accuracy of uptake detection at early time points of incubation.

Simultaneous depletion of two major proteins significantly increased the cellular uptake of Phy/MaMo hexosomes in comparison to untreated and control siRNA treated cells after 20 min and 60 min incubation (Figure 27A and B, respectively). These results may be in correlation to the increased uptake observed for single knockdown of GRAF1 (Figure 26A). Abundant membrane invaginations (caveolae)²¹⁵ and tubovesicular formations (CLICs)¹³⁵ are natural membrane reserves able to protect cells against mechanical stresses. Depletion of proteins associated with such structures may cause a disturbance of the cell membrane and increase its permeability.²¹³ It is likely that the silencing of GRAF1 and Cav1 influenced membrane tension and may explain the significantly higher uptake. A very contrasting

scenario was observed for DOPC/DOPE liposomes. We found that the double knockdowns investigated had a significant additive effect and reduced the uptake by approximately 70% and 88% after 20 min (Figure 27A) and 60 min (Figure 27B) incubation, respectively. Overall these results seem to indicate the contribution of more than one endocytic pathway for the internalization of liposomes and an unusual mechanism of interaction between hexosomes and the cell membrane.

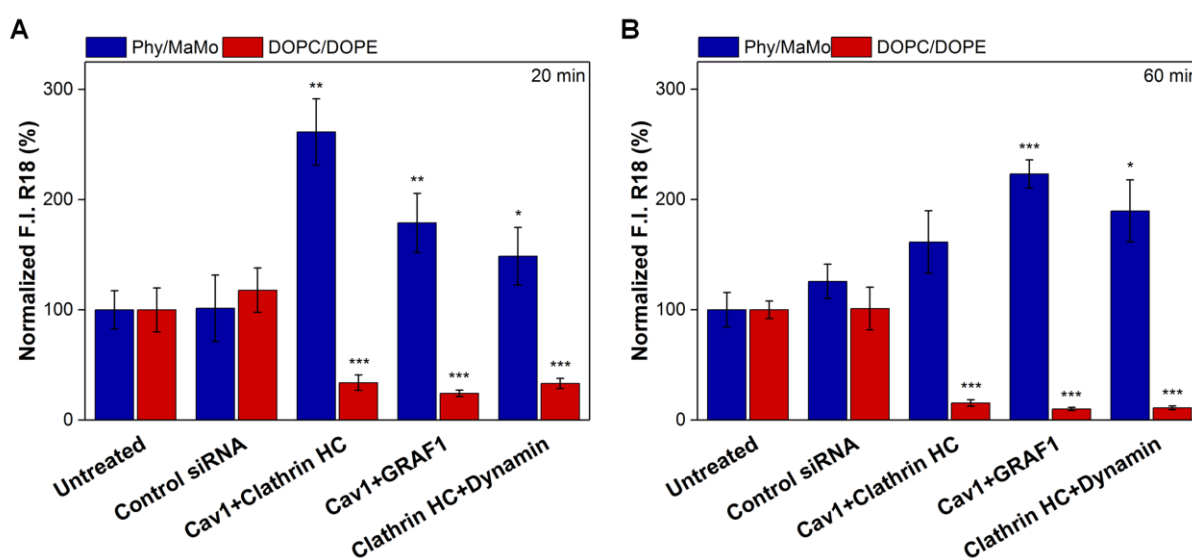


Figure 27: Quantification of nanoparticle uptake by HeLa cells after silencing of regulatory proteins in various combinations using siRNA treatment. HeLa cells were incubated with nanoparticles at 30 nmol/ml (total lipid) at 37°C. The uptake was monitored using live-cell confocal microscopy after 20 min (A) and 60 min (B). Per condition z-stacks of at least ten different cells were analyzed (mean + SEM, $n = 2$). *, $p \leq 0.05$; **, $p \leq 0.01$; ***, $p \leq 0.001$ compared to untreated.

4.4. Internalization of Phy/MaMo hexosomes is not affected by cytochalasin D, but is drastically lowered after hypotonic cell swelling

To better understand the intriguing internalization dynamics of the Phy/MaMo hexosomes, the cells were further challenged with uptake inhibition strategies of broader effect. The aim was to identify factors able to block or significantly reduce the uptake of Phy/MaMo hexosomes.

Considering that internalization of particles is blocked at 4°C (Figure 23), and that the lower temperature diminishes energy-dependent processes and increases cell membrane

tension²⁰⁹ it was coherent to analyze one of these effects separately. Since the downregulation of specific proteins involved in endocytosis might have impacted membrane tension, we decided to further investigate this aspect.

One way to alter the tension of the plasma membrane is to expose the cells to medium with reduced osmolarity and so induce cell swelling. To visualize the acute cell volume changes, we used induced Cav1-GFP Flp-In TRex HeLa cells and recorded z-stacks to monitor the volume increase after 10 min incubation with a hypotonic solution (Figure 28A, side views). The internalization of R18-labeled nanoparticles was then measured by live cell confocal microscopy after 20 min. Increasing the membrane tension led to 91% and 69% reduction in uptake of Phy/MaMo hexosomes and DOPC/DOPE liposomes, respectively (Figure 28B).

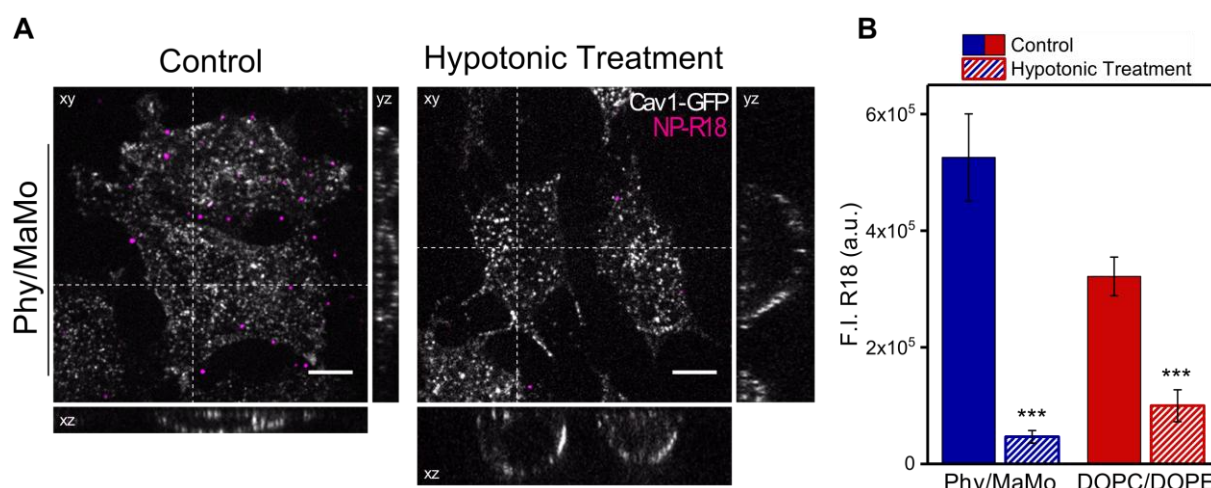


Figure 28: Representative confocal images of hypotonic swelling of induced Cav1-GFP Flp-In TRex HeLa cells (white). To investigate the role of membrane tension on the particle uptake, cells were either untreated or a hypotonic solution was added for 10 min before R18-labeled Phy/MaMo hexosomes (magenta) were added and the uptake measured by live cell confocal microscopy after 20 min. Orthogonal views of a single optical plane (xy, xz, yz) showing the intersection planes at the position of the white cross-hair (A). The bar plot shows a quantification of internalized nanoparticles after 20 min (B). Per condition z-stacks of at least ten different cells were analyzed at the indicated time-points (mean + SEM, $n = 2$). Data are shown as mean values + SEM ($n = 2$). ***, $p \leq 0.001$ compared to control. Scale bars, 10 μm .

It is known that increases in membrane tension reduce endocytic processes.²¹⁶ Therefore, the uptake inhibition observed for liposomes after the hypotonic treatment is consistent with our findings from the knockdown experiments. The fact that the increase in membrane tension nearly blocked the internalization of hexosomes is remarkable. This, together with

the fact that Phy/MaMo hexosomes are not internalized via any major endocytosis routes, suggested a direct interaction of these particles with the cell membrane. Considering that an increase in membrane tension was able to reduce the uptake, it could be expected that a decrease in membrane tension may facilitate the uptake of hexosomes. Several studies propose a “tension buffer” function for the invaginations of the cell membrane.^{135, 215} Therefore, the double knockdowns, through the disruption of such invaginations, might have promoted a decrease of membrane tension. This ultimately culminated with an increase of the internalization of hexosomes. Analogously, the single depletion of GRAF-1 also appeared to facilitate the uptake of hexosomes. GRAF1 is a protein involved in CLICs pathways, stabilizing tubulovesicular structures of several micrometers in length.^{135, 136} This pleiomorphic tubulation is a major regulator of the cell membrane area.¹³⁵ Therefore, the positive effect on the uptake of hexosomes observed after the knockdown of GRAF1 might have been a consequence of an increase in cell membrane area, which generated a decrease in cell membrane tension.

Cell tension is a combination of two parameters: membrane tension and cortical tension. While the former represents the tension of the lipid bilayer itself, the latter is the contribution of the actin cytoskeleton.²¹⁷ To investigate the role of cortical tension and to study actin-dependent uptake mechanisms, such as macropinocytosis, HeLa cells were treated with cytochalasin D. Cytochalasin D is a potent inhibitor of actin polymerization and may impact several endocytic pathways, even if actin is not directly involved. This actin depolymerization triggers a reorganization of actin filaments in the cell, which can modify the function of plasma membrane proteins.²¹⁸ Despite the rather broad impact expected for this inhibitor, cytochalasin D did not affect the cell entry of Phy/MaMo hexosomes (Figure 29A). However, it significantly reduced the uptake of DOPC/DOPE liposomes after 60 min incubation (Figure 29B).

Together, the results confirm that hexosomes and liposomes undergo different cellular internalization processes. While liposomes are internalized through common and well-described endocytic pathways, hexosomes appear to enter the cell in a distinct manner that is independent of endocytic machineries but dependent on membrane tension.

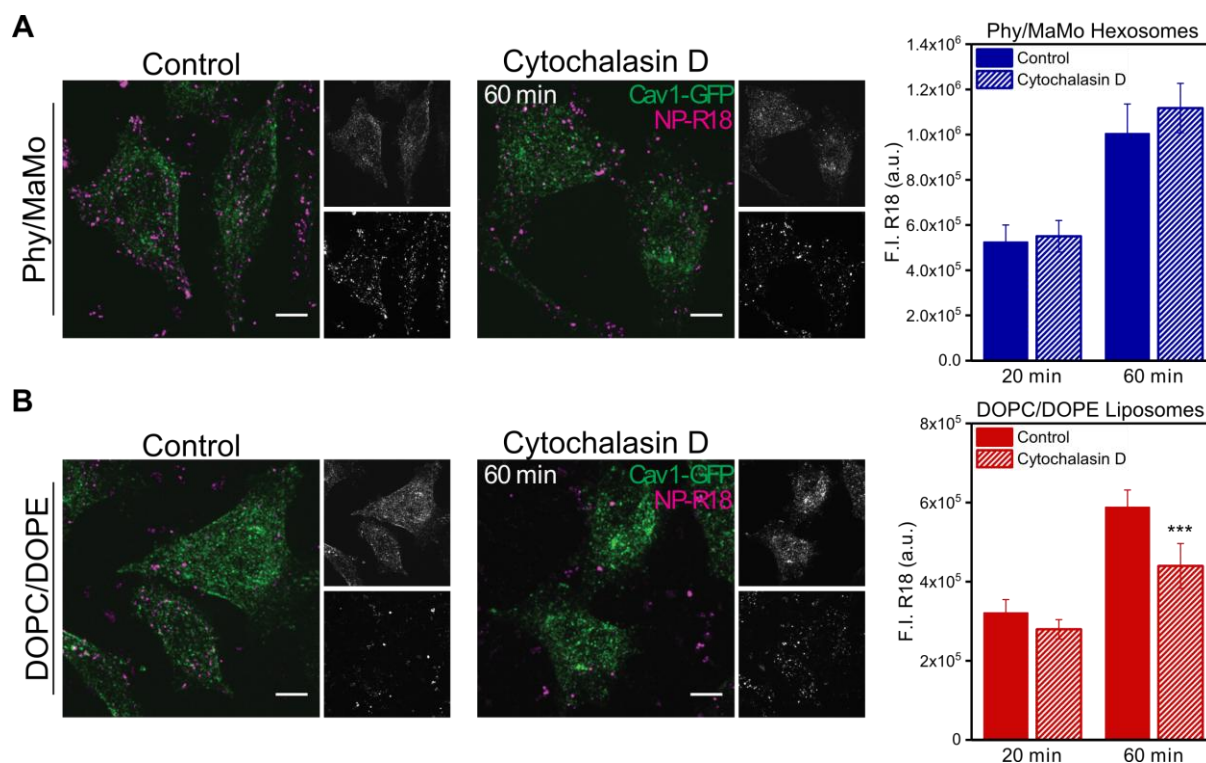


Figure 29: Representative confocal images of induced Cav1-GFP Flp-In TRex HeLa cells (green) incubated with R18-labeled Phy/MaMo hexosomes (A) and DOPC/DOPE liposomes (B), both are shown in magenta). Cells were either untreated (control) or pre-treated with 1 μ M cytochalasin D for 30 min prior to incubation with the nanoparticles (30 nmol/ml total lipid) at 37°C. The uptake was monitored using live-cell confocal microscopy after 20 min and 60 min. The bar plots to the right show a quantification of internalized R18-labeled Phy/MaMo hexosomes (A) and DOPC/DOPE liposomes (B). Per condition z-stacks of at least ten different cells were analyzed at the indicated time-points (mean + SEM, $n = 2$). Data are shown as mean values \pm SEM ($n = 2$). ***, $p \leq 0.001$ compared to control. Scale bars, 10 μ m.

4.5. Phy/MaMo hexosomes directly interact with models of the plasma membrane

To enhance our understanding of the way Phy/MaMo hexosomes enter cells, we explored how they interact with models of the cell membrane using different techniques. We prepared the artificial membrane models using POPC, a zwitterionic phospholipid abundantly found in eukaryotic cell membranes.^{219, 220}

The calcein leakage assay is widely used to measure membrane perturbation and permeabilization. The fluorescent dye calcein is thereby entrapped in POPC vesicles at self-quenching concentrations. To evaluate whether Phy/MaMo hexosomes, DOPC/DOPE

liposomes or the neat components (Phy, MaMo and P407) exert membrane activity, we measured their abilities to induce calcein leakage from POPC.^{221, 222}

Phy/MaMo hexosomes exhibited a significantly higher leakage activity (Figure 30) compared to DOPC/DOPE liposomes and to the negative control (calcein loaded liposomes in PBS). Among the neat components, Phy+P407 showed leakage activity, while the MaMo+P407 and P407 did not lead to increased fluorescence (Figure 30). Phy+P407 is known to form cubosomes, particles internally structured with the non-lamellar inverse bicontinuous cubic phase.^{88, 148} Thus, our findings suggested that non-lamellar phases, such as inverse hexagonal and inverse bicontinuous cubic phase, were able to destabilize the POPC bilayer resulting in membrane perturbation and calcein leakage.

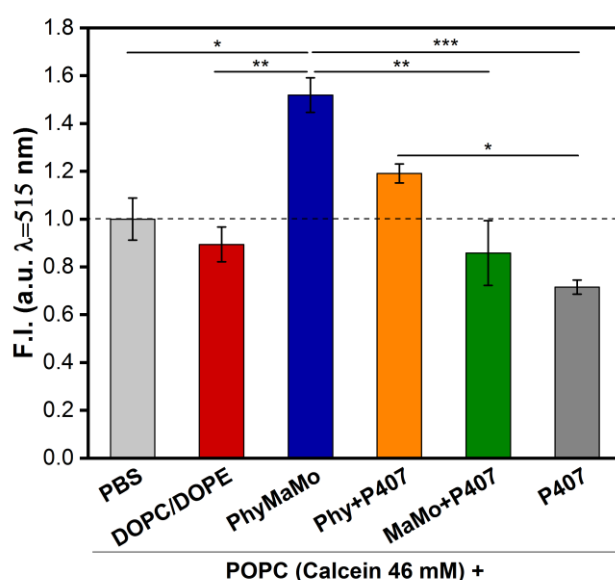


Figure 30: Membrane activity assayed by release of calcein dye from POPC vesicles upon incubation with either DOPC/DOPE liposomes, Phy/MaMo hexosomes or the neat components (Phy, MaMo and P407) at a ratio of 5:1 for 1 h at rt. The calcein leakage was determined by fluorescence intensities superior as the negative control (calcein liposomes + PBS) and is indicated by the dashed line. Data are presented as mean + SEM ($n = 2$).

To further evaluate the interactions between particles and model membranes, the Langmuir monolayer approach was employed. A POPC film was created on a subphase of PBS at 37°C and compressed to an initial surface pressure (π_0) of 30 mN/m, corresponding to lateral pressure in membranes.²²³ To study the interactions of Phy/MaMo hexosomes, DOPC/DOPE liposomes or combinations of the neat components (Phy, MaMo and P407) with the POPC monolayer, they were injected underneath the film and the surface pressure was monitored over time (Figure 31). Changes in surface pressure give information on the

interactions with the monolayer: While a positive increase indicates penetration into the lipid film, a negative change suggests loss of phospholipids from the interface into the subphase.^{224, 225}

Injection of Phy/MaMo hexosomes under the equilibrated lipid monolayer resulted in an immediate steep rise in surface pressure (Figure 31, $\Delta\pi \approx 17$ mN/m). This shows that the hexosomes adsorb to, and insert into the POPC lipid monolayer. The neat components of this formulation (Phy+P407, MaMo+P407, and P407) showed weaker interactions and caused increases of approximately 6 mN/m, 3 mN/m, and 4 mN/m, respectively. These particles might have interacted predominantly with the headgroups of the POPC molecules. In contrast, the surface pressure slowly decreased over time after the injection of DOPC/DOPE liposomes (Figure 31). Similarly to our findings, Jabłowska E et al.²²⁶ reported that monoolein based cubosomes, featuring primitive bicontinuous cubic phase (Im3m), induced surface pressure increase in a 1,2-dipalmitoyl-sn-glycero-3-phosphocholine (DPPC) monolayer. This effect was associated to the incorporation of the nanoparticles into the monolayer. Interestingly, this phenomenon was found to be more pronounced in monolayers that are initially less compressed (5 mN/m) than in highly packed monolayers (35 mN/m).²²⁶

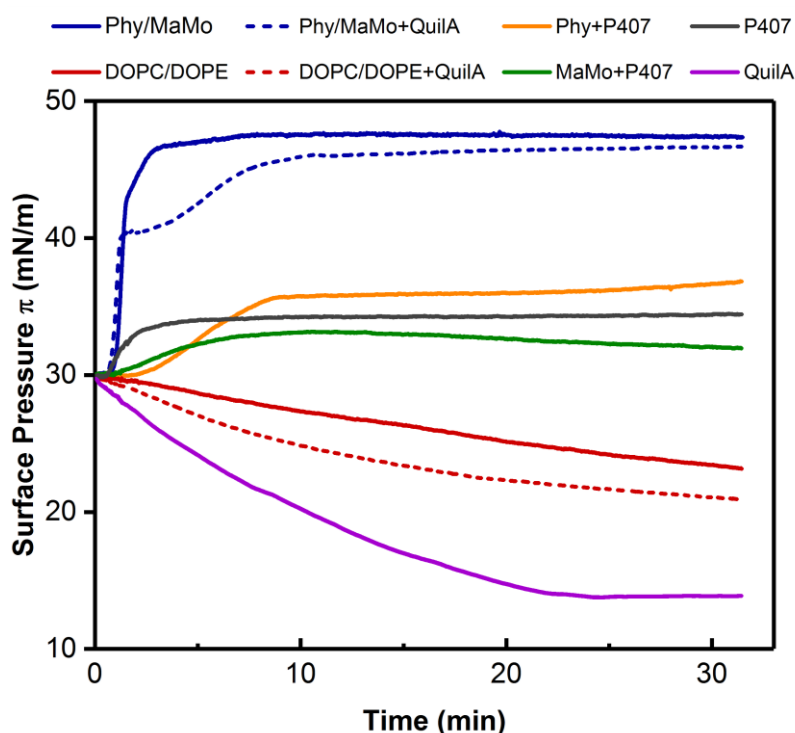


Figure 31: Adsorption isotherms of nanoparticles or neat components (Quil-A[®], Phy, MaMo and P407) onto POPC monolayers (solid lines). The nanoparticles were further modified with Quil-A[®] (dashed lines). The lipid monolayer was compressed to an initial surface pressure (π) of 30 mN m⁻¹ and the samples injected underneath the film at time 0.

Quil-A[®] is a saponin-based adjuvant that is known to intercalate into cell membranes and so induces cell permeabilization.²⁰⁶ To enable a comparison to a well characterized and pharmaceutically relevant molecule, we included Quil-A[®] in these experiments, investigating its surface activity alone and when included in the nanoparticles. Upon Quil-A[®] injection (Figure 31), a drastic decrease of the surface pressure was observed, achieving a plateau after approximately 20 min ($\Delta\pi \approx -3.4$ mN/m). Quil-A[®] had the ability to disturb the POPC monolayer and induced the migration of the phospholipids into the subphase, consequently reducing the surface pressure. This is consistent with the detergent effects typical of saponins.²²⁷ The incorporation of Quil-A[®] into hexosomes resulted in an increase of the surface pressure, which is similar to the effect promoted by hexosomes without Quil-A[®]. Analogously, liposomes containing Quil-A[®] induced a slight decrease of the surface pressure, which is comparable to the effect of liposomes without Quil-A[®] (Figure 31). These findings provided strong evidence that the properties of the carrier are able to surpass the properties of its isolated components, even when these are chemically active like Quil-A[®].

Next, we used confocal fluorescence microscopy to visualize the interactions between POPC-based giant unilamellar vesicles (GUVs, labeled with Marina Blue DHPE) and hexosomes or liposomes (both labeled with R18). GUVs have been extensively used to study interactions of molecules with model membranes in fusion experiments mainly due to their size. Their large dimensions of around 3-30 μm exceed the intrinsic resolution limit of light microscopy, and so make them easily visualized.^{225, 228, 229}

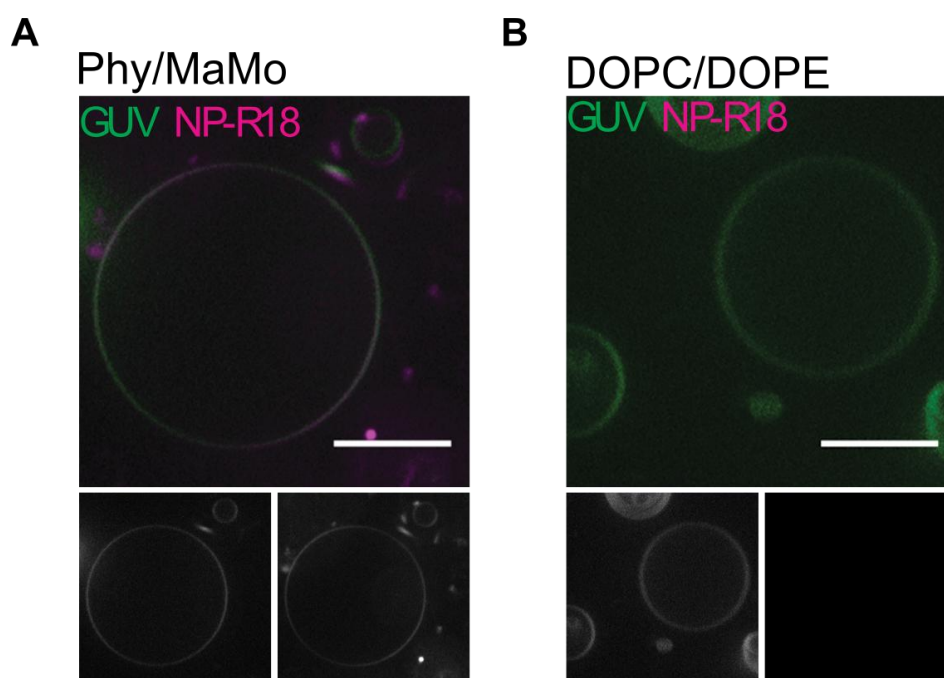


Figure 32: Representative confocal images showing fusion experiment between POPC GUVs labeled with Marina Blue DHPE (green) and either Phy/MaMo hexosomes (A) or DOPC/DOPE liposomes (B), both labeled with R18 (magenta). The GUVs and nanoparticles were mixed and incubated at 37°C for 4 h before acquiring the images. Scale bars, 10 μm .

When R18 labeled hexosomes or liposomes were mixed with POPC GUVs, we detected rhodamine fluorescence in the GUV membrane only for hexosomes (Figure 32). This reaffirmed the superior capacity of hexosomes to directly interact with lipid membranes. Interestingly, R-18 labeled hexosomes were not observed inside the GUVs. The vesicles based on POPC represent a simplification of the plasma membrane and have, due to the larger dimensions, a higher membrane tension.^{228, 229} This may explain why the hexosomes were indeed able to interact with the membrane, but may not have penetrated through the bilayer as we saw in live cell experiments (Figure 24).

To better understand the interactions of hexosomes with membranes, we used smaller POPC vesicles (liposomes) as a model, and employed cryo-TEM to enable visualization of the interactions. Depending on the observation angle, hexosomes appear in cryo-TEM images as internally structured particles with hexagonal shape and/or as round particles displaying parallel lines.²³⁰ Due to the lower rigidity of the hexagonal arrangement, it is also common to observe elongated structures with curved striations as seen in Figure 33 (upper panel Phy/MaMo). These are formed when the tube endings converge and so connect both sides of the structure²³⁰ and has also been seen in earlier experiments.⁸⁸ POPC liposomes appeared mainly as unilamellar spherical vesicles in the size range of approximately 50-200 d.nm (Figure 33). We found that co-incubation of Phy/MaMo hexosomes and POPC liposomes influences the highly ordered lamellar structure of the vesicles as indicated by the white arrows in Figure 33. This effect on the integrity of the liposomal lipid bilayer suggests an ability of hexosomes to distort membranes. It is possible that such a distortion is directly responsible for a higher permeability of the membrane and hence could explain the calcein leakage from liposomes (Figure 30). This is also in agreement with the capacity of hexosomes to insert into lipid monolayers as demonstrated in Figure 31.

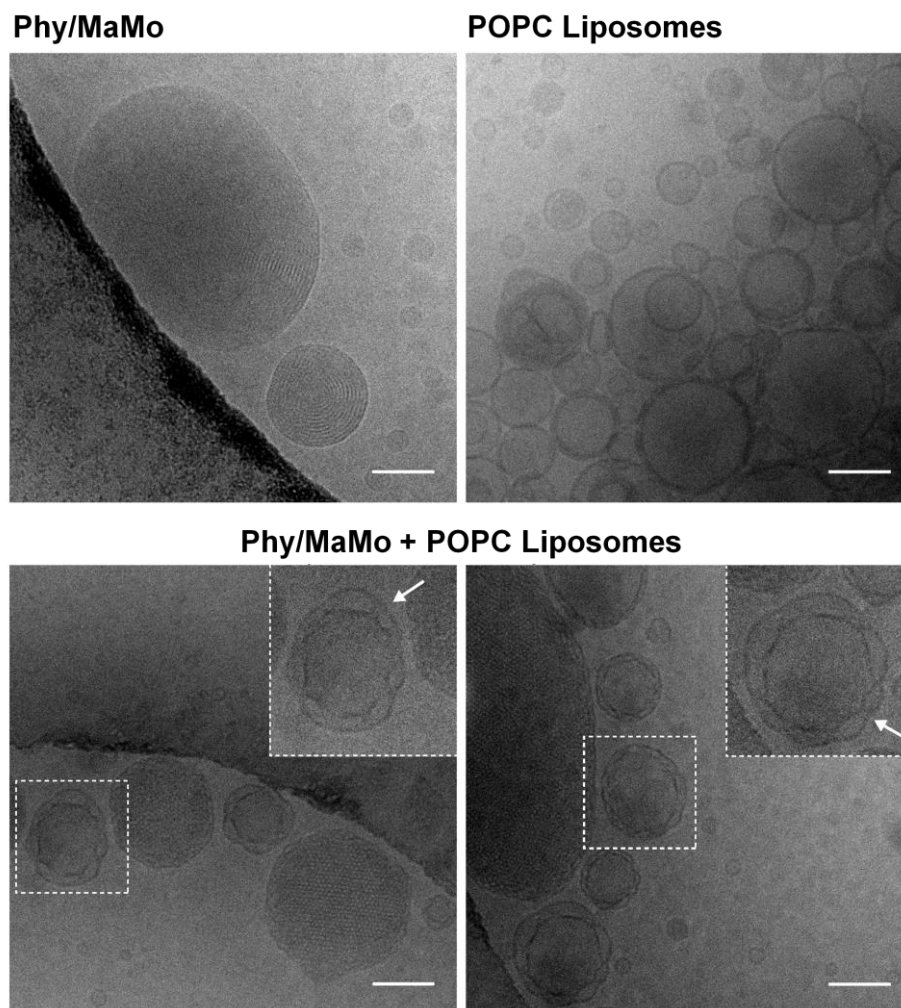


Figure 33: Representative cryo-TEM images of control Phy/MaMo hexosomes and POPC liposomes (top panels) and their mixture (lower panels). Phy/MaMo and POPC liposomes were mixed at a 4:1 ratio and incubated for 1 h at rt before specimen preparation. White arrows in the lower panels highlight the distortion of the POPC lipid bilayer caused by hexosomes. Scale bars, 100 nm.

Together, our data indicated that Phy/MaMo hexosomes have a remarkable ability to directly interact with lipid bilayers and pass through mammalian cell membranes. Having an overall negative zeta potential, their interaction with negatively charged cell membranes is particularly striking. In contrast to DOPC/DOPE liposomes, which are non-specifically endocytosed, the internalization of Phy/MaMo hexosomes does not rely on any of the major endocytic pathways, but rather depends on direct interactions with the lipid bilayer. Our findings are comparable to a recently published study on monoolein based cubosomes.²³¹ According to it, these cubosomes are internalized through an uncommon pathway, which

appears to be cholesterol-dependent and partially energy-independent.²³¹ In addition, the internalized particles seem to mostly circumvent endosomal trafficking and accumulate in lipid droplets.²³¹ The uncommon internalization of cubosomes²³¹ as well as hexosomes is most likely related to their non-lamellar structure. Our results point to the probability that hexosomes distort membranes allowing them to rapidly cross this barrier, without the occurrence of fusion or the creation of permanent pores.

5 CONCLUSION AND OUTLOOK

This work has investigated the cellular internalization of hexosomes and elucidated which role their internal inverse hexagonal phase plays in this process. The evidence from this study implies that the internalization of hexosomes is not dependent on any of the major endocytic routes, but is rather mediated through a direct interaction with the cell membrane. We found that only increased membrane tension and rigidity limits the cellular uptake of hexosomes. Accordingly, an increase in membrane area and consequent decrease of membrane tension are thought to facilitate their cell entry. Hexosomes also showed impressive affinity for POPC model membranes, which was unexpected since they are negatively charged and steric stabilized with poloxamer 407. Cryo-TEM micrographs displayed strong evidence that hexosomes might promote distortions in the cell membrane, which is probably the key to understand their uptake dynamics and the effects associated with their non-lamellar structure. These distortions are not a sort of “surfactant effect” since hexosomes were shown to intercalate into a lipid monolayer, without promoting its damage or solubilization, as demonstrated by the saponin Quil-A®.

Our findings highlight a significant role for hexosomes as powerful drug delivery system and considerable progress has been made in understanding hexosome-cell interactions. We are confident that this research will serve as a basis to understand its full potential. With regards to this, additional research is required to elucidate the intracellular fate of hexosomes and their cargo molecules.

CHAPTER IV

The Supramolecular Structure of Nano-Self-Assemblies Influences the Adjuvant Efficacy of a Synthetic Mycobacterial Monomycoloyl Glycerol Analogue

A version of this chapter is submitted for publication.

Rodrigues L., Raftopoulos N. K., Tandrup Schmidt S., Schneider F., Dietz H., Rades T., Franzyk H., Elm Pedersen A., Papadakis C. M., Christensen D., Foged C., Winter G., Hubert M. „Adjuvants based on a monomycoloyl glycerol analogue in hexosomes and liposomes induce different immune responses after vaccination with the *Chlamydia trachomatis* major outer membrane protein”.

This work was conducted in collaboration with the Soft Matter Physics Group and Institute for Advanced Study of the Technische Universität München, the Translational Immunology Group and the group for Vaccine Design and Delivery of the University of Copenhagen, and the section for vaccine research of the Statens Serum Institut in Copenhagen. The manuscript was written by Rodrigues L. The SAXS measurements were performed by Rodrigues L and Raftopoulos N K under

the supervision of Papadakis C M. Cryo-TEM image acquisition was conducted by Schneider F and supervised by Dietz H. The animal immunization and collection of biological samples were conducted by the veterinarians of the animal facility of the Statens Serum Institut. Rodrigues L and Tandrup Schmidt S performed together the experiments with the collected biological samples under the supervision of Christensen D. The in-vitro studies with PBMCs were conducted by Rodrigues L under the supervision of Elm Pedersen A. All data analyses and additional experimental work were performed by Rodrigues L and supervised by Foged C, Winter G and Hubert M.

1 ABSTRACT

The mycobacterial lipid monomycoloyl glycerol (MMG) and its synthetic analogue MMG-1 exert promising adjuvanticity, but little is known about how immunopotentiality is influenced by the supramolecular structure of the delivery system used to target MMG and antigen to the immune system. Here, we demonstrate that the nanostructure of MMG-based particles remarkably influence the responses against the *Chlamydia trachomatis* major outer membrane protein (MOMP) antigen. Hexosomes are self-assemblies of amphiphilic lipid molecules, internally structured with inverse hexagonal phase. They have the potential to deliver antigens directly to the cytosol of antigen-presenting cells, and therefore represent a field of great interest. Differently charged MMG-1-based hexosomes were compared to established cationic MMG-1-based liposomes. *In vitro*, hexosomes did not induce maturation of human dendritic cells derived from peripheral blood mononuclear cells, whereas liposomes up-regulated CCR7. In mice, while liposomes induced predominantly cell-mediated responses against MOMP, hexosomes elicited mainly humoral responses, with high IgG titers and minimal potential T-cell effector function. This immune profile appeared to be independent of the zeta-potential of the hexosomes. In conclusion, this study emphasizes profound differences in the immunopotentiating behavior of MMG-1-based liposomes and hexosomes, and highlights the importance of rational particle engineering to achieve customized and optimal immunological responses upon vaccination.

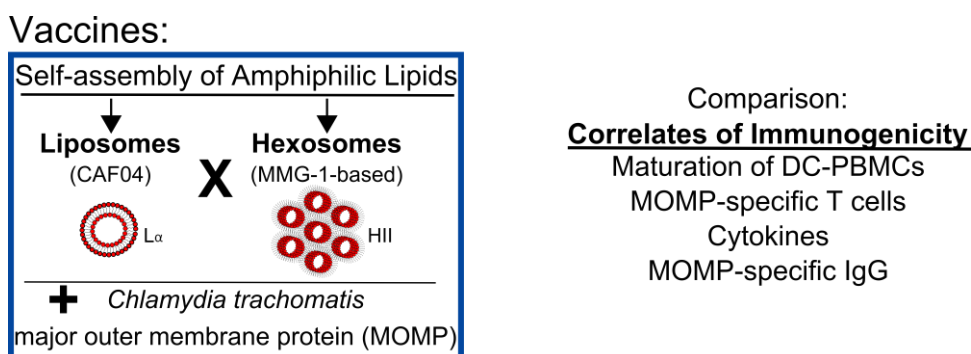


Figure 34: Graphical Abstract - The Supramolecular Structure of Nano-Self-Assemblies Influences the Adjuvant Efficacy of a Synthetic Mycobacterial Monomycoloyl Glycerol Analogue.

2 INTRODUCTION

Despite the fact that vaccines constitute one of the greatest medical successes, diseases that are potentially preventable by vaccination are still a major global health problem ². These diseases include so-called difficult prophylactic vaccine targets, *e.g.*, tuberculosis, malaria and HIV, and therapeutic targets like cancer, for which efficacious and safe vaccines do not yet exist ^{2, 232}. It is well known that the majority of the existing vaccines mediate protection through stimulation of humoral immunity. However, there is an unmet medical need for novel safe and efficacious vaccines that also stimulate cell-mediated immune (CMI) responses, which appear to be critical in providing protection against intracellular pathogens, *e.g.* *Mycobacterium tuberculosis*, HIV and *Chlamydia trachomatis*. ^{1, 233}

Vaccine safety has been substantially improved with the introduction of subunit vaccines. Unlike the traditional vaccines based on live attenuated or inactivated whole pathogens, subunit vaccines contain only specifically defined subunits of the pathogens, which can be synthetic peptides, highly purified recombinant proteins, or DNA/RNA encoding the antigen(s). ¹ The result is increased safety, yet these systems show lower immunogenicity. Co-administration of adjuvants is therefore required to provoke persistent and protective immune responses. Ideally, adjuvants improve vaccine efficacy with minimal impact on safety. For a specific vaccine, the immune profile of the adjuvant has to be carefully

designed and optimized to induce adequate protective immunity and immunological memory against the pathogen.²³³

Vaccine adjuvants constitute a large group of structurally heterogeneous compounds that generally are classified as either immunopotentiators, delivery systems or a combination of both.²⁰ Recently, it was shown that synthetic analogues of lipid components from the cell wall of *M. tuberculosis* are extraordinarily strong CMI-stimulating immunopotentiators, and they are therefore highly promising as subunit vaccine adjuvants.^{66, 68, 234, 235} Examples are synthetic analogues of monomycoloyl glycerol (MMG).^{24, 66, 234} The combination of the MMG analogue referred to as MMG-1 and a cationic liposomal delivery system [the so-called cationic adjuvant formulation (CAF) 04, Statens Serum Institut, DK] has shown promising adjuvant activity. CAF04 induced strong Th1/Th17 biased responses, polyfunctional T cells and specific IgG against the tuberculosis fusion antigen Ag85B-ESAT-6⁶⁸ and the *C. trachomatis* serovar D major outer membrane protein (MOMP) antigen.⁶⁹

We recently performed a detailed analysis of the influence of MMG structure on the adjuvant activity of CAF04 employing an array of MMG analogues with different alkyl chain lengths displaying different stereochemistry in the hydrophobic moiety and in the polar headgroup.^{24, 69} However, little is known about the influence of the structural characteristics of the delivery system on the adjuvanticity of MMG. The aim of the present study was to compare the adjuvant activity of MMG-1-based cationic liposomes (CAF04) and hexosomes loaded with MOMP antigen, and to investigate the effect of surface charge. The hypothesis was that the nanostructural characteristics of the lipid-based delivery system are decisive for the way the antigen is delivered to and interacts with antigen-presenting cells (APCs), which in turn affects the induced immune responses qualitatively and quantitatively. In this way, rational particle engineering may be applied to stimulate customized and optimal immunological responses upon vaccination.

Hexosomes are self-assembled particles of amphiphilic lipids, internally structured with an inverse hexagonal (HII) structure and dispersed in an aqueous system. They consist of rod-shaped inverse micelles organized in a hexagonal geometry with closed water channels.¹⁰⁰ Due to a high amount of lipid per particle and a network of water channels, the intricate structure of hexosomes allows for high loading efficiencies of hydrophilic, hydrophobic and

amphiphilic drug cargoes.¹⁰⁰ This is a promising property for overcoming encapsulation constraints encountered with other particulate systems applied for vaccination (*e.g.* liposomes).¹⁰⁰ Moreover, non-lamellar assemblies, *e.g.* inverse hexagonal phases, have been reported to show fusogenic properties.⁷⁸ Thus, hexosomes have potential for delivery of antigens directly to the cytosol of APCs, and in this way facilitate stimulation of cytotoxic T lymphocyte (CTL) immune responses.²³⁶

We therefore compared the immunogenicity of MOMP adjuvanted with MMG-1-based hexosomes and liposomes, respectively. Correlates of immunogenicity were analyzed, *e.g.*, activated populations of MOMP-specific T cells (CD44^{hi}), cytokine responses, and induction of MOMP-specific IgG responses. Our results demonstrate for the first time striking differences between these self-assembled, lipid-based delivery systems in all aspects analyzed. This supports the importance of particle design in the rational formulation engineering of subunit vaccines and reveals a potential application of this knowledge as a tool to tailor vaccine-induced immune responses.

3 MATERIALS AND METHODS

3.1. Materials

Phytantriol (Phy) from DSM Nutritional Products Europe Ltd was a gift from Nordmann, Rassmann GmbH (Hamburg, DE). Dimethyldioctadecylammonium (DDA) bromide and poloxamer 407 were purchased from Sigma-Aldrich (Taufkirchen, DE). 1,2-Dipalmitoyl-*sn*-glycero-3-phosphocholine (DPPC) and 1,2-dipalmitoyl-*sn*-glycero-3-phosphoglycerol sodium salt (DPPG) were gifts from Lipoid GmbH (Ludwigshafen, DE). Chicken egg ovalbumin (OVA) conjugated with Alexa Fluor 488 (OVA-Alexa488) was purchased from Life Technologies GmbH (Darmstadt, DE). The modified *C. trachomatis* serovar D MOMP antigen referred to by Knudsen *et al.* as rMOMP²³⁷ was used as antigen (Statens Serum Institut). All other chemicals and reagents were of analytical grade and were purchased from commercial suppliers.

3.2. Synthesis of Mycobacterial Monomycoloyl Glycerol Analogue 1 (MMG-1)

MMG-1 was synthesized, purified and characterized as previously described.⁶⁸

3.3. Preparation of Liposomes

Cationic liposomes (CAF04) were prepared as previously described with modifications.²⁴ Weighed amounts of DDA (5.3 mg) and MMG-1 (2.1 mg, equivalent to 31 mol% of total lipid) were dissolved in CHCl₃ (Table 1). The organic solvent was completely removed by rotary evaporation followed by incubation for 72 h in a vacuum drying chamber at 25°C and 15 mBar. Subsequently, 1 ml of phosphate-buffered saline (PBS, pH 7.4) was added to rehydrate the lipid film, and probe-type ultrasonication was performed in three cycles of 2 min with 2 s pulse, 2 s pause, and 30% amplitude (Bandelin Sonopuls HD3200 with sonotrode MS72, Berlin, DE).

3.4. Preparation of Hexosomes

Hexosomes were prepared as previously reported.⁸⁸ Briefly, appropriate amounts of each lipid (Table 5) were weighed and melted at 70°C using the Thermomixer comfort (Eppendorf, Hamburg, Germany). The samples were agitated for 30 min in a dual asymmetric centrifuge (SpeedMixer™ DAC 150.1 CM41) at 3500 rpm to homogenize the lipid melt. Subsequently, 1 ml of poloxamer 407 solution in PBS was added to each sample (3.25 mol% of the total lipid content). The samples were probe-type ultrasonicated in three cycles of 2 min with 2 s pulse and 2 s pause at an amplitude of 30% (Bandelin Sonopuls HD3200 with sonotrode MS72).

Table 5: Adjuvant compositions.

Adjuvant	Phase	Phy (mg/ml)	MMG-1 (mg/ml)	Charged lipid (mg/ml)	Lipid adjuvants ^c
CAF04	L α	0.0	2.1	5.30 (DDA)	MMG-1 and DDA
Phy/MMG-1 ^a	HII	18.4	6.9	---	MMG-1
Phy/MMG-1 ^a + DDA ^b	HII	16.5	6.2	0.78 (DDA)	MMG-1 and DDA
Phy/MMG-1 ^a + DPPC ^b	HII	18.4	6.9	1.00 (DPPC)	MMG-1
Phy/MMG-1 ^a + DPPG ^b	HII	18.4	6.9	1.02 (DPPG)	MMG-1

^aAll hexosome dispersions contain 18 mol% MMG-1 of the total lipid content (Phy+MMG-1).

^bCharged lipids (DPPC/DPPG/DDA) were added to hexosomes at 2 mol% of total lipid (Phy+MMG-1).

^cTotal concentration of lipid adjuvants was kept constant at 2.42 mmol/ml in all formulations.

3.5. Small-Angle X-ray Scattering (SAXS)

SAXS analyses were performed using a Ganesha 300XL instrument (SAXSLAB ApS, Copenhagen, DK) equipped with a GENIX 3D microfocuss Cu X-ray source (XENOX, Sassenage, FR) and a 2D Pilatus 300K detector (Dectris, Baden-Daettwil, CH). The sample chamber and beam path were under vacuum. Concentrated particle dispersions (Table 5) were loaded into glass capillaries (1 mm light path, SAXSLAB), which were hermetically sealed and mounted in a temperature-controlled cell. The samples were measured after 10 min of equilibration at 37 °C. The wavelength was $\lambda = 1.54 \text{ \AA}$, the sample-to-detector distance was 406.2 mm, and the acquisition time was 180 min. A pin diode was used to measure the transmission of the sample. The 2D images were azimuthally averaged, and the background from the glass capillaries was subtracted, taking the transmission into account.

To identify the different liquid crystalline phases, the q -position [$q = 4\pi \sin(\theta/2)/\lambda$ is the momentum transfer] of each Bragg reflection was determined by fitting a Lorentz function (θ is the scattering angle). The ratios of the relative peak positions were calculated and compared to patterns described in the literature.¹⁵² The repeat distance, d , was calculated using Bragg's law, $d = 2\pi/q_1$, where q_1 is the position of the first peak. The mean lattice parameter, a , was determined according to the scattering law for the inverse hexagonal phase, namely $a = 2d/\sqrt{3}$.¹⁵⁴

3.6. Cryogenic Transmission Electron Microscopy (Cryo-TEM)

Vitrified specimens of selected dispersions at approximately 5 % (w/w) of total lipid were prepared using a Vitrobot (FEI, Eindhoven, NL) at 22.0°C and 90% humidity. A volume of 3

μl of the particle dispersion was applied on 400-mesh C-Flat CF-2/1-4C copper grids (Protochips, Morrisville, NC, USA) negatively glow discharged with a Plasma Cleaner (EMS, Hatfield, PA, USA) at 35 mA for 45 s. After 30 s equilibration, the excess of liquid was removed by blotting (3 s, “force” -1), and the grids were automatically vitrified in liquid ethane below -172°C . A subset of samples was imaged using a Tecnai Spirit microscope (FEI) equipped with a Tietz TemCam-F416 charge-couple device (CCD) camera and a Cryo-Transfer Holder (Gatan, Inc., Pleasanton, CA, USA). The system was operated at an acceleration voltage of 120 kV under low-dose conditions (SerialEM Tecnai v3.5.6 acquisition software) with 26.000-, 30.000-, 40.000- and 50.000-fold magnification. The second subset of samples was imaged using a Titan Krios microscope (FEI), equipped with a Falcon 3EC direct electron detector. The system was operated at an acceleration voltage of 300 kV under low-dose conditions (EPU Titan v1.9 acquisition software) with 37.000- and 47.000-fold magnification. Image analysis was performed using the Fiji software (National Institutes of Health, Bethesda, MD, USA).

3.7. Dynamic Light Scattering (DLS)

A Malvern Zetasizer Nano ZS (Malvern Instruments, Worcestershire, UK) was used to measure the intensity-weighted average hydrodynamic diameter (z-average), polydispersity index (PDI) and zeta potential of the particles. The dispersions were diluted (1:100) and added into PMMA cuvettes (BRAND®) or DTS1060C capillary cells (Malvern Instruments) for the analysis of z-average and zeta potential, respectively. The measurements were not affected by the sample concentration within the range used in this study. For viscosity and refractive indexes, the values of PBS were used. The measurements were carried out in triplicate at 25°C under buffering conditions relevant for biological experiments (PBS, pH 7.4). Zetasizer Software version 7.03 (Macromedia, Inc.) was used for acquisition and analysis of the data.

3.8. *In vitro* Experiments:

3.8.1. Preparation of Primary Dendritic Cells (DCs) Derived from Peripheral Blood Mononuclear Cells (PBMCs)

Leukocytes were isolated from fresh human venous blood (provided by the blood bank at Rigshospitalet, Copenhagen, DK) by gradient centrifugation using Lymphoprep™ (Fresenius Kabi, Oslo, NO). The cells were washed three times with PBS and resuspended in RPMI1640. Using 0.2% eosin as an indicator of viability, the cells were counted and subsequently cultured in 6-well plates (1×10^7 viable cells/well) with complete medium (RPMI1640 supplemented with Glutamax™, 100 U/ml penicillin, and 100 µg/ml streptomycin) with 15% (v/v) human AB serum (Valley Biomedical Inc., Winchester, VA, USA). After 1.5 h incubation (37°C, 5% CO₂), the wells were carefully washed to remove non-adherent cells. In order to differentiate the PBMCs into DCs, 2 ml complete medium containing 5% (v/v) human AB serum, 50 ng/ml granulocyte-macrophage colony-stimulating factor (GM-CSF) and 25 ng/ml interleukin (IL)-4 (both from PeproTech Nordic, Stockholm, SE) were added to each well. After three days of incubation, the cytokine-containing medium was renewed, and the cells were incubated for additional three days. The purity of the DC cultures was higher than 70% on day 6. This was evaluated based on the surface expression of CD11c (PE-labeled anti-mouse CD11c antibody, clone B-ly6, BD Pharmingen, San Diego, CA, USA), which was quantified by flow cytometry using a BD FACScalibur (BD Biosciences, San Jose, CA, USA).

3.8.2. Viability Assay

PBMC-derived DCs were harvested on day 6, and then the cells were seeded in 96-well plates (3×10^4 cells/well) in complete medium supplemented with 5% (v/v) human AB serum. Different concentrations of the particle dispersions (0-0.102 nmol of lipid adjuvant/ml) were added to each well, and the cells were incubated with the samples for 24 h (37°C, 5% CO₂). The medium was subsequently replaced with 100 µl of [3-(4,5-dimethylthiazol-2-yl)-5-(carboxymethoxyphenyl)-2-(4-sulfenyl)-2H-tetrazolium]/phenazine methosulfate (MTS/PMS) reagent solution (140 µg/ml MTS and 2.4 µg/ml PMS in PBS)

according to the vendor's recommendations (Promega, Madison, WI, USA). Following 4 h of incubation, the absorbance was measured at 492 nm.

3.8.3. Uptake Experiments

To investigate cellular uptake *in vitro*, 50 µg/ml of the fluorescently labeled model antigen OVA (OVA-Alexa488) was added to the prepared liposomal dispersion. The net negative charge of OVA at physiological pH [isoelectric point (pI) = 4.5²³⁸] is suggested to contribute to the adsorption of the antigen to the cationic liposomes via attractive electrostatic interactions.²³⁹ To prepare hexosomes for the uptake studies, 50 µg/ml of OVA-Alexa488 were added to the lipid melt together with the poloxamer solution, followed by sonication. PBMC-derived DCs were harvested on day 6 of differentiation, and the cells were cultured in 96-well plates (1×10⁵ cells/well) in complete medium supplemented with 5% (v/v) human AB serum. Selected nanoparticle dispersions, loaded with OVA-Alexa488 were added to the cells in triplicate at 20 pmol of lipid adjuvant/ml. The uptake experiments were performed at 37°C and 4°C, respectively, to distinguish particle internalization from interaction with the cell membrane (blockage of membrane trafficking at 4°C).²⁰⁴ After 2 h incubation, the cells were harvested, washed three times with PBS, and the uptake was quantified by flow cytometry (BD FACScalibur).

3.8.4. Stimulation of DCs and Evaluation of Surface Marker Expression

PBMC-derived DCs were incubated on day 5 of differentiation with the dispersions at 20 pmol of lipid adjuvant/ml for 24 and 48 h (37°C and 5% CO₂). Cells stimulated with lipopolysaccharide (LPS, 3 µg/ml) served as positive control. After incubation, the cells were harvested, washed twice with PBS, and incubated for 10 min at room temperature (rt) with blocking buffer [PBS containing 2% (v/v) human AB serum]. Subsequently, the cell suspensions were centrifuged (5 min at 600 g and 4°C), and the cell pellets were resuspended in 50 µl antibody staining solution (single staining). The staining solutions were PE-labelled anti-mouse CD11c antibody (clone B-ly6, BD Pharmingen), FITC-labelled anti-mouse CD80 antibody (clone L307.4, BD Pharmingen), APC-labelled anti-mouse CD83 antibody (clone HB15e, Biolegend), FITC-labelled anti-mouse CD86 antibody (clone 2331/FUN-1, BD Pharmingen), FITC-labelled anti-mouse HLA-DR antibody (clone AB3, Dako), APC-labelled anti-mouse CD40 antibody (clone 5C3, Biolegend), PerCP-Cy5.5-

labelled anti-mouse CD197 (CCR7) antibody (clone G043H7, Biolegend), and proper isotype controls (BD Pharmingen) diluted according to manufacturer's recommendations in staining buffer [PBS containing 1% (w/v) BSA]. The cells were incubated with the staining solutions on ice and protected from light for 45 min. The cells were subsequently washed twice with cold staining buffer, and resuspended in 150 μ l 4% (v/v) paraformaldehyde (PFA) and 150 μ l staining buffer. The samples were stored at 4°C and protected from light until analysis by flow cytometry (BD FACScalibur).

3.9. Animal Experiments

Five-fold dilutions of CAF04 and MMG-based hexosomes (Table 5) were loaded with 25 μ g/ml *C. trachomatis* serovar D MOMP antigen, and then aliquoted in dose volumes of 200 μ l. For the hexosomal formulations, MOMP was incorporated into the lipid melt together with the poloxamer solution. For CAF04, MOMP was surface-adsorbed to the prepared liposomes. To enable comparability between the different vaccine delivery systems, all formulations contained the same concentration of MOMP antigen (5 μ g/200 μ l dose) and the same molar concentration of total lipid adjuvant (0.484 mmol adjuvant/ml, Table 5). Female CB6/F1 (6-8 weeks old) were purchased from Harlan (Horst, NL). All experiments were carried out in accordance with the European Community Directive (86/609), and the experimental protocol (2014-15-2934-01065) was approved by the Danish Council for Animal Experiments. The mice in each group ($n = 6$) were immunized twice subcutaneously at the base of the tail, with an interval of two weeks. A group of mice immunized with the non-adsorbed antigen in PBS (without carrier system and adjuvant) was used as negative control. The mice were euthanized ten days after the last immunization, and the spleen, inguinal lymph nodes, and plasma were harvested and analyzed.

3.9.1. Intracellular Cytokine Staining (ICS)

Single cell suspensions from lymph nodes and spleen were prepared by homogenization of the organs through a nylon mesh. The cells were washed twice with RPMI1640 (Gibco Invitrogen, Carlsbad, CA, USA) and seeded in 96-well plates at a density of 2×10^5 cells/well in complete medium [RPMI1640 supplemented with 1 mM L-glutamine, 10% (v/v) fetal calf serum, 5 μ M 2-mercaptoethanol, 100 U/ml penicillin, 100 μ g/ml streptomycin, 1% (v/v)

sodium pyruvate, and 10 mM 4-(2-hydroxyethyl)-1-piperazineethanesulfonic acid (HEPES)]. Cells isolated from three mice were pooled to ensure sufficient cell numbers in samples from the lymph nodes, resulting in a total of two groups per treatment group. The cells were restimulated for 1 h (37°C, 5% CO₂) with 2 µg/ml MOMP in the presence of 1 µg/ml of the co-stimulatory anti-mouse CD28 (clone 37.51) and CD49d (clone MFR4.B, both from BD Biosciences) antibodies. Cells stimulated with phorbol-12-myristate-13-acetate (PMA, 0.05 µg/ml, Sigma Aldrich) and ionomycin (1 µg/ml, Sigma Aldrich) served as positive controls, and cells incubated with complete medium only served as negative control. Subsequently, brefeldin A (10 µg/ml, Sigma Aldrich) and Monensin/GolgiStop (0.7 µl/ml, BD Biosciences) were added and the cells were further incubated for 5 h (37°C). The cells were washed with FACS buffer [PBS containing 1% (v/w) fetal calf serum] and stained for surface markers with the anti-mouse antibodies CD4:eFluor780 (clone RM4-5), CD8:PerCp-Cy5.5 (clone 53-6.7), and CD44:FITC (clone IM7, all from eBioscience, San Diego, CA, USA) (30 min at 4°C). Following permeabilization with the Cytfix/Cytoperm kit (BD Biosciences) according to the manufacturer's recommendations, the cells were stained intracellularly with the anti-mouse antibodies interferon-γ (IFN-γ):PE-Cy7 (clone XMG1.2), tumor necrosis factor-α (TNF-α):PE (clone MP6-XT22), and IL-2:APC (clone JES6-5H4, all from eBiosciences) (30 min at 4°C). All antibodies used for the stainings were diluted 1:200 in FACS buffer. After three washing steps in FACS buffer, the cells were submitted to quantification via flow cytometry using a FACSCanto (BD Biosciences) and analyzed by using the FlowJo 10 software (FlowJo, LLC, Ashland, OR, USA).

3.9.2. Evaluation of Cytokine Release

Cells isolated from spleen and lymph nodes were restimulated for 72 h with 2 µg/ml MOMP. Cells stimulated with concanavalin A (ConA, Sigma Aldrich, 5 µg/ml) and complete medium only were used as positive and negative controls, respectively. After incubation, the concentrations of IFN-γ, IL-17, and IL-5 in the supernatants were quantified using enzyme-linked immunosorbent assay (ELISA) kits (BD Biosciences). MaxiSorp plates (Nunc, Roskilde, DK) were coated with the respective capture anti-mouse antibodies (IFN-γ, IL-17 and IL-5) overnight at 4°C, and subsequently blocked with 2% (w/v) bovine serum albumin (BSA) or skim milk powder in PBS. The supernatants were added at eight-fold dilution in PBS and allowed to incubate for 2 h at rt. Biotin-conjugated anti-IFN-γ, anti-IL-17

and anti-IL-5 antibodies were added (1 h, rt) followed by addition of streptavidin-conjugated horseradish peroxidase (HRP, 30 min, rt). Detection was performed with 3,3',5,5'-tetramethylbenzidine (TMB, Kem-En-Tec, Taastrup, DK), and the reaction was stopped with 0.2 M H₂SO₄. The optical density was read at 450 nm with correction at 570 nm.

3.9.3. Evaluation of Antibody Responses in Serum

Ten days after the last immunization, blood was collected from the heart, and serum was isolated by centrifugation (10,000 g for 10 min). MaxiSorp plates (96-well) were coated with MOMP (1 µg/well) overnight at 4°C, and blocked with 2% (w/v) BSA in PBS. The serum was added in serial dilutions in PBS and incubated for 2 h at rt, followed by addition of HRP-conjugated anti-mouse IgG antibody. TMB was used for detection, and the reaction was stopped with 0.2 M H₂SO₄. The optical density was detected at 450 nm with correction at 570 nm. A cutoff based on the average background observed for the negative control (samples isolated from mice immunized with non-loaded antigen in PBS) added by three times the standard deviation was established. The reciprocal value of the highest dilution giving a signal higher than the cutoff was considered the antibody titer.

3.10. Statistical analyses

Statistics were performed by one-way ANOVA using Tukey's comparison test to analyze the differences between the groups. All calculations were carried out using OriginPro 2016 (Northampton, MA, USA).

4 RESULTS AND DISCUSSION

When designing nanoparticle-based antigen delivery systems, a number of parameters are decisive for the quality and magnitude of the immune response. In the present study, we compared the immunostimulatory activity of liposomes and hexosomes *in vitro* and *in vivo*. Although both types of self-assembled systems are based on lipids, their composition, shape and internal structure are highly diverse. For example, addition of stabilizer is required for

the self-assembly of hexosomes, and charged lipids were included to study the effect of surface charge.¹⁰³ These parameters may influence the biodistribution upon administration, cellular internalization and, most importantly, the quality and the quantity of the triggered immune response.²⁴⁰ Here we compared the physicochemical and adjuvant properties of a novel MMG-1-based hexosomal adjuvant with those of MMG-1/DDA liposomes (CAF04).⁶⁸

4.1. Systems composed of MMG-1 and phytantriol self-assemble into an inverse hexagonal phase.

Hexosomes and liposomes based on MMG-1 were prepared to study the effect of particle structure and composition on adjuvanticity. The physical characteristics of the CAF04 liposomal adjuvant were thoroughly investigated in previous studies.^{68, 69} Strong immunological responses were measured for liposomes containing 31 mol% MMG-1.⁶⁸ For this reason, a content of MMG-1 corresponding to a molar ratio of 31% was selected for the liposomes tested in the present study. To design MMG-1-based hexosomes, phytantriol (Phy) was combined with 18 mol% MMG-1 and dispersed with poloxamer 407 in PBS. At this molar ratio, the respective bulk phases displayed appropriate physical stability, *i.e.* no phase separation or precipitation was observed after several weeks of storage at rt (data not shown). In addition, the SAXS measurements revealed three distinct peaks for Phy/MMG-1 (18 mol%) at $1.617 \pm 0.001 \text{ nm}^{-1}$, $2.805 \pm 0.004 \text{ nm}^{-1}$ and $3.247 \pm 0.009 \text{ nm}^{-1}$ (Figure 35). These peaks correspond to the 1, $\sqrt{3}$ and $\sqrt{4}$ reflections, which are characteristic for the inverse hexagonal (HII) structures of hexosomes.¹⁵²

For a number of adjuvant systems, DDA has been shown to play an important role for induction of immune responses.^{68, 69, 241} This activity has been largely attributed to the positive headgroup charge, but the adjuvant mechanisms of DDA are not fully clarified yet.^{242, 243} To investigate the impact of DDA on the biological performance of hexosomes, DDA was included in one of the formulations. Likewise, formulations containing zwitterionic DPPC or anionic DPPG were included to study the effect of surface charge (Table 6).

DDA, DPPC, and DPPG were added at 2 mol%, resulting in the self-assembly of hexosomes (Figure 35) with highly diverse zeta potentials (Table 6). Reflections characteristic for HII

structures were measured for all dispersions (Figure 35), indicating that the internal arrangement of the self-assembled nanoparticles is similar to that measured for Phy/MMG-1 hexosomes. Interestingly, the addition of charged lipids induced an enlargement of the lattice parameter from 4.48 ± 0.01 nm for Phy/MMG-1 to 4.56 ± 0.01 nm, 4.62 ± 0.01 nm, and 4.80 ± 0.01 nm for dispersions containing DDA, DPPC, and DPPG, respectively. Preservation of the HII structure and an increase of the lattice parameter upon incorporation of charged lipids have also been observed for hexosomes based on Phy and mannide monooleate in previous studies.⁸⁸ In the present work, DPPG had the most pronounced impact on the hexagonal arrangement, inducing an increase in the lattice parameter of approximately 0.32 nm. This can be explained by the negative charge and the larger headgroup volume of DPPG as compared to DDA or DPPC.¹⁶⁹ Taking into account that the Phy/MMG-1 dispersion has a net negative zeta potential (Table 6), the inclusion of a more bulky group with the same net charge may induce repulsion in the headgroup region of the hexagonal arrangement, eventually resulting in an increased lattice parameter. Similarly, DPPC also has a bulky headgroup. However, due to the zwitterionic character, the overall charge of DPPC is neutral. As a result, both the repulsion and its impact on the lattice parameter were weaker for DPPC, as compared to DPPG. The HII structure appears to have a high accommodation capacity for DDA, which promotes minimal increase of the lattice parameter due to its relatively small and positively charged headgroup.

Measurements of the z-average hydrodynamic radius suggested that the hexosomes are smaller than the CAF04 liposomes and show a more heterogeneous size distribution (Table 6). However, these results should be interpreted with caution because the measurements of the hydrodynamic diameter are based on the assumption that the nanoparticles are spherical.²⁴⁴ While liposomes are known to adopt a spherical shape, hexosomes can be elongated.²⁴⁵ In addition, hexosomes are coated with a layer of steric stabilizer (poloxamer 407), which may influence the diffusion rate of the particles, and thus may alter their hydrodynamic size. For this reason, the dispersions were also characterized by cryo-TEM, which enables a detailed morphological evaluation of the particles in the frozen-hydrated state.⁹⁶ Electron micrographs revealed that CAF04 liposomes are unilamellar vesicles displaying a faceted morphology (Figure 36A).⁶⁹ The faceted appearance of liposomes containing DDA has been previously reported, and it may be attributed to the fluidity/rigidity of the bilayer and the phase transition temperature of the lipid mixture.⁶⁸

The electron micrographs of the hexosomes (Figure 36B-E) corroborated the SAXS data, as they showed internally-structured particles featuring curved striations and/or a hexagonal shape, which is characteristic for hexosomes.⁹⁷ In addition, the images of the hexosomes (Figure 36B-E) confirm the size heterogeneity also suggested by the DLS measurements (Table 6).

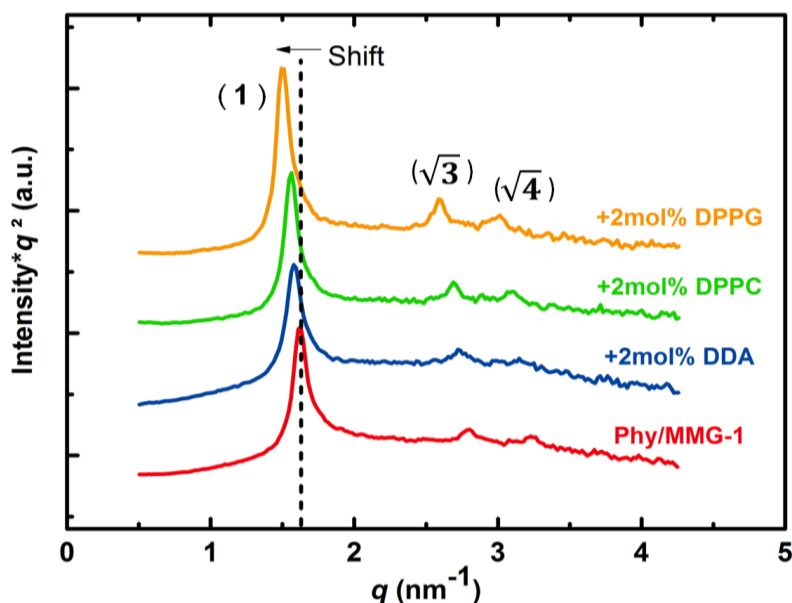


Figure 35: SAXS curves recorded at 37°C for hexosomes dispersed in PBS (pH = 7.4) composed of either Phy/MMG-1 (—) or Phy/MMG-1 + 2 mol% of either DDA (—), DPPC (—) or DPPG (—), stabilized with 3.25 mol% poloxamer 407. The curves are shifted vertically for clarity. The dashed line indicates a shift of the Bragg reflections to lower q -values for samples containing charged lipids.

Table 6: z -average, PDI, and zeta-potential of MMG-1-based liposomes and hexosomes dispersed in PBS (mean values \pm SD, $n = 3$)

Adjuvant	z -Average (d.nm)	PDI	Zeta-potential (mV)
CAF04	186 \pm 1	0.17 \pm 0.01	50.7 \pm 2.5
Phy/MMG-1	151 \pm 2	0.34 \pm 0.04	-8.1 \pm 0.4
Phy/MMG-1 +DDA	107 \pm 1	0.29 \pm 0.03	18.6 \pm 0.8
Phy/MMG-1 +DPPC	140 \pm 3	0.46 \pm 0.05	-8.9 \pm 0.8
Phy/MMG-1 +DPPG	143 \pm 2	0.42 \pm 0.01	-30.2 \pm 0.7

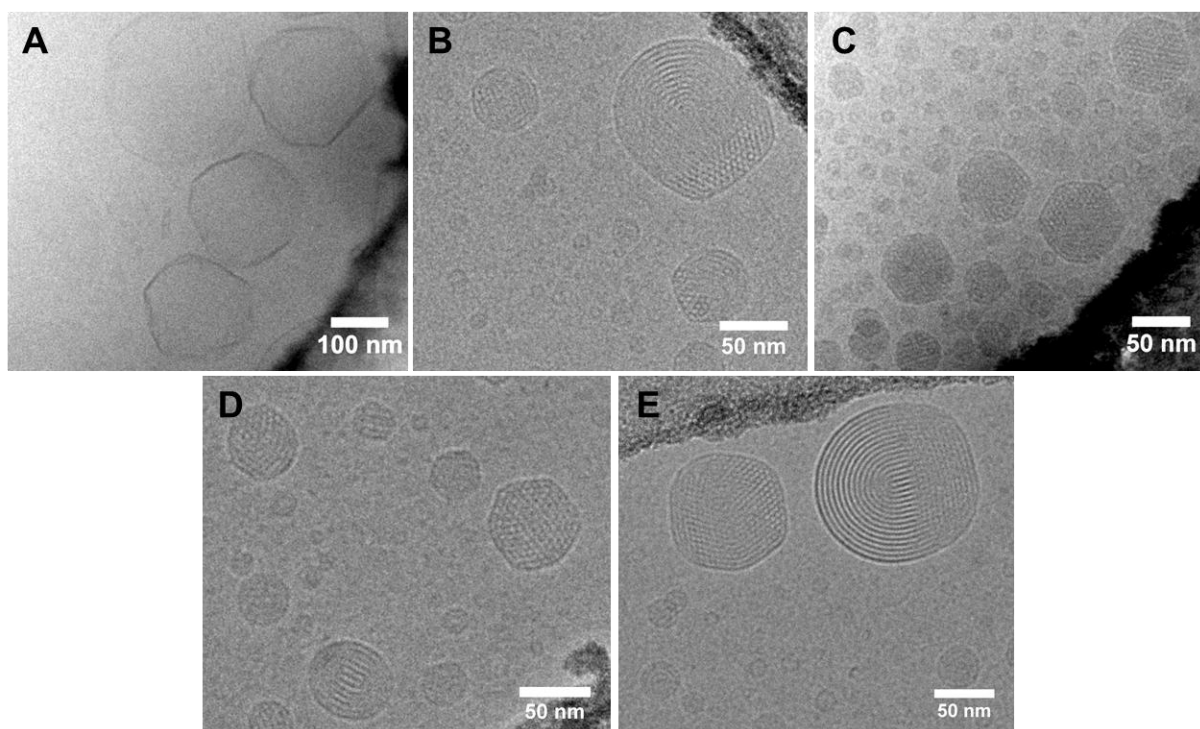


Figure 36: Representative cryo-TEM images of CAF04 liposomes (A) and hexosomes composed of Phy/MMG-1 (B), Phy/MMG-1 + 2 mol% of either DDA (C), DPPC (D) or DPPG (E), all stabilized with 3.25 mol% poloxamer 407.

4.2. MMG-1-based hexosomes do not induce DC maturation, whereas CAF04 liposomes stimulate up-regulation of CCR7.

Initially, the immunostimulatory potential of the adjuvants was evaluated *in vitro* in cultures of human PBMC-derived DCs by examining their effects on the expression level of selected, relevant maturation markers using flow cytometry (Figure 37). The nanoparticle dispersions were administered to the cells at a well-tolerated adjuvant concentration of 20 pmol/ml, which was pre-determined using the MTS/PMS viability assay (data not shown). Incubation of PBMC-derived DCs with MMG-1-based hexosomes did not affect the expression level of any of the examined maturation markers (Figure 37). In contrast, CAF04 liposomes induced an increase in the expression of CC-chemokine receptor 7 (CCR7). The homing receptor CCR7 is expressed only at very low levels by immature DCs. In response to up-regulation of CCR7, DCs migrate to the draining lymph nodes.²⁴⁶ These results suggest that CAF04 liposomes may have the capacity to induce lymph node homing of human PBMC-derived

DCs. To exclude that the absence of DC stimulation upon incubation with hexosomes was not due to lack of internalization, uptake experiments were performed and analyzed via flow cytometry, which clearly showed internalization of hexosomes to the same extent as found for liposomes in an energy-dependent manner (Figure 38).

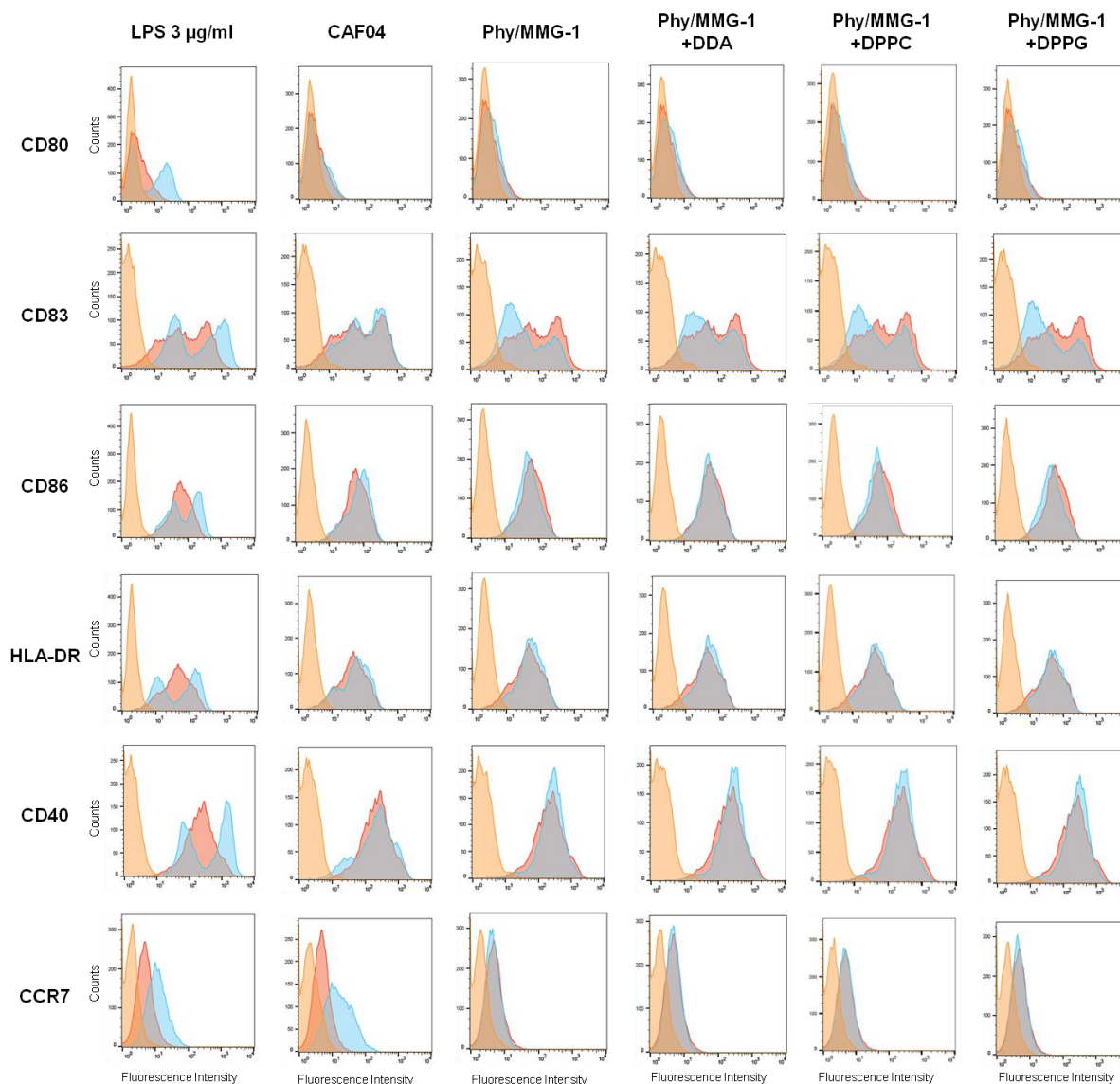


Figure 37: Histograms showing the expression of the surface activation markers CD80, CD83, CD86, HLA-DR, CD40 and CCR7 by PBMC-derived DCs after 48 h of stimulation with liposomes (CAF04) and hexosomes (Phy/MMG-1; Phy/MMG-1+DDA; Phy/MMG-1+DPPC; Phy/MMG-1+DPPG). Yellow: isotype control; Red: unstimulated cells; Blue: stimulated cells. Representative plots of three analyses are shown. Acquisition gates were introduced in the granulocyte cell population in the forward scatter (FSC) versus side scatter (SSC) plot (not shown).

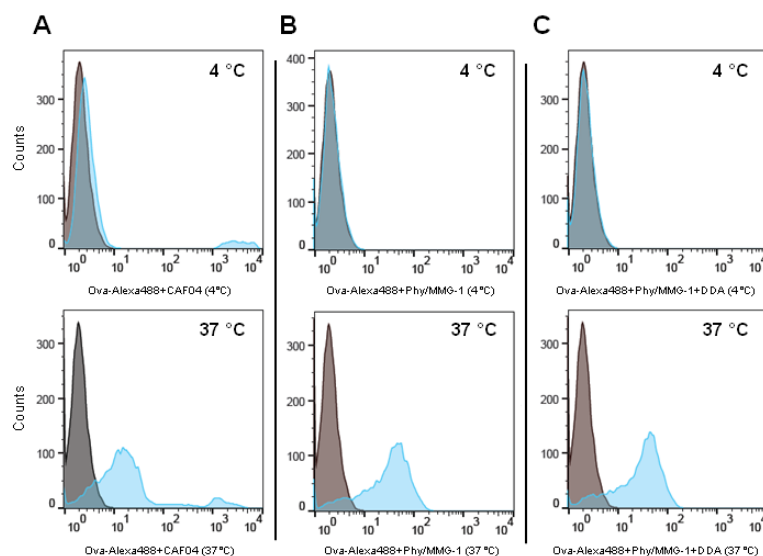


Figure 38: Histograms showing the uptake of formulations by DC-PBMCs *in vitro*. DC-PBMCs were incubated with CAF04 liposomes (A), Phy/MMG-1 hexosomes (B) and Phy/MMG-1 + DDA hexosomes (C) at 4 °C and 37 °C for 2 h. Particle internalization was quantified by flow cytometry. Gray: cells incubated with unlabeled formulations. Blue: cells incubated with formulations containing Alexa488-labeled OVA. Representative plots of three analyses are shown.

4.3. MMG-1-based hexosomes and CAF04 liposomes induce antigen-specific CD4⁺ T-cell responses characterized by different cytokine profiles.

The adjuvanticity of cationic liposomes and hexosomes *in vivo* was compared using the MOMP antigen from *C. trachomatis*. In the present work, mice were immunized twice subcutaneously with MOMP antigen alone or with MOMP adjuvanted with the particle dispersions. Activation of MOMP-specific CD4⁺ and CD8⁺ T cells in the spleen and lymph nodes was measured as CD44 upregulation. The expression level of CD44 was used to distinguish naïve T cells (CD44^{low}) from activated antigen-specific T cells (CD44^{hi}).²⁴⁷ Using ICS and flow cytometry, CD8⁺CD44^{hi} and CD4⁺CD44^{hi} T cells were subsequently analyzed for their secretion of IL-2, IFN- γ , and TNF- α .

Analyses of the antigen-specific CD4⁺CD44^{hi} and CD8⁺CD44^{hi} T-cell populations revealed significantly larger populations of activated cells only for splenocytes from mice immunized with hexosomes containing either DDA, DPPC or DPPG, compared to those from mice immunized with unadjuvanted MOMP (Figure 39). Significant differences were not

observed between the effects of these three differently charged hexosomes. It has already been reported that unadjuvanted MOMP induces immune responses (self-adjuvant effect).²³⁷ This could explain the similarity between the activated antigen-specific T-cell populations encountered in lymph nodes for all formulations (Figure 40) and in the spleens of mice vaccinated with MOMP adjuvanted with either CAF04 or Phy/MMG-1 compared to unadjuvanted MOMP (Figure 39).

In the lymph nodes of mice vaccinated with MMG-1-based particles, there was no measurable statistically significant advantage regarding the expansion of antigen-specific CD4⁺ and CD8⁺ T-cell (CD44^{hi}) populations in comparison to unadjuvanted MOMP (Figure 40).

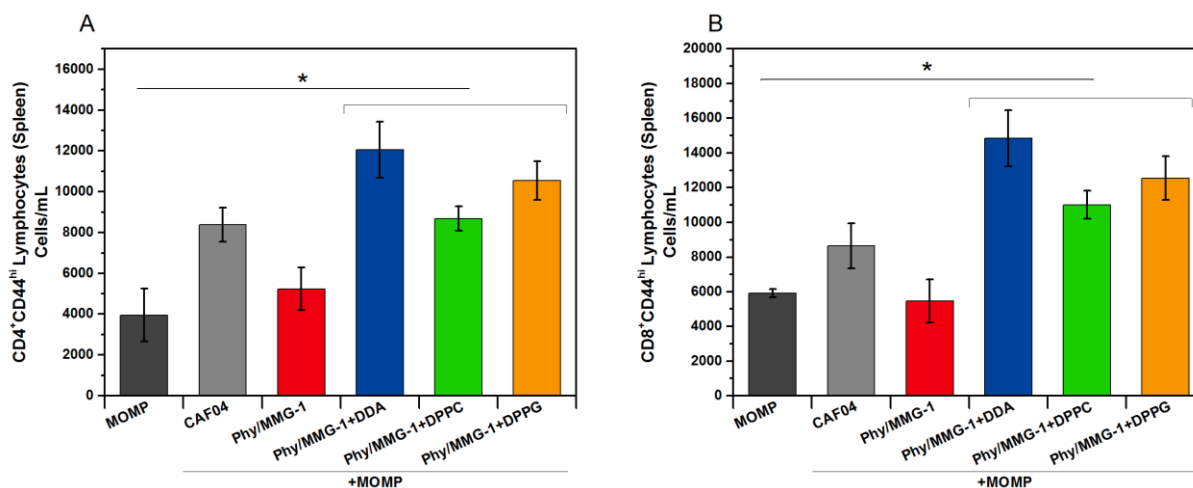


Figure 39: MOMP-specific, activated (CD44^{hi}) CD4⁺ (A) and CD8⁺ (B) T cells from spleen. Ten days after the second immunization, splenocytes were isolated and restimulated with MOMP *ex vivo*. The frequencies of MOMP-specific CD4⁺CD44^{hi} and CD8⁺CD44^{hi} lymphocytes were measured by flow cytometry. Columns represent average values \pm SEM ($n = 6$). *, $p < 0.01$ (comparison between control mice immunized with unadjuvanted MOMP in PBS and mice immunized with MOMP adjuvanted with hexosomes containing DDA, DPPC or DPPG).

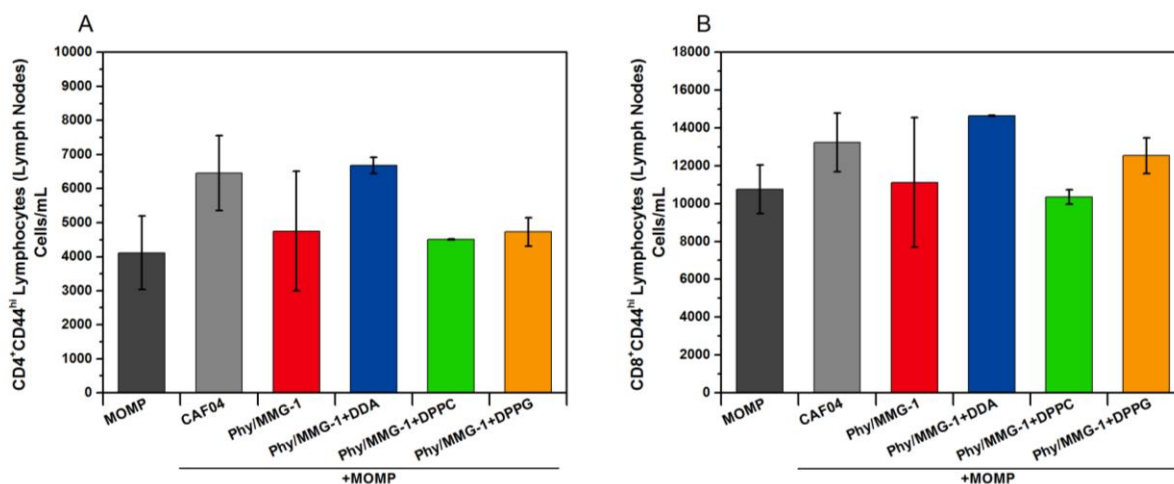


Figure 40: MOMP-specific, activated (CD44^{hi}) CD4⁺ (A) and CD8⁺ (B) T cells from inguinal lymph nodes. Ten days after the second immunization, cells were isolated from the lymph nodes and restimulated with MOMP *ex vivo*. Frequencies (cell numbers) of MOMP-specific CD4⁺CD44^{hi} and CD8⁺CD44^{hi} lymphocytes were analyzed by flow cytometry. Columns represent average values \pm SEM ($n = 6$).

Measurement of the MOMP-specific intracellular cytokine levels in CD4⁺CD44^{hi} splenocytes revealed significantly higher numbers of IL-2-producing cells in mice immunized with hexosomes containing either DDA, DPPC or DPPG than in mice immunized with CAF04-adjuvanted MOMP or unadjuvanted MOMP (Figure 41A). Interestingly, these three different hexosome-based adjuvants also induced the largest populations of CD4⁺CD44^{hi} and CD8⁺CD44^{hi} T cells (Figure 39). These findings may be explained by the growth-promoting function of IL-2, which induces survival and proliferation of antigen-specific T cells.²⁴⁸ In contrast, significantly larger populations of CD4⁺CD44^{hi} splenocytes producing intracellular IFN- γ and TNF- α were measured following immunization with CAF04 liposomes compared to unadjuvanted MOMP and MOMP adjuvanted with hexosomes. These findings suggest that hexosomes and liposomes induce qualitatively different immunological responses. While IL-2 promotes differentiation and expansion of T-cell populations, IFN- γ and TNF- α have effector functions, and are essential for processes related to the direct killing of infected cells and the elimination of intracellular pathogens.^{249, 250} The levels of all three intracellular cytokines in mice vaccinated with hexosomes containing either DDA, DPPC or DPPG were comparable.

In contrast to the intracellular cytokine levels in spleen cells (Figure 41A), the frequency of cytokine-producing cells from the inguinal lymph nodes (Figure 41B) was significantly increased only for TNF- α in mice vaccinated with MOMP adjuvanted with CAF04 liposomes in comparison with MOMP antigen alone. There were no statistical differences in the IL-2 and IFN- γ levels in cells from the lymph nodes of mice vaccinated with the different formulations.

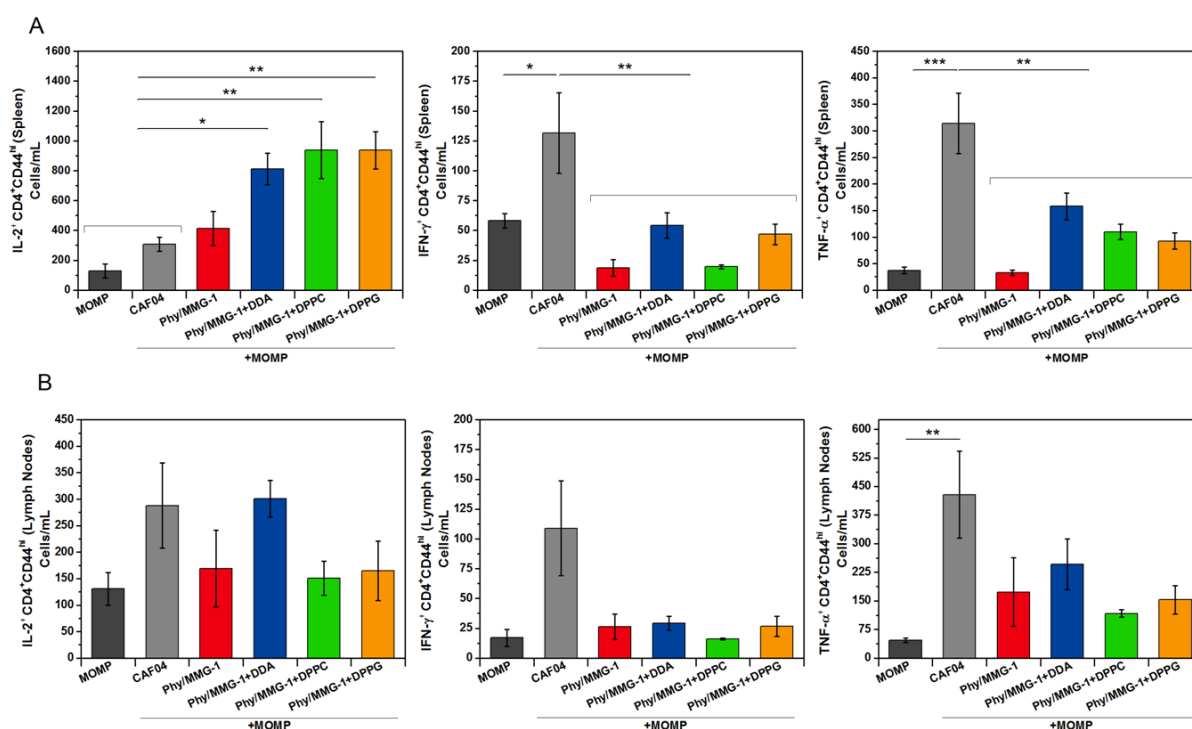


Figure 41: MOMP-specific CD4⁺ T-cell responses of cells from spleen (A) and inguinal lymph nodes (B) restimulated with MOMP, measured by intracellular cytokine staining. Ten days after the second immunization, the spleens and lymph nodes were collected, and the numbers of MOMP-specific CD44^{hi}CD4⁺ T cells producing either IL-2, IFN- γ , or TNF- α were analyzed by flow cytometry. Columns represent mean values \pm SEM ($n = 6$). *, $p \leq 0.05$; **, $p \leq 0.01$; ***, $p \leq 0.001$ compared to the highlighted groups.

4.4. MOMP adjuvanted with CAF04 liposomes induces higher CMI responses than MOMP adjuvanted with MMG-1-based hexosomes.

In addition to the magnitude of the T-cell response, several recent studies suggest that the quality of the T-cell response is an additional crucial factor for vaccine-induced protection.⁷

Polyfunctional T cells produce different cytokines simultaneously and exert multiple effector functions.²⁵¹ A number of studies have linked the induction of polyfunctional T-cell responses with improved protective efficacy, as compared to the efficacy of monofunctional T-cell responses.^{7, 252, 253} The T cells within the CD4⁺CD44^{hi} population were divided in seven groups, based on their secretion of IL-2, IFN- γ or TNF- α alone, or in any combination to further investigate the relative frequencies of multifunctional cells. Unadjuvanted MOMP induced predominantly single-positive cells and minor populations of multifunctional cells (Figure 42A). MOMP adjuvanted with CAF04 liposomes induced single-positive but also multifunctional cell subsets expressing IL-2 and TNF- α , as well as triple-positive cells (Figure 42B). The IL-2 single positive cells dominated the T-cell response after vaccination with hexosomes, representing 75-90% of the subpopulation (Figure 42C-F). IL-2 plays an important role for T-cell proliferation, survival and the longevity of the response.²⁴⁸ Several studies suggest that IL-2-single positive cells are potential central memory T cells (T_{CM}), which remain after the infection has been reduced or the antigen has been eliminated.^{7, 254} T_{CM} cells are crucial for long-term immunity by mediating rapid antigen recall responses, which are characterized by high expression of IL-2 and induction of killing mechanisms.⁷

In contrast, the subpopulation profile observed in mice vaccinated with MOMP adjuvanted with CAF04 liposomes was more diverse, including potential T_{CM} cells and potential effector/effector memory T cells (T_{E/EM}) characterized by IFN- γ production.²⁵⁵ This suggests improved T-cell response induced by MOMP adjuvanted with CAF04 liposomes in comparison with the responses elicited by unadjuvanted MOMP and MOMP adjuvanted with hexosomes. Through the simultaneous secretion of IFN- γ and TNF- α , functions related to direct killing of parasites may be activated. The combined secretion with IL-2 supports survival and expansion of this cell population.⁷

Since other studies imply that the quality and frequency of subsets of cytokine-secreting T cells may depend on the strength and duration of the antigen signal,²⁴⁹ we suggest that the observed differences may be explained by different clearance kinetics of hexosomes and liposomes. For instance, it is well known that the adjuvant mechanism of cationic liposomes involves the formation of a depot at the injection site, which causes binding and retention of the antigen.^{68, 256} This results in a delayed clearance of the antigen and prolonged vaccine exposure compared to vaccination with unadjuvanted antigen.^{68, 256} Thus, this adjuvant

enhances antigen presentation, and the consequence is induction of stronger CMI responses.²⁵⁷ In contrast, hexosomes are sterically stabilized with poloxamer 407, and depot formation at the site of injection is therefore less likely. However, further studies of the biodistribution profile of hexosomes are needed to confirm this hypothesis. Induction of IL-2-only secreting cells may be an indication of insufficient T-cell stimulation, or suggestive of the termination of T-cell effector responses and differentiation into T_{CM} cells.^{254, 255}

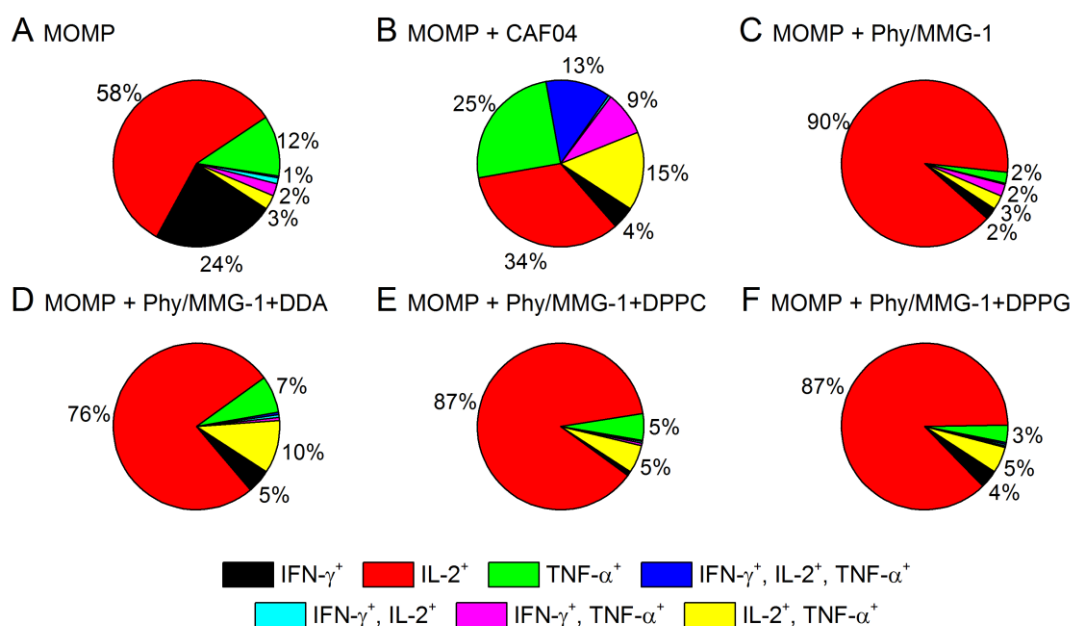


Figure 42: Polyfunctionality analysis by Boolean gating of cytokine-producing MOMP-specific CD4⁺CD44^{hi} splenocytes. Cells isolated from mice immunized with unadjuvanted MOMP (A), MOMP surface-adsorbed to CAF04 liposomes (B), and MOMP loaded in MMG-1-based hexosomes (C-F). Only groups with data $\geq 1\%$ are shown.

The polyfunctionality profiles of CD4⁺CD44^{hi} T cells isolated from lymph nodes were again very different between the groups of mice vaccinated with unadjuvanted MOMP, MOMP surface-adsorbed to CAF04 liposomes, and MOMP loaded in MMG-1-based hexosomes (Figure 43). However, a general observation was an increase in the frequency of multifunctional cell populations for all groups compared to the distribution found in spleens. In addition, the number of TNF- α positive cells (alone or in combination with IL-2) was increased remarkably in all groups. This was most pronounced for the hexosome-adjuvanted vaccines, which also induced higher frequencies of IFN- γ positive cells in the

lymph nodes (Figure 43C-F) than in the spleens. This suggests a stronger effector character of the activated cells and potential differentiation into both T_{CM} and T_{E/EM} cells.²⁵⁵ Therefore, vaccination with MOMP adjuvanted with CAF04 liposomes displayed again a T-cell stimulation profile of improved quality in comparison with unadjuvanted and hexosome-adjuvanted MOMP vaccines. CAF04 liposomes showed the largest subsets of double- and triple-positive cells, which could be an indication of induction of durable protection.⁷ However, further studies are needed to prove this hypothesis.

Unexpectedly, hexosomes displaying different zeta-potentials showed similar profiles with respect to the polyfunctionality of T cells in both spleen and lymph nodes.

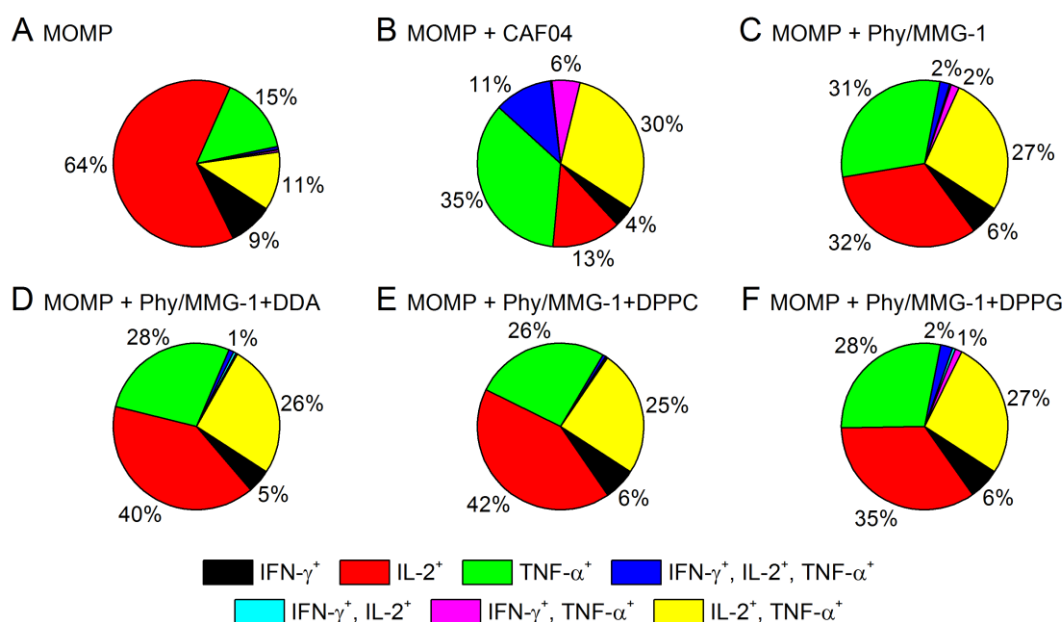


Figure 43: Polyfunctionality analysis by Boolean gating of cytokine-producing CD4⁺CD44^{hi} cells from inguinal lymph nodes. Cells were isolated from mice immunized with unadjuvanted MOMP (A), MOMP surface-adsorbed to CAF04 liposomes (B), and MOMP loaded in MMG-1-based hexosomes (C-F). Only groups with data $\geq 1\%$ are shown.

4.5. MMG-1-based hexosomes and CAF04 liposomes induce different immunostimulation

Next, we investigated the capability of antigen-specific CD4⁺ T cells from lymph nodes and spleen to produce cytokines following *in vitro* restimulation with MOMP (Figure 44). The overall cytokine secretion profile provides useful information on the quality of the cellular immune responses.^{258, 259} The release of IFN- γ , IL-17, and IL-5 was evaluated as an indication of potential Th1-, Th17-, and Th2-biased responses, respectively.

Cells isolated from spleen and lymph nodes of mice vaccinated with MOMP adjuvanted with CAF04 liposomes showed a significant increase in IFN- γ and IL-17 titers compared to the titers for mice vaccinated with unadjuvanted MOMP or MOMP adjuvanted with hexosomes (Figure 43, $p \leq 0.001$). Together with the low levels of IL-5 (Figure 43), this demonstrates that CAF04 liposomes stimulates immune responses *via* the Th1/Th17 pathway as previously reported.^{69, 260} MOMP adjuvanted with MMG-1-based hexosomes induced low levels of all three cytokines under investigation, similar to levels measured for unadjuvanted MOMP. Compared to the cytokine secretion pattern measured for mice vaccinated with CAF04-adjuvanted MOMP, these results suggest a different mechanism of immunostimulation for the hexosomes.

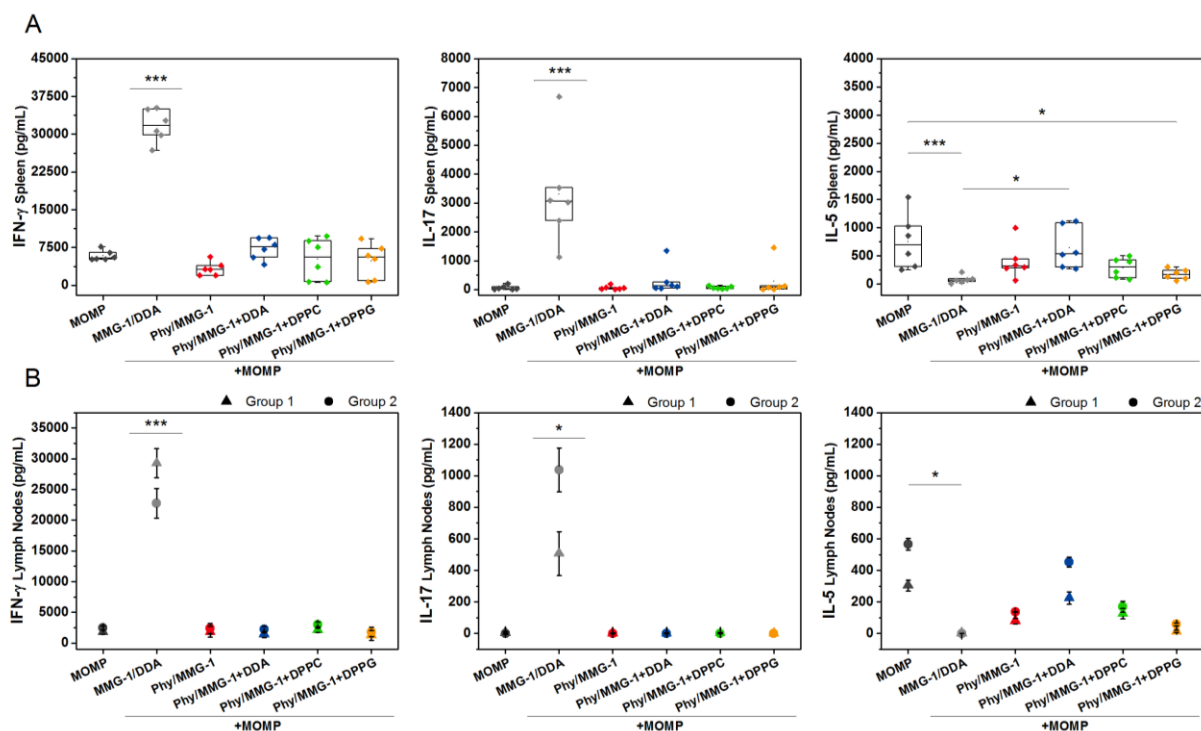


Figure 44: Release of IFN- γ , IL-17, and IL-5 determined by ELISA in the supernatant of cell cultures obtained from the spleen (A) and the inguinal lymph nodes (B). In A, each data point represents samples obtained from one mouse (n = 6). In B, each data point represents three mice pooled (average of triplicates \pm SD). *, $p \leq 0.05$ and ***, $p \leq 0.001$ compared to the group vaccinated with unadjuvanted MOMP and mice immunized with hexosome-adjuvanted MOMP, unless otherwise indicated in the graphics.

4.6. MMG-1-based hexosomes induce stronger humoral responses than CAF04 liposomes.

The MOMP-specific serum IgG titers were quantified by ELISA. Data suggest that MMG-1-based hexosomes were more efficient in inducing MOMP-specific IgG responses than MOMP surface-adsorbed to CAF04 liposomes or unadjuvanted MOMP (Figure 45). No significant differences were observed for the IgG titers between the differently charged hexosomes. The narrow data distribution within each hexosome group may indicate a more concerted and faster drainage to the lymph nodes.²⁶¹ This may be due to the steric stabilization of hexosomes by poloxamer 407. The higher IgG titers indicate that at least a fraction of the hexosomes are retained in the lymph nodes, which enables uptake by tissue-resident DCs, B cell activation and improved antibody responses.^{261, 262} Zhuang et al.

suggested that a similar mechanism is involved in the overall improvement of the immune responses elicited by PEGylated dioleoyl-trimethylammoniumpropane (DOTAP) liposomes loaded with OVA, as compared to those elicited by non-PEGylated liposomes.²⁶¹ However, in contrast to the findings of the present work, the PEGylated DOTAP liposomes studied by Zhuang et al. induced higher levels of IgG, but also levels of IFN- γ comparable to the non-PEGylated formulation.²⁶¹ These findings support the hypothesis that steric stabilization and reduction of depot formation are crucial for the induction of diverse immunological pathways and for the enhancement of humoral responses. However, other factors, *e.g.*, particle composition and structure, may also contribute to the induction of these highly diverse immune responses mediated by hexosomes and liposomes. Complementary studies are necessary to fully understand the mechanisms of action of these systems, and to determine the basis of each response. We speculate that combining the attributes of hexosomes and liposomes into one single vaccine formulation may offer a promising strategy to design new adjuvant systems capable of potentiating concomitant humoral and CMI responses. For instance, T-cell activation combined with lymphatic targeting would be optimal properties of a *Chlamydia* vaccine. Further, rational combination of the two different carriers may be used to modify immunological outcomes, and thereby induce optimal responses needed for protective immunity against a given pathogen. The present work demonstrates that the type of vaccine formulation used to deliver the antigen has a strong impact on the elicited immune responses.

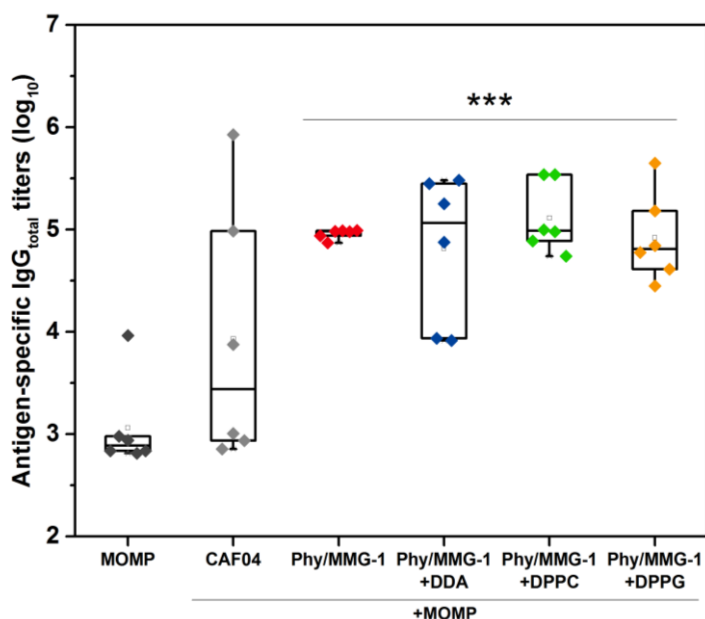


Figure 45: MOMP-specific serum IgG titers measured by ELISA. Each data point represents samples obtained from one mouse (n = 6). ***, $p \leq 0.001$ compared with the group of control mice immunized with unadjuvanted MOMP in PBS.

5 CONCLUSIONS AND OUTLOOK

This study highlights differences between the immunostimulatory behavior of MMG-1-based hexosomes and liposomes as vaccine delivery systems. While MMG-1-based liposomes induced predominantly cellular-mediated responses against the MOMP antigen, hexosomes elicited mainly humoral responses with high IgG titers, but with minimal effector T-cell stimulation. Differently charged hexosomal formulations induced comparable immune responses. The diverse immunological behavior of cationic hexosomes and CAF04 liposomes, both containing DDA and MMG-1, suggests that the nanostructure of the particles, rather than the surface charge or the adjuvant composition, dictates the immune response. This highlights a significant role of the structural features of the nanoassemblies in terms of antigen presentation to B cells, activation of DCs and overall kinetics of the immune responses. To understand further the biological performance of the novel MMG-1-based hexosomes and explain their immune profile, comprehensive biodistribution studies

monitoring kinetics, characterization of memory T cells, and tracking of antigen-positive cells will be essential.

CHAPTER V

General Conclusions and Outlook

The principal objective of this work was the development and characterization of new vaccine carriers with adjuvant properties, based on lyotropic liquid crystalline structures. Due to the great potential of these systems and the uncountable open questions surrounding them, our attention was focused on one of the less studied assemblies, the hexosomes. In the literature only very few reports describe the development of this kind of formulation combined with an evaluation of its applicability in the biological context. The present work greatly advanced the state of knowledge in this field and gives a comprehensive description of the formulation development and biological performance of hexosomes.

In Chapter II, we showed the development of stable hexosomes based on Phy and MaMo. SAXS, cryo-TEM, and polarization microscopy were used throughout this process to characterize the self-assembled structure. Additionally, we demonstrated a great versatility of these particles by modifying size, surface charge, and internal structure in a controlled manner. We were also able to show that these systems can be stabilized by a range of different surfactants including poloxamer 407, Myrj 59, and Pluronic F108. These findings argued against the common knowledge that particles internally structured with lyotropic liquid crystals are difficult to customize due to their highly sensitive internal structures.¹⁰⁰ When compared to the development of liposomal formulations, where measurements of size

and zeta potential usually drive the initial establishment of the systems, the formulation development of non-lamellar structured particles is much slower and challenging. In this case, the formulation development is initially guided exclusively by the resulting internal structure of the particles and the size optimization is performed in a posterior stage. Thus, at the beginning, the development work is driven by laborious methods and techniques that are not easily accessible (*e.g.* SAXS, cryo-TEM). This highlights the need to establish other approaches that enable the acquisition of structural information. In this work, we chose a less costly approach by using polarization microscopy to create a phase diagram to screen compositions before employing SAXS measurements. This strategy clearly facilitated the formulation development and allowed for drastic reduction of the number of samples measured with SAXS. However, it is only applicable for bulk phases. This is an important limitation, because the particle preparation requires the addition of steric stabilizer and this might impact the internal structure of the particles. Other approaches based on sample turbidity and viscosity could also be developed to investigate bulk phases.¹⁰⁰ However, their application in particle dispersions is also difficult due the fundamental role played by sample concentration in the determination of turbidity and viscosity. Differential scanning calorimetry (DSC) of high sensitivity has been used to determine the phase transition temperatures of lipid-based particles.²⁶³⁻²⁶⁵ This may assist the strategic planning of SAXS measurements and allow for a reduction of the number of temperature points measured per sample. If SAXS lab sources are used, acquisition times can be very long (up to hours) and a previous scanning of phase transitions with DSC may optimize the overall experiment duration.

In this study, we also investigated the particle loading of two different model antigens, OVA and LYS. Our data indicated a geometric mismatch between the dimensions of the repeating unit (lattice parameter) and the cargo proteins. This suggested that the loaded proteins could not be entrapped in the water channels of the hexosomes without considerably impacting the HII structure. Based on these findings we proposed a loading mechanism based on interactions with the lipidic network. However, this hypothesis has not been confirmed yet and the localization of the entrapped macromolecule has yet to be clarified. This is an interesting matter, but also very challenging to solve. We believe that small angle neutron scattering (SANS) combined with computer simulation and modeling might be the most suitable approach to investigate this issue. SANS enables the differentiation between

different molecules, based on the scattering length density and contrast-match in D₂O.²⁶⁶ Approaches based on fluorescent labeling of components, such as Förster resonance energy transfer (FRET), are not suitable for this investigation, because the staining might change the properties of the molecule and change the manner in which the protein interacts with the lipid molecules. Thus, as generally observed in the field of lyotropic liquid crystalline dispersion for biomedical uses, the interdisciplinary work is essential for the obtention of fast progress. Considering a potential application of hexosomes as vaccine carriers, it will be crucial to elucidate the loading mechanism of different antigens (*e.g.* surface adsorption, encapsulation) as this is known to play an important role in the induction of immune responses.²⁶⁷ Although we were unable to clarify how exactly proteins are entrapped into hexosomes, we demonstrated a reproducible approach to produce stable and versatile hexosomes loaded with model antigens, which have a potential as vaccine delivery systems.

Following the development of Phy/MaMo hexosomes, Chapter III focuses more in detail on the interaction of these systems with HeLa cells and model membranes. It has been hypothesized that one of the most advantageous properties of non-lamellar structured particles is their potential fusogenic character, which would enable delivery of sensitive biomolecules directly to the cytoplasm.^{103, 104} In the context of vaccination, this may play a major role in antigen presentation via MHC class I and a consequent induction of CTL.¹⁴³ Contrary to the expectations, the hexosomes used in our study did not appear to have the ability to fuse with membranes. We found that the uptake of Phy/MaMo hexosomes was not mediated by any of the major endocytic mechanisms but instead induced through distortions of the cell membrane that allowed their rapid passage through this barrier. This was only reduced or inhibited by high membrane tension and rigidity, which further supports the hypothesis of a cell entry mechanism based on a direct interaction of the particles with the membrane. In comparison to DOPC/DOPE-based liposomes, the internalization efficiency of hexosomes was particularly superior. However, this rapid uptake kinetics appeared to correlate with higher toxicity. It is important to highlight that all experiments were performed with the formulations at concentrations considered safe according to the viability assay (MTT test). Comprehensive analysis using POPC model membranes (calcein leakage assay, Langmuir monolayer and giant vesicles) indicated a surprisingly high affinity of hexosomes for the lipid membranes when compared to their neat components and to liposomes. These results suggest that hexosomes could be

promising delivery systems for therapeutic molecules whose target is localized intracellularly or molecules that normally do not have the ability to get through the cell membrane. To the best of our knowledge, this study reports for the first time how hexosomes are internalized by cells. Despite of the encouraging findings, further efforts are necessary to evaluate the reproducibility of our results with other cell types. In addition to this, considering a potential application of hexosomes as cytoplasmatic delivery systems for sensitive biomolecules, it is of utmost importance to elucidate the intracellular fate of their cargo molecules. In this regard, the analysis of uptake and fate of hexosomes loaded with different molecules may provide clear insights about their capacity to circumvent the endosomal/lysosomal system. To this end, we believe that transmission electron microscopy is the method of choice. Despite being laborious and time consuming, this method could enable direct visualization of the integrity and fate of hexosomes after cell entry. Other techniques, such as confocal microscopy, require fluorescent labeling and enable solely an indirect analysis. Considering that our findings suggested a direct interaction of the hexosomes with the cell membrane, it is of fundamental importance to evaluate how the surface properties of these particles (*e.g.* charge, different densities and lengths of steric stabilizers) affect the cellular uptake. For this purpose, the customization strategies described in Chapter II could be applied. Overall, the findings reported in Chapter III provide a good starting point to understand the performance of hexosomes in the biological environment. Moreover, these data open new horizons with respect to potential applications for hexosomes in the biomedical context. However, it is evident that much remains to be done in order to establish these particles as vaccine/drug delivery vehicles.

In Chapter IV, the adjuvancity of hexosomes based on Phy and MMG-1 was studied *in vitro* and *in vivo*. MMG-1 is a synthetic analogue of the mycobacterial lipid monomycoloyl glycerol found to have promising adjuvancity especially when combined to cationic liposomes.^{68, 69} In our studies, to enable comparability to established and well known delivery systems with immunostimulatory character, the positive control used consisted of cationic liposomes based on MMG-1 and DDA (CAF04). A limiting factor in the formulation development of Phy/MMG-1 hexosomes was the challenging preparation of synthetic MMG-1. By applying the knowledge that we gained from the studies shown in Chapter II, we were able to significantly shorten and to simplify this process. Hence, a range of differently charged hexosomes was created and compared to CAF04.

Interestingly, all aspects evaluated (*e.g.* expression of surface markers by DCs derived from PBMCs, T-cell activation, cytokine expression and release, polyfunctionality, specific serum IgG) revealed highly contrasting results for liposomes and hexosomes. Overall, the immunogenicity of liposomes was determined mainly by cellular-mediated responses, and the responses induced by hexosomes were predominantly humoral. Furthermore the different hexosomal formulations showed similar activity, indicating that the charges played only a minor role (if any) in the adjuvancity of these particles. It is extremely challenging to explain the differences between the performances of hexosomes and liposomes and to track the origin of each outcome. This is because, besides structural aspects, the two types of nanoparticles comprise different amounts of lipid per particle, vary in their physicochemical properties and interact differently with the entrapped antigen. Considering that all these aspects may influence the type and kinetics of the immune responses elicited, an unequivocal and straightforward interpretation of the experimental outcomes is difficult in this stage. Additionally, it is important to consider that the punctual analysis of the correlates of immunogenicity does not reveal the whole immunological outcome. Therefore, additional experiments to monitor the kinetics of the responses and determine their profile as a whole seem to be critical. Moreover, to explain the type and magnitude of the responses elicited, the investigation of biodistribution of the carriers and tracking of antigen-positive cells are fundamental.

In these experiments we studied the responses against the *Chlamydia* antigen MOMP. The protection against MOMP is typically induced via the CD4 signaling pathway.²⁶⁸ For this reason, another important open research question is whether hexosomes are able to delivery antigen directly to the cytosol, which may help to induce CTL responses. In Chapter III, we reported interesting evidences suggesting that hexosomes are internalized through an uncommon uptake mechanism based on the direct interaction of these particles with the cell membrane. Based on this, it could be speculated that hexosomes are potential cytoplasmatic delivery systems. This kind of antigen delivery could mimic the antigen presentation of intracellular pathogens and facilitate CTL responses.¹⁴³ To investigate this hypothesis it would be necessary to perform *in vivo* immunization studies with an antigen characterized by both signaling pathways (*i.e.* CD4 and CD8), such as OVA.^{73, 269}

The present work presents new insights in the fields of vaccine delivery and lyotropic liquid crystalline dispersions. Great progress was made regarding the development and application of hexosomes. Further efforts are needed to continue increasing the understanding about these remarkable particulate systems and to ultimately establish them as vaccine/drug carriers. Overall, this thesis provides an essential contribution to provoke new discussions and guide future works in the field of vaccine delivery and lyotropic liquid crystalline dispersions.

SUMMARY

In this work, combined interdisciplinary research in the fields of Pharmaceutical Technology, (Bio)Materials Science, and Biology is presented to understand and promote lyotropic liquid crystalline dispersions as novel vaccine carriers.

The work was initiated with a detailed development of lyotropic mesophases based on phytantriol. The aim was to gain knowledge on the phase behavior of the system and also on the structural impact of additives. Therefore, formulations with increasing degree of complexity were sequentially characterized. The study started establishing a phase diagram, in which bulk phases of phytantriol in excess of highly purified water were characterized, upon temperature increase, applying polarization microscopy and small angle X-ray scattering (SAXS). Subsequently, pursuing the development of a system with immunostimulatory properties, the impact of mannide monooleate on phytantriol-based mesophases was investigated. Mannide monooleate is an emulsifier widely used in adjuvant formulations and found to promote immune responses in emulsion form. Thus, progressively higher amounts of mannide monooleate were incorporated into the system and the structural modifications were monitored upon temperature increase. The phase diagram allowed for a deep understanding of the mesophase behavior and enabled the selection of a feasible phytantriol/mannide monooleate ratio for the subsequent investigations. In this way, a stable formulation, featuring inverse hexagonal structure was identified. Next, to enable dispersion of the characterized bulk and to produce a nanoparticulate system, different steric stabilizers were evaluated. Here, the selection criteria were based on the dispersion efficiency at low concentrations and on the impact on the internal structure of the particles. The last part of the formulation development was concerning the application and customization of the formed hexosomes. Thus, the particle loading with the model antigens ovalbumin and lysozyme was studied, as well as strategies to introduce new features to the particulate system in a controlled way, preserving the inverse hexagonal structure. Here, negatively and positively charged hexosomes could be prepared through the incorporation of charged phospholipids into the formulation. Additionally, a formulation based on phytantriol and mannide monooleate, which typically formed an inverse hexagonal structure was shown to self-assemble with bicontinuous cubic double diamond structure upon addition of octyl- β -D-glucopyranoside.

The aim of the second part of this work was the verification of one of the most important hypothesis with respect to the biological performance of non-lamellar lyotropic liquid crystalline dispersions. More specifically, it is known that non-lamellar structures are involved in fusogenic processes of the cell membrane. For this reason, it was speculated that particles internally structured with non-lamellar phases, such as hexosomes, could have fusogenic properties. Thus, to verify this hypothesis and elucidate the cellular uptake mechanism of hexosomes, we investigated the interactions of these particles with cells and with models of the cell membrane. For this purpose, the established hexosomes, based on phytantriol/mannide monooleate, were fluorescently labeled and their toxicity in cultures of HeLa cells was determined. Series of uptake experiments were carried out after suppression of the major endocytic pathways using highly specific approaches (*e.g.* single and double knockdown of regulatory proteins), and also inhibition strategies of broader effect (*e.g.* temperature reduction to 4°C, hypotonic treatment, cytochalasin D treatment). Additionally, experiments using models of the cell membrane (*e.g.* phospholipid monolayers and bilayers) were performed. All the analyses were carried out with hexosomes and liposomes in parallel to enable the comparison between particles featuring non-lamellar and lamellar structures, respectively. The results revealed a steeper toxicity curve and faster internalization kinetics for hexosomes in comparison to liposomes. Interestingly, against the expectations, indications of fusogenic properties were not observed. However, strong evidences that hexosomes have an alternative cell entry pathway that bypasses standard endocytosis were identified. In contrast, liposomes appeared to enter the cells through well-known endocytic pathways, such as caveolae-mediated and clathrin-mediated endocytosis.

The final part of this work consisted of the evaluation of the biological performance of hexosomes within the vaccination context. The experiments were performed *in vitro* and *in vivo*, in parallel with the already established and promising cationic liposomal formulation CAF04, which is based on dimethyldioctadecylammonium (DDA) and on a synthetic analogue of monomycoloyl glycerol (MMG-1). Since MMG-1 and the positive charge of DDA are considered the core of the success of this formulation, differently charged hexosomes containing MMG-1 were developed and included in the study. The development process was driven by the lessons learned in the first phase of the project with phytantriol/mannide monooleate systems. In this way, to create particles internally structured with inverse hexagonal phase, MMG-1 was combined to phytantriol. After the

establishment of the formulations, the immunogenicity of plain particles (without antigen) was investigated *in vitro* in cultures of dendritic cells derived from human peripheral blood mononuclear cells. Through the evaluation of the expression of several surface markers, it was found that, while CAF04 liposomes induced the upregulation of the homing receptor CCR7, all hexosomal formulations tested did not provoke any sign of adjuvanticity. Considering that the cultures of dendritic cells represent a dramatic simplification of the immune system, further experiments were performed *in vivo*. Thus, mice were immunized with the formulations loaded with *Chlamydia trachomatis* major outer membrane protein (MOMP) antigen. The immunological output was analyzed through several parameters (*e.g.* T-cell activation, cytokine expression and release, polyfunctionality, specific serum IgG) and all of them revealed dramatic differences between the immunizations performed with the unadjuvanted antigen and antigen adjuvanted with either liposomes or hexosomes. In comparison to the unadjuvanted systems, liposomes and hexosomes were both able to increase the magnitude of the immune responses. However, the immune responses elicited by CAF04 liposomes and by hexosomes were very distinct, the first eliciting mainly cellular mediated responses and the second humoral responses.

Throughout this work, it was shown that stable and robust lipid-based lyotropic liquid formulations, that allow customization without impairment of the internal structure, can be rationally designed. In addition, keeping track of the structural modifications induced by each additive (separately) was shown to be a key strategy to enable further optimization in advanced stages of the formulation development. Regarding the performance of hexosomes in the biological environment, we have obtained accurate results demonstrating, *in vitro* and *in vivo*, drastic differences in comparison to liposomes. This intriguing outcome was observed for different formulations and in completely independent experiments. Overall, the insights presented in this thesis show hexosomes as promising delivery systems with uncommon properties and an applicability potential that goes beyond the vaccination context.

REFERENCES

1. Delany, I.; Rappuoli, R.; De Gregorio, E., Vaccines for the 21st century. *EMBO Mol. Med.* 2014, 6, 708-720.
2. Oyston, P.; Robinson, K., The current challenges for vaccine development. *J. Med. Microbiol.* 2012, 61, 889-894.
3. Sullivan, N. J.; Martin, J. E.; Graham, B. S.; Nabel, G. J., Correlates of protective immunity for Ebola vaccines: implications for regulatory approval by the animal rule. *Nature reviews. Microbiology* 2009, 7, 393.
4. Koff, W. C.; Burton, D. R.; Johnson, P. R.; Walker, B. D.; King, C. R.; Nabel, G. J.; Ahmed, R.; Bhan, M. K.; Plotkin, S. A., Accelerating next-generation vaccine development for global disease prevention. *Science* 2013, 340, 1232910.
5. Burton, D. R.; Poignard, P.; Stanfield, R. L.; Wilson, I. A., Broadly neutralizing antibodies present new prospects to counter highly antigenically diverse viruses. *Science* 2012, 337, 183-186.
6. Krammer, F., The quest for a universal flu vaccine: headless HA 2.0. *Cell host & microbe* 2015, 18, 395-397.
7. Thakur, A.; Pedersen, L. E.; Jungersen, G., Immune markers and correlates of protection for vaccine induced immune responses. *Vaccine* 2012, 30, 4907-4920.
8. Plotkin, S. A.; Plotkin, S. A., Correlates of vaccine-induced immunity. *Clinical infectious diseases* 2008, 47, 401-409.
9. Mestas, J.; Hughes, C. C., Of mice and not men: differences between mouse and human immunology. *J. Immunol.* 2004, 172, 2731-2738.
10. Fowler, V.; Proctor, R. A., Where does a Staphylococcus aureus vaccine stand? *Clinical Microbiology and Infection* 2014, 20, 66-75.
11. Levine, M. M.; Sztein, M. B., Vaccine development strategies for improving immunization: the role of modern immunology. *Nature immunology* 2004, 5, 460.
12. Weinberger, B.; Herndler-Brandstetter, D.; Schwanninger, A.; Weiskopf, D.; Grubeck-Loebenstien, B., Biology of immune responses to vaccines in elderly persons. *Clinical Infectious Diseases* 2008, 46, 1078-1084.
13. Beigi, R. H.; Fortner, K. B.; Munoz, F. M.; Roberts, J.; Gordon, J. L.; Han, H. H.; Glenn, G.; Dormitzer, P. R.; Gu, X. X.; Read, J. S., Maternal immunization: opportunities for scientific advancement. *Clinical Infectious Diseases* 2014, 59, S408-S414.
14. Moyle, P. M.; Toth, I., Modern subunit vaccines: development, components, and research opportunities. *ChemMedChem* 2013, 8, 360-76.

15. Kallerup, R. S.; Foged, C., Classification of vaccines. In *Subunit vaccine delivery*, Springer: 2015; pp 15-29.
16. Moyle, P. M., Biotechnology approaches to produce potent, self-adjuvanting antigen-adjuvant fusion protein subunit vaccines. *Biotechnology advances* 2017, 35, 375-389.
17. Foged, C., Subunit vaccines of the future: the need for safe, customized and optimized particulate delivery systems. *Therapeutic delivery* 2011, 2, 1057-1077.
18. Bruno, G., The perfect mix: recent progress in adjuvant research. *Nature reviews. Microbiology* 2007, 5, 505.
19. Reed, S. G.; Orr, M. T.; Fox, C. B., Key roles of adjuvants in modern vaccines. *Nat. Med.* 2013, 19, 1597-1608.
20. Alving, C. R.; Peachman, K. K.; Rao, M.; Reed, S. G., Adjuvants for human vaccines. *Curr. Opin. Immunol.* 2012, 24, 310-315.
21. Bachmann, M. F.; Jennings, G. T., Vaccine delivery: a matter of size, geometry, kinetics and molecular patterns. *Nat Rev Immunol* 2010, 10, 787-96.
22. Rizwan, S. B.; McBurney, W. T.; Young, K.; Hanley, T.; Boyd, B. J.; Rades, T.; Hook, S., Cubosomes containing the adjuvants imiquimod and monophosphoryl lipid A stimulate robust cellular and humoral immune responses. *Journal of controlled release : official journal of the Controlled Release Society* 2013, 165, 16-21.
23. Nordly, P.; Madsen, H. B.; Nielsen, H. M.; Foged, C., Status and future prospects of lipid-based particulate delivery systems as vaccine adjuvants and their combination with immunostimulators. *Expert opinion on drug delivery* 2009, 6, 657-72.
24. Martin-Bertelsen, B.; Korsholm, K. S.; Rose, F.; Nordly, P.; Franzyk, H.; Andersen, P.; Agger, E. M.; Christensen, D.; Yaghmur, A.; Foged, C., The supramolecular structure is decisive for the immunostimulatory properties of synthetic analogues of a mycobacterial lipid in vitro. *Rsc Adv* 2013, 3, 20673-20683.
25. Pulendran, B.; Ahmed, R., Immunological mechanisms of vaccination. *Nature immunology* 2011, 12, 509-17.
26. He, P.; Zou, Y.; Hu, Z., Advances in aluminum hydroxide-based adjuvant research and its mechanism. *Human vaccines & immunotherapeutics* 2015, 11, 477-488.
27. Lindblad, E. B., Aluminum Adjuvants: Basic Concepts and Progress in Understanding. In *Subunit Vaccine Delivery*, Springer: 2015; pp 33-57.
28. Correia-Pinto, J. F.; Csaba, N.; Alonso, M. J., Vaccine delivery carriers: insights and future perspectives. *Int J Pharm* 2013, 440, 27-38.
29. Shah, R. R.; Brito, L. A.; O'Hagan, D. T.; Amiji, M. M., Emulsions as vaccine adjuvants. In *Subunit Vaccine Delivery*, Springer: 2015; pp 59-76.
30. Brito, L. A.; Malyala, P.; O'Hagan, D. T. In *Vaccine adjuvant formulations: a pharmaceutical perspective*, Seminars in immunology, Elsevier: 2013; pp 130-145.

31. Aucouturier, J.; Dupuis, L.; Deville, S.; Ascarateil, S.; Ganne, V., Montanide ISA 720 and 51: a new generation of water in oil emulsions as adjuvants for human vaccines. *Expert review of vaccines* 2002, 1, 111-118.
32. O'Hagan, D. T.; Ott, G. S.; De Gregorio, E.; Seubert, A., The mechanism of action of MF59 - An innately attractive adjuvant formulation. *Vaccine* 2012, 30, 4341-4348.
33. Mbow, M. L.; De Gregorio, E.; Valiante, N. M.; Rappuoli, R., New adjuvants for human vaccines. *Curr Opin Immunol* 2010, 22, 411-416.
34. O'Hagan, D. T.; Fox, C. B., New generation adjuvants—from empiricism to rational design. *Vaccine* 2015, 33, B14-B20.
35. Singh, M.; O'Hagan, D., Advances in vaccine adjuvants. *Nature biotechnology* 1999, 17, 1075.
36. Krieg, A. M., Therapeutic potential of Toll-like receptor 9 activation. *Nature reviews. Drug discovery* 2006, 5, 471.
37. Desel, C.; Werninghaus, K.; Ritter, M.; Jozefowski, K.; Wenzel, J.; Russkamp, N.; Schleicher, U.; Christensen, D.; Wirtz, S.; Kirschning, C., The Mincle-activating adjuvant TDB induces MyD88-dependent Th1 and Th17 responses through IL-1R signaling. *PLoS One* 2013, 8, e53531.
38. Rabes, A.; Zimmermann, S.; Reppe, K.; Lang, R.; Seeberger, P. H.; Suttorp, N.; Witznath, M.; Lepenies, B.; Opitz, B., The C-type lectin receptor Mincle binds to *Streptococcus pneumoniae* but plays a limited role in the anti-pneumococcal innate immune response. *PLoS One* 2015, 10, e0117022.
39. Guy, B., The perfect mix: recent progress in adjuvant research. *Nature Reviews Microbiology* 2007, 5, 505-517.
40. Ogawa, C.; Liu, Y.-J.; Kobayashi, K., Muramyl dipeptide and its derivatives: peptide adjuvant in immunological disorders and cancer therapy. *Current bioactive compounds* 2011, 7, 180-197.
41. Lemesre, J.-L.; Holzmüller, P.; Cavaleyra, M.; Gonçalves, R. B.; Hottin, G.; Papierok, G., Protection against experimental visceral leishmaniasis infection in dogs immunized with purified excreted secreted antigens of *Leishmania infantum* promastigotes. *Vaccine* 2005, 23, 2825-2840.
42. Tritto, E.; Mosca, F.; De Gregorio, E., Mechanism of action of licensed vaccine adjuvants. *Vaccine* 2009, 27, 3331-3334.
43. Gregory, A. E.; Williamson, D.; Titball, R., Vaccine delivery using nanoparticles. *Frontiers in cellular and infection microbiology* 2013, 3, 13.
44. Rattanapak, T.; Young, K.; Rades, T.; Hook, S., Comparative study of liposomes, transfersomes, ethosomes and cubosomes for transcutaneous immunisation: characterisation and in vitro skin penetration. *J Pharm Pharmacol* 2012, 64, 1560-1569.

45. Brito, L. A.; Malyala, P.; O'Hagan, D. T., Vaccine adjuvant formulations: a pharmaceutical perspective. *Seminars in immunology* 2013, 25, 130-45.
46. Donaldson, B.; Al-Barwani, F.; Young, V.; Scullion, S.; Ward, V.; Young, S., Virus-like particles, a versatile subunit vaccine platform. In *Subunit Vaccine Delivery*, Springer: 2015; pp 159-180.
47. Buonaguro, F. M.; Tornesello, M. L.; Buonaguro, L., Virus-like particle vaccines and adjuvants: the HPV paradigm. *Expert Rev Vaccines* 2009, 8, 1379-1398.
48. Brito, L. A.; O'Hagan, D. T., Designing and building the next generation of improved vaccine adjuvants. *J. Controlled Release* 2014, 190, 563-579.
49. Grgacic, E. V. L.; Anderson, D. A., Virus-like particles: Passport to immune recognition. *Methods* 2006, 40, 60-65.
50. Nielsen, H. M.; Hübschmann, H. B.; Rades, T., ISCOMs as a vaccine delivery system. In *Subunit Vaccine Delivery*, Springer: 2015; pp 141-158.
51. Brugmann, M.; Drommer, W.; Reichl, U.; Boge, A., [Iscom (Immuno Stimulating Complex)-vaccine of equine influenza virus--transmission electron microscopic investigation and literature review]. *DTW. Deutsche tierärztliche Wochenschrift* 1997, 104, 196-202.
52. Zhao, L.; Seth, A.; Wibowo, N.; Zhao, C.-X.; Mitter, N.; Yu, C.; Middelberg, A. P., Nanoparticle vaccines. *Vaccine* 2014, 32, 327-337.
53. Akagi, T.; Baba, M.; Akashi, M., Biodegradable Nanoparticles as Vaccine Adjuvants and Delivery Systems: Regulation of Immune Responses by Nanoparticle-Based Vaccine. *Adv Polym Sci* 2012, 247, 31-64.
54. Akagi, T.; Baba, M.; Akashi, M., Biodegradable nanoparticles as vaccine adjuvants and delivery systems: regulation of immune responses by nanoparticle-based vaccine. In *Polymers in nanomedicine*, Springer: 2011; pp 31-64.
55. Mahony, D.; Cavallaro, A. S.; Stahr, F.; Mahony, T. J.; Qiao, S. Z.; Mitter, N., Mesoporous Silica Nanoparticles Act as a Self-Adjuvant for Ovalbumin Model Antigen in Mice. *Small* 2013, 9, 3138-3146.
56. Chen, Y.-S.; Hung, Y.-C.; Liao, I.; Huang, G. S., Assessment of the in vivo toxicity of gold nanoparticles. *Nanoscale research letters* 2009, 4, 858.
57. Chen, Y.-S.; Hung, Y.-C.; Lin, W.-H.; Huang, G. S., Assessment of gold nanoparticles as a size-dependent vaccine carrier for enhancing the antibody response against synthetic foot-and-mouth disease virus peptide. *Nanotechnology* 2010, 21, 195101.
58. Niikura, K.; Matsunaga, T.; Suzuki, T.; Kobayashi, S.; Yamaguchi, H.; Orba, Y.; Kawaguchi, A.; Hasegawa, H.; Kajino, K.; Ninomiya, T., Gold nanoparticles as a vaccine platform: influence of size and shape on immunological responses in vitro and in vivo. *ACS nano* 2013, 7, 3926-3938.
59. Chang, H. I.; Yeh, M. K., Clinical development of liposome-based drugs: formulation, characterization, and therapeutic efficacy. *International journal of nanomedicine* 2012, 7, 49-60.

60. Maurer, N.; Fenske, D. B.; Cullis, P. R., Developments in liposomal drug delivery systems. *Expert opinion on biological therapy* 2001, 1, 923-47.
61. Kastner, E.; Schmidt, S. T.; Wilkinson, A.; Christensen, D.; Perrie, Y., The Application of Liposomes as Vaccine Adjuvants. In *Subunit Vaccine Delivery*, Springer: 2015; pp 77-94.
62. Watson, D. S.; Endsley, A. N.; Huang, L., Design considerations for liposomal vaccines: influence of formulation parameters on antibody and cell-mediated immune responses to liposome associated antigens. *Vaccine* 2012, 30, 2256-2272.
63. Kaur, R.; Bramwell, V. W.; Kirby, D. J.; Perrie, Y., Pegylation of DDA: TDB liposomal adjuvants reduces the vaccine depot effect and alters the Th1/Th2 immune responses. *J. Controlled Release* 2012, 158, 72-77.
64. Christensen, D.; Henriksen-Lacey, M.; Kamath, A. T.; Lindenstrøm, T.; Korsholm, K. S.; Christensen, J. P.; Rochat, A.-F.; Lambert, P.-H.; Andersen, P.; Siegrist, C.-A., A cationic vaccine adjuvant based on a saturated quaternary ammonium lipid have different in vivo distribution kinetics and display a distinct CD4 T cell-inducing capacity compared to its unsaturated analog. *J. Controlled Release* 2012, 160, 468-476.
65. Agger, E. M.; Rosenkrands, I.; Hansen, J.; Brahimi, K.; Vandahl, B. S.; Aagaard, C.; Werninghaus, K.; Kirschning, C.; Lang, R.; Christensen, D., Cationic liposomes formulated with synthetic mycobacterial cordfactor (CAF01): a versatile adjuvant for vaccines with different immunological requirements. *PloS One* 2008, 3, e3116.
66. Andersen, C. S.; Agger, E. M.; Rosenkrands, I.; Gomes, J. M.; Bhowruth, V.; Gibson, K. J.; Petersen, R. V.; Minnikin, D. E.; Besra, G. S.; Andersen, P., A simple mycobacterial monomycolated glycerol lipid has potent immunostimulatory activity. *J. Immunol.* 2009, 182, 424-432.
67. Andersen, C. A. S.; Rosenkrands, I.; Olsen, A. W.; Nordly, P.; Christensen, D.; Lang, R.; Kirschning, C.; Gomes, J. M.; Bhowruth, V.; Minnikin, D. E., Novel generation mycobacterial adjuvant based on liposome-encapsulated monomycoloyl glycerol from *Mycobacterium bovis* bacillus Calmette-Guerin. *J. Immunol.* 2009, 183, 2294-2302.
68. Nordly, P.; Korsholm, K. S.; Pedersen, E. A.; Khilji, T. S.; Franzyk, H.; Jorgensen, L.; Nielsen, H. M.; Agger, E. M.; Foged, C., Incorporation of a synthetic mycobacterial monomycoloyl glycerol analogue stabilizes dimethyldioctadecylammonium liposomes and potentiates their adjuvant effect in vivo. *Eur. J. Pharm. Biopharm.* 2011, 77, 89-98.
69. Martin-Bertelsen, B.; Korsholm, K. S.; Roces, C. B.; Nielsen, M. H.; Christensen, D.; Franzyk, H.; Yaghmur, A.; Foged, C., Nano-self-assemblies based on synthetic analogues of mycobacterial monomycoloyl glycerol and DDA: Supramolecular structure and adjuvant efficacy. *Mol. Pharmaceutics* 2016, 13, 2771-2781.
70. Watson, D. S.; Endsley, A. N.; Huang, L., Design considerations for liposomal vaccines: influence of formulation parameters on antibody and cell-mediated immune responses to liposome associated antigens. *Vaccine* 2012, 30, 2256-72.
71. Altin, J. G.; Parish, C. R., Liposomal vaccines - targeting the delivery of antigen. *Methods* 2006, 40, 39-52.

72. Boyd, B. J.; Dong, Y. D.; Rades, T., Nonlamellar liquid crystalline nanostructured particles: advances in materials and structure determination. *Journal of liposome research* 2009, 19, 12-28.
73. Burgdorf, S.; Kautz, A.; Böhnert, V.; Knolle, P. A.; Kurts, C., Distinct pathways of antigen uptake and intracellular routing in CD4 and CD8 T cell activation. *science* 2007, 316, 612-616.
74. Dierking, I., States of Matter. In *Textures of liquid crystals*, John Wiley & Sons: 2003; pp 1-3.
75. Birdi, K., Liquid Crystals. In *Surface and colloid chemistry: principles and applications*, CRC press: 2009; pp 186-192.
76. Kaasgaard, T.; Drummond, C. J., Ordered 2-D and 3-D nanostructured amphiphile self-assembly materials stable in excess solvent. *Phys. Chem. Chem. Phys.* 2006, 8, 4957-4975.
77. Yagmur, A.; Glatter, O., Characterization and potential applications of nanostructured aqueous dispersions. *Advances in colloid and interface science* 2009, 147, 333-342.
78. Fong, C.; Le, T.; Drummond, C. J., Lyotropic liquid crystal engineering-ordered nanostructured small molecule amphiphile self-assembly materials by design. *Chem. Soc. Rev.* 2012, 41, 1297-1322.
79. Mulet, X.; Boyd, B. J.; Drummond, C. J., Advances in drug delivery and medical imaging using colloidal lyotropic liquid crystalline dispersions. *Journal of colloid and interface science* 2013, 393, 1-20.
80. Yagmur, A.; De Campo, L.; Sagalowicz, L.; Leser, M. E.; Glatter, O., Emulsified microemulsions and oil-containing liquid crystalline phases. *Langmuir* 2005, 21, 569-577.
81. Yagmur, A.; Østergaard, J.; Larsen, S. W.; Jensen, H.; Larsen, C.; Rappolt, M., Drug formulations based on self-assembled liquid crystalline nanostructures. *Liposomes, Lipid Bilayers and Model Membranes: From Basic Research to Application* 2014, 341.
82. Torchilin, V. P., Recent advances with liposomes as pharmaceutical carriers. *Nature reviews Drug discovery* 2005, 4, 145-160.
83. Wörle, G.; Siekmann, B.; Koch, M. H.; Bunjes, H., Transformation of vesicular into cubic nanoparticles by autoclaving of aqueous monoolein/poloxamer dispersions. *Eur. J. Pharm. Sci.* 2006, 27, 44-53.
84. Spicer, P. T.; Hayden, K. L.; Lynch, M. L.; Ofori-Boateng, A.; Burns, J. L., Novel process for producing cubic liquid crystalline nanoparticles (cubosomes). *Langmuir : the ACS journal of surfaces and colloids* 2001, 17, 5748-5756.
85. Phan, S.; Fong, W. K.; Kirby, N.; Hanley, T.; Boyd, B. J., Evaluating the link between self-assembled mesophase structure and drug release. *Int J Pharmaceut* 2011, 421, 176-182.
86. Dong, Y. D.; Boyd, B. J., Applications of X-ray scattering in pharmaceutical science. *Int J Pharm* 2011, 417, 101-111.

87. Angelova, A.; Angelov, B.; Garamus, V. M.; Couvreur, P.; Lesieur, S., Small-Angle X-ray Scattering Investigations of Biomolecular Confinement, Loading, and Release from Liquid-Crystalline Nanochannel Assemblies. *J Phys Chem Lett* 2012, 3, 445-457.
88. Rodrigues, L.; Kyriakos, K.; Schneider, F.; Dietz, H.; Winter, G.; Papadakis, C. M.; Hubert, M., Characterization of Lipid-Based Hexosomes as Versatile Vaccine Carriers. *Mol. Pharmaceutics* 2016, 13, 3945-3954.
89. Schnablegger, H.; Singh, Y., The SAXS Guide. *Anton Paar GmbH* 2013.
90. Dong, Y.-D.; Boyd, B. J., Applications of X-ray scattering in pharmaceutical science. *Int. J. Pharm.* 2011, 417, 101-111.
91. Gottstein, G., Experimentelle Verfahren zur kristallographischen Struktur- und Orientierungsbestimmung. In *Physikalische Grundlagen der Materialkunde*, Springer-Verlag: 2007; pp 41-44.
92. Bragg, W. H.; Bragg, W. L., The reflection of X-rays by crystals. *Proceedings of the Royal Society of London. Series A, Containing Papers of a Mathematical and Physical Character* 1913, 88, 428-438.
93. Muller, F.; Salonen, A.; Glatter, O., Phase behavior of Phytantriol/water bicontinuous cubic $Pn3m$ cubosomes stabilized by Laponite disc-like particles. *J. Colloid Interface Sci.* 2010, 342, 392-398.
94. Pieranski, P., Faceting of Soft Crystals. In *Advances in Planar Lipid Bilayers and Liposomes*, Elsevier: 2011; Vol. 14, pp 1-43.
95. Sagalowicz, L.; Mezzenga, R.; Leser, M. E., Investigating reversed liquid crystalline mesophases. *Curr Opin Colloid In* 2006, 11, 224-229.
96. Kuntsche, J.; Horst, J. C.; Bunjes, H., Cryogenic transmission electron microscopy (cryo-TEM) for studying the morphology of colloidal drug delivery systems. *Int. J. Pharm.* 2011, 417, 120-137.
97. Sagalowicz, L.; Michel, M.; Adrian, M.; Frossard, P.; Rouvet, M.; Watzke, H. J.; Yaghmur, A.; de Campo, L.; Glatter, O.; Leser, M. E., Crystallography of dispersed liquid crystalline phases studied by cryo-transmission electron microscopy. *Journal of microscopy* 2006, 221, 110-21.
98. Hyde, S. T., Identification of lyotropic liquid crystalline mesophases. *Handbook of applied surface and colloid chemistry* 2001, 2, 299-332.
99. Yaghmur, A.; Glatter, O., Characterization and potential applications of nanostructured aqueous dispersions. *Advances in colloid and interface science* 2009, 147-148, 333-42.
100. Mulet, X.; Boyd, B. J.; Drummond, C. J., Advances in drug delivery and medical imaging using colloidal lyotropic liquid crystalline dispersions. *J. Colloid Interface Sci.* 2013, 393, 1-20.

101. Rosevear, F., The microscopy of the liquid crystalline neat and middle phases of soaps and synthetic detergents. *Journal of the American Oil Chemists' Society* 1954, 31, 628-639.
102. Angelova, A.; Angelov, B.; Mutafchieva, R.; Lesieur, S.; Couvreur, P., Self-Assembled Multicompartment Liquid Crystalline Lipid Carriers for Protein, Peptide, and Nucleic Acid Drug Delivery. *Acc. Chem. Res.* 2011, 44, 147-156.
103. Fong, C.; Le, T.; Drummond, C. J., Lyotropic liquid crystal engineering-ordered nanostructured small molecule amphiphile self-assembly materials by design. *Chem. Soc. Rev.* 2012, 41, 1297-322.
104. Tenchov, B. G.; MacDonald, R. C.; Siegel, D. P., Cubic phases in phosphatidylcholine-cholesterol mixtures: cholesterol as membrane "fusogen". *Biophys J* 2006, 91, 2508-16.
105. Rodriguez, A.; Regnault, A.; Kleijmeer, M.; Ricciardi-Castagnoli, P.; Amigorena, S., Selective transport of internalized antigens to the cytosol for MHC class I presentation in dendritic cells. *Nature cell biology* 1999, 1, 362-368.
106. Boyd, B. J.; Whittaker, D. V.; Khoo, S.-M.; Davey, G., Lyotropic liquid crystalline phases formed from glycerate surfactants as sustained release drug delivery systems. *Int. J. Pharm.* 2006, 309, 218-226.
107. Phan, S.; Fong, W.-K.; Kirby, N.; Hanley, T.; Boyd, B. J., Evaluating the link between self-assembled mesophase structure and drug release. *Int. J. Pharm.* 2011, 421, 176-182.
108. Swarnakar, N. K.; Jain, V.; Dubey, V.; Mishra, D.; Jain, N., Enhanced oromucosal delivery of progesterone via hexosomes. *Pharm. Res.* 2007, 24, 2223-2230.
109. Lopes, L. B.; Ferreira, D. A.; de Paula, D.; Garcia, M. T. J.; Thomazini, J. A.; Fantini, M. C.; Bentley, M. V. L., Reverse hexagonal phase nanodispersion of monoolein and oleic acid for topical delivery of peptides: in vitro and in vivo skin penetration of cyclosporin A. *Pharm. Res.* 2006, 23, 1332-1342.
110. Nilsson, C.; Barrios-Lopez, B.; Kallinen, A.; Laurinmäki, P.; Butcher, S. J.; Raki, M.; Weisell, J.; Bergström, K.; Larsen, S. W.; Østergaard, J., SPECT/CT imaging of radiolabeled cubosomes and hexosomes for potential theranostic applications. *Biomaterials* 2013, 34, 8491-8503.
111. Meli, V.; Caltagirone, C.; Sinico, C.; Lai, F.; Falchi, A. M.; Monduzzi, M.; Obiols-Rabasa, M.; Picci, G.; Rosa, A.; Schmidt, J., Theranostic hexosomes for cancer treatments: an in vitro study. *New Journal of Chemistry* 2017, 41, 1558-1565.
112. Rizwan, S.; McBurney, W.; Young, K.; Hanley, T.; Boyd, B.; Rades, T.; Hook, S., Cubosomes containing the adjuvants imiquimod and monophosphoryl lipid A stimulate robust cellular and humoral immune responses. *J. Controlled Release* 2013, 165, 16-21.
113. Han, S.; Shen, J.-q.; Gan, Y.; Geng, H.-m.; Zhang, X.-x.; Zhu, C.-l.; Gan, L., Novel vehicle based on cubosomes for ophthalmic delivery of flurbiprofen with low irritancy and high bioavailability. *Acta Pharmacologica Sinica* 2010, 31, 990-998.

114. Yameen, B.; Choi, W. I.; Vilos, C.; Swami, A.; Shi, J.; Farokhzad, O. C., Insight into nanoparticle cellular uptake and intracellular targeting. *J. Controlled Release* 2014, 190, 485-499.
115. Garnacho, C., Intracellular drug delivery: mechanisms for cell entry. *Current pharmaceutical design* 2016, 22, 1210-1226.
116. Hillaireau, H.; Couvreur, P., Nanocarriers' entry into the cell: relevance to drug delivery. *Cellular and Molecular Life Sciences* 2009, 66, 2873-2896.
117. Mayor, S.; Pagano, R. E., Pathways of clathrin-independent endocytosis. *Nature reviews Molecular cell biology* 2007, 8, 603-612.
118. Gessner, A.; Waicz, R.; Lieske, A.; Paulke, B.-R.; Mäder, K.; Müller, R., Nanoparticles with decreasing surface hydrophobicities: influence on plasma protein adsorption. *Int. J. Pharm.* 2000, 196, 245-249.
119. Gessner, A.; Lieske, A.; Paulke, B. R.; Müller, R. H., Influence of surface charge density on protein adsorption on polymeric nanoparticles: analysis by two-dimensional electrophoresis. *Eur. J. Pharm. Biopharm.* 2002, 54, 165-170.
120. Gessner, A.; Lieske, A.; Paulke, B. R.; Müller, R. H., Functional groups on polystyrene model nanoparticles: influence on protein adsorption. *Journal of Biomedical Materials Research Part A* 2003, 65, 319-326.
121. Vonarbourg, A.; Passirani, C.; Saulnier, P.; Benoit, J.-P., Parameters influencing the stealthiness of colloidal drug delivery systems. *Biomaterials* 2006, 27, 4356-4373.
122. Peracchia, M.; Harnisch, S.; Pinto-Alphandary, H.; Gulik, A.; Dedieu, J.; Desmaele, D.; d'Angelo, J.; Müller, R.; Couvreur, P., Visualization of in vitro protein-rejecting properties of PEGylated stealth® polycyanoacrylate nanoparticles. *Biomaterials* 1999, 20, 1269-1275.
123. Mathaes, R.; Winter, G.; Besheer, A.; Engert, J., Influence of particle geometry and PEGylation on phagocytosis of particulate carriers. *Int. J. Pharm.* 2014, 465, 159-164.
124. Dobrovolskaia, M. A.; McNeil, S. E., Immunological properties of engineered nanomaterials. *Nature nanotechnology* 2007, 2, 469-478.
125. Conner, S. D.; Schmid, S. L., Regulated portals of entry into the cell. *Nature* 2003, 422, 37.
126. Hillaireau, H.; Couvreur, P., Nanocarriers' entry into the cell: relevance to drug delivery. *Cellular and molecular life sciences : CMLS* 2009, 66, 2873-96.
127. Royle, S. J., The cellular functions of clathrin. *Cellular and molecular life sciences* 2006, 63, 1823-1832.
128. Carver, L. A.; Schnitzer, J. E., Caveolae: mining little caves for new cancer targets. *Nature Reviews Cancer* 2003, 3, 571-581.

129. Parton, R. G.; Del Pozo, M. A., Caveolae as plasma membrane sensors, protectors and organizers. *Nature reviews Molecular cell biology* 2013, 14, 98-112.
130. Pelkmans, L.; Kartenbeck, J.; Helenius, A., Caveolar endocytosis of simian virus 40 reveals a new two-step vesicular-transport pathway to the ER. *Nature cell biology* 2001, 3, 473-483.
131. Hayer, A.; Stoeber, M.; Ritz, D.; Engel, S.; Meyer, H. H.; Helenius, A., Caveolin-1 is ubiquitinated and targeted to intraluminal vesicles in endolysosomes for degradation. *The Journal of cell biology* 2010, 191, 615-629.
132. Kiss, A. L.; Botos, E., Endocytosis via caveolae: alternative pathway with distinct cellular compartments to avoid lysosomal degradation? *Journal of cellular and molecular medicine* 2009, 13, 1228-1237.
133. Lundmark, R.; Doherty, G. J.; Howes, M. T.; Cortese, K.; Vallis, Y.; Parton, R. G.; McMahon, H. T., The GTPase-activating protein GRAF1 regulates the CLIC/GEEC endocytic pathway. *Current Biology* 2008, 18, 1802-1808.
134. Howes, M. T.; Kirkham, M.; Riches, J.; Cortese, K.; Walser, P. J.; Simpson, F.; Hill, M. M.; Jones, A.; Lundmark, R.; Lindsay, M. R., Clathrin-independent carriers form a high capacity endocytic sorting system at the leading edge of migrating cells. *The Journal of cell biology* 2010, 190, 675-691.
135. Gauthier, N. C.; Masters, T. A.; Sheetz, M. P., Mechanical feedback between membrane tension and dynamics. *Trends in cell biology* 2012, 22, 527-535.
136. Lundmark, R.; Carlsson, S. R. In *Driving membrane curvature in clathrin-dependent and clathrin-independent endocytosis*, Seminars in cell & developmental biology, Elsevier: 2010; pp 363-370.
137. Rejman, J.; Oberle, V.; Zuhorn, I. S.; Hoekstra, D., Size-dependent internalization of particles via the pathways of clathrin-and caveolae-mediated endocytosis. *Biochemical Journal* 2004, 377, 159-169.
138. Lai, S. K.; Hida, K.; Man, S. T.; Chen, C.; Machamer, C.; Schroer, T. A.; Hanes, J., Privileged delivery of polymer nanoparticles to the perinuclear region of live cells via a non-clathrin, non-degradative pathway. *Biomaterials* 2007, 28, 2876-2884.
139. Kim, H. R.; Andrieux, K.; Gil, S.; Taverna, M.; Chacun, H.; Desmaële, D.; Taran, F.; Georgin, D.; Couvreur, P., Translocation of poly (ethylene glycol-co-hexadecyl) cyanoacrylate nanoparticles into rat brain endothelial cells: role of apolipoproteins in receptor-mediated endocytosis. *Biomacromolecules* 2007, 8, 793-799.
140. Garcia-Garcia, E.; Gil, S.; Andrieux, K.; Desmaele, D.; Nicolas, V.; Taran, F.; Georgin, D.; Andreux, J.; Roux, F.; Couvreur, P., A relevant in vitro rat model for the evaluation of blood-brain barrier translocation of nanoparticles. *Cellular and molecular life sciences* 2005, 62, 1400-1408.

141. Nordly, P.; Madsen, H. B.; Nielsen, H. M.; Foged, C., Status and future prospects of lipid-based particulate delivery systems as vaccine adjuvants and their combination with immunostimulators. *Expert opinion on drug delivery* 2009, 6, 657-672.
142. Pulendran, B.; Ahmed, R., Immunological mechanisms of vaccination. *Nature immunology* 2011, 12, 509-517.
143. Siegrist, C.-A., Vaccine immunology. *Vaccines* 2008, 5, 17-36.
144. Rock, K. L.; Shen, L., Cross-presentation: underlying mechanisms and role in immune surveillance. *Immunological reviews* 2005, 207, 166-183.
145. Bachmann, M. F.; Jennings, G. T., Vaccine delivery: a matter of size, geometry, kinetics and molecular patterns. *Nat. Rev. Immunol.* 2010, 10, 787-96.
146. Rizwan, S. B.; Assmus, D.; Boehnke, A.; Hanley, T.; Boyd, B. J.; Rades, T.; Hook, S., Preparation of phytantriol cubosomes by solvent precursor dilution for the delivery of protein vaccines. *Eur. J. Pharm. Biopharm.* 2011, 79, 15-22.
147. Tenchov, B. G.; MacDonald, R. C.; Siegel, D. P., Cubic phases in phosphatidylcholine-cholesterol mixtures: cholesterol as membrane "fusogen". *Biophys. J.* 2006, 91, 2508-2516.
148. Dong, Y.-D.; Larson, I.; Hanley, T.; Boyd, B. J., Bulk and dispersed aqueous phase behavior of phytantriol: effect of vitamin E acetate and F127 polymer on liquid crystal nanostructure. *Langmuir* 2006, 22, 9512-9518.
149. Guy, B., The perfect mix: recent progress in adjuvant research. *Nat. Rev. Microbiol.* 2007, 5, 505-517.
150. Oda, K.; Sato, Y.; Katayama, S.; Ito, A.; Ohgitani, T., Separation and characterization of adjuvant oligosaccharide oleate ester derived from product mixture of mannitol-oleic acid esterification. *Vaccine* 2004, 22, 2812-2821.
151. Boyd, B. J.; Dong, Y. D.; Rades, T., Nonlamellar liquid crystalline nanostructured particles: advances in materials and structure determination. *J. Liposome Res.* 2009, 19, 12-28.
152. Garti, N., *Self-assembled Supramolecular Architectures: Lyotropic Liquid Crystals*. John Wiley & Sons: 2012; Vol. 3.
153. Muller, F.; Salonen, A.; Glatter, O., Phase behavior of Phytantriol/water bicontinuous cubic Pn3m cubosomes stabilized by Laponite disc-like particles. *J. Colloid Interface Sci.* 2010, 342, 392-398.
154. Zhai, J.; Waddington, L.; Wooster, T. J.; Aguilar, M. I.; Boyd, B. J., Revisiting beta-casein as a stabilizer for lipid liquid crystalline nanostructured particles. *Langmuir* 2011, 27, 14757-66.
155. Dong, Y. D.; Larson, I.; Hanley, T.; Boyd, B. J., Bulk and dispersed aqueous phase behavior of phytantriol: effect of vitamin E acetate and F127 polymer on liquid crystal nanostructure. *Langmuir* 2006, 22, 9512-8.

156. Sagalowicz, L.; Guillot, S.; Acquistapace, S.; Schmitt, B.; Maurer, M.; Yaghmur, A.; De Campo, L.; Rouvet, M.; Leser, M.; Glatter, O., Influence of vitamin E acetate and other lipids on the phase behavior of mesophases based on unsaturated monoglycerides. *Langmuir* 2013, 29, 8222-8232.
157. Barauskas, J.; Landh, T., Phase behavior of the phytantriol/water system. *Langmuir* 2003, 19, 9562-9565.
158. Dong, Y.-D.; Dong, A. W.; Larson, I.; Rappolt, M.; Amenitsch, H.; Hanley, T.; Boyd, B. J., Impurities in commercial phytantriol significantly alter its lyotropic liquid-crystalline phase behavior. *Langmuir* 2008, 24, 6998-7003.
159. Borné, J.; Nylander, T.; Khan, A., Microscopy, SAXD, and NMR studies of phase behavior of the monoolein-diolein-water system. *Langmuir* 2000, 16, 10044-10054.
160. Nakano, M.; Teshigawara, T.; Sugita, A.; Leesajakul, W.; Taniguchi, A.; Kamo, T.; Matsuoka, H.; Handa, T., Dispersions of liquid crystalline phases of the monoolein/oleic acid/Pluronic F127 system. *Langmuir* 2002, 18, 9283-9288.
161. Murgia, S.; Falchi, A. M.; Mano, M.; Lampis, S.; Angius, R.; Carnerup, A. M.; Schmidt, J.; Diaz, G.; Giacca, M.; Talmon, Y.; Monduzzi, M., Nanoparticles from lipid-based liquid crystals: emulsifier influence on morphology and cytotoxicity. *J. Phys. Chem. B* 2010, 114, 3518-25.
162. Chong, J. Y. T.; Mulet, X.; Waddington, L. J.; Boyd, B. J.; Drummond, C. J., Steric stabilisation of self-assembled cubic lyotropic liquid crystalline nanoparticles: high throughput evaluation of triblock polyethylene oxide-polypropylene oxide-polyethylene oxide copolymers. *Soft Matter* 2011, 7, 4768-4777.
163. Chong, J. Y.; Mulet, X.; Waddington, L. J.; Boyd, B. J.; Drummond, C. J., High-throughput discovery of novel steric stabilizers for cubic lyotropic liquid crystal nanoparticle dispersions. *Langmuir* 2012, 28, 9223-32.
164. Martiel, I.; Sagalowicz, L.; Mezzenga, R., Phospholipid-based nonlamellar mesophases for delivery systems: Bridging the gap between empirical and rational design. *Adv. Colloid Interface Sci.* 2014, 209, 127-143.
165. Barauskas, J.; Johnsson, M.; Joabsson, F.; Tiberg, F., Cubic phase nanoparticles (Cubosome): principles for controlling size, structure, and stability. *Langmuir* 2005, 21, 2569-77.
166. Nakano, M.; Sugita, A.; Matsuoka, H.; Handa, T., Small-angle x-ray scattering and ¹³C NMR investigation on the internal structure of "cubosomes". *Langmuir* 2001, 17, 3917-3922.
167. Johnsson, M.; Lam, Y.; Barauskas, J.; Tiberg, F., Aqueous phase behavior and dispersed nanoparticles of diglycerol monooleate/glycerol dioleate mixtures. *Langmuir* 2005, 21, 5159-5165.

168. Li, S. J.; Yamashita, Y.; Yamazaki, M., Effect of electrostatic interactions on phase stability of cubic phases of membranes of monoolein/dioleoylphosphatidic acid mixtures. *Biophys. J.* 2001, 81, 983-993.
169. Liu, Q.; Dong, Y.-D.; Hanley, T. L.; Boyd, B. J., Sensitivity of nanostructure in charged cubosomes to phase changes triggered by ionic species in solution. *Langmuir* 2013, 29, 14265-14273.
170. Murgia, S.; Bonacchi, S.; Falchi, A. M.; Lampis, S.; Lippolis, V.; Meli, V.; Monduzzi, M.; Prodi, L.; Schmidt, J.; Talmon, Y., Drug-loaded fluorescent cubosomes: versatile nanoparticles for potential theranostic applications. *Langmuir* 2013, 29, 6673-6679.
171. Angelov, B.; Angelova, A.; Garamus, V. M.; Lebas, G.; Lesieur, S.; Ollivon, M.; Funari, S. S.; Willumeit, R.; Couvreur, P., Small-angle neutron and X-ray scattering from amphiphilic stimuli-responsive diamond-type bicontinuous cubic phase. *Journal of the American Chemical Society* 2007, 129, 13474-13479.
172. Clogston, J.; Caffrey, M., Controlling release from the lipidic cubic phase. Amino acids, peptides, proteins and nucleic acids. *J. Controlled Release* 2005, 107, 97-111.
173. Steinrauf, L., Preliminary X-ray data for some new crystalline forms of β -lactoglobulin and hen-egg-white lysozyme. *Acta Crystallogr.* 1959, 12, 77-79.
174. Erickson, H. P., Size and shape of protein molecules at the nanometer level determined by sedimentation, gel filtration, and electron microscopy. *Biol. Proced. Online* 2009, 11, 32-51.
175. Francescangeli, O.; Pisani, M.; Stanić, V.; Bruni, P.; Weiss, T., Evidence of an inverted hexagonal phase in self-assembled phospholipid-DNA-metal complexes. *Europhys. Lett.* 2004, 67, 669.
176. Angelova, A.; Ollivon, M.; Campitelli, A.; Bourgaux, C., Lipid cubic phases as stable nanochannel network structures for protein biochip development: X-ray diffraction study. *Langmuir* 2003, 19, 6928-6935.
177. Conn, C. E.; Drummond, C. J., Nanostructured bicontinuous cubic lipid self-assembly materials as matrices for protein encapsulation. *Soft Matter* 2013, 9, 3449-3464.
178. Simpson-Abelson, M. R.; Purohit, V. S.; Pang, W. M.; Iyer, V.; Odunsi, K.; Demmy, T. L.; Yokota, S. J.; Loyall, J. L.; Kelleher, R. J.; Balu-Iyer, S., IL-12 delivered intratumorally by multilamellar liposomes reactivates memory T cells in human tumor microenvironments. *Clinical Immunology* 2009, 132, 71-82.
179. Allen, T. M.; Cullis, P. R., Drug delivery systems: entering the mainstream. *Science* 2004, 303, 1818-1822.
180. Couvreur, P., Nanoparticles in drug delivery: past, present and future. *Adv. Drug Delivery Rev.* 2013, 65, 21-23.
181. Hafez, I. M.; Cullis, P. R., Roles of lipid polymorphism in intracellular delivery. *Adv. Drug Delivery Rev.* 2001, 47, 139-148.

182. Goñi, F. M., The basic structure and dynamics of cell membranes: an update of the Singer-Nicolson model. *Biochimica et Biophysica Acta (BBA)-Biomembranes* 2014, 1838, 1467-1476.
183. Peetla, C.; Vijayaraghavalu, S.; Labhasetwar, V., Biophysics of cell membrane lipids in cancer drug resistance: Implications for drug transport and drug delivery with nanoparticles. *Adv. Drug Delivery Rev.* 2013, 65, 1686-1698.
184. Van Meer, G.; Voelker, D. R.; Feigenson, G. W., Membrane lipids: where they are and how they behave. *Nature reviews Molecular cell biology* 2008, 9, 112-124.
185. Sercombe, L.; Veerati, T.; Moheimani, F.; Wu, S. Y.; Sood, A. K.; Hua, S., Advances and challenges of liposome assisted drug delivery. *Frontiers in pharmacology* 2015, 6, 286.
186. Bruni, N.; Stella, B.; Giraudo, L.; Della Pepa, C.; Gastaldi, D.; Dosio, F., Nanostructured delivery systems with improved leishmanicidal activity: a critical review. *International journal of nanomedicine* 2017, 12, 5289.
187. Zeng, N.; Gao, X.; Hu, Q.; Song, Q.; Xia, H.; Liu, Z.; Gu, G.; Jiang, M.; Pang, Z.; Chen, H., Lipid-based liquid crystalline nanoparticles as oral drug delivery vehicles for poorly water-soluble drugs: cellular interaction and in vivo absorption. *International journal of nanomedicine* 2012, 7, 3703.
188. Koltover, I.; Salditt, T.; Rädler, J. O.; Safinya, C. R., An inverted hexagonal phase of cationic liposome-DNA complexes related to DNA release and delivery. *Science* 1998, 281, 78-81.
189. Chemelli, A.; Maurer, M.; Geier, R.; Glatter, O., Optimized loading and sustained release of hydrophilic proteins from internally nanostructured particles. *Langmuir* 2012, 28, 16788-16797.
190. Bitan-Cherbakovsky, L.; Libster, D.; Appelhans, D.; Voit, B.; Aserin, A.; Garti, N., Reversed hexagonal lyotropic liquid-crystal and open-shell glycodendrimers as potential vehicles for sustained release of sodium diclofenac. *The Journal of Physical Chemistry B* 2014, 118, 4016-4024.
191. Angelova, A.; Angelov, B.; Mutafchieva, R.; Lesieur, S.; Couvreur, P., Self-assembled multicompartiment liquid crystalline lipid carriers for protein, peptide, and nucleic acid drug delivery. *Accounts of chemical research* 2010, 44, 147-156.
192. Barauskas, J.; Johnsson, M.; Joabsson, F.; Tiberg, F., Cubic phase nanoparticles (cubosome[†]): principles for controlling size, structure, and stability. *Langmuir* 2005, 21, 2569-2577.
193. Varkouhi, A. K.; Scholte, M.; Storm, G.; Haisma, H. J., Endosomal escape pathways for delivery of biologicals. *J. Controlled Release* 2011, 151, 220-228.
194. Dominska, M.; Dykxhoorn, D. M., Breaking down the barriers: siRNA delivery and endosome escape. *J Cell Sci* 2010, 123, 1183-1189.

195. Brooks, N. A.; Pouniotis, D. S.; Tang, C.-K.; Apostolopoulos, V.; Pietersz, G. A., Cell-penetrating peptides: application in vaccine delivery. *Biochimica et Biophysica Acta (BBA)-Reviews on Cancer* 2010, 1805, 25-34.
196. Kwon, E. J.; Bergen, J. M.; Pun, S. H., Application of an HIV gp41-derived peptide for enhanced intracellular trafficking of synthetic gene and siRNA delivery vehicles. *Bioconjugate chemistry* 2008, 19, 920-927.
197. Gonzalez, M. E.; Carrasco, L., Viroporins. *FEBS letters* 2003, 552, 28-34.
198. Leal, C.; Boussein, N. F.; Ewert, K. K.; Safinya, C. R., Highly efficient gene silencing activity of siRNA embedded in a nanostructured gyroid cubic lipid matrix. *Journal of the American Chemical Society* 2010, 132, 16841-16847.
199. Zhen, G.; Hinton, T. M.; Muir, B. W.; Shi, S.; Tizard, M.; McLean, K. M.; Hartley, P. G.; Gunatillake, P., Glycerol monooleate-based nanocarriers for siRNA delivery in vitro. *Mol. Pharmaceutics* 2012, 9, 2450-2457.
200. Yang, L.; Huang, H. W., Observation of a membrane fusion intermediate structure. *Science* 2002, 297, 1877-1879.
201. Doherty, G. J.; Åhlund, M. K.; Howes, M. T.; Morén, B.; Parton, R. G.; McMahon, H. T.; Lundmark, R., The endocytic protein GRAF1 is directed to cell-matrix adhesion sites and regulates cell spreading. *Molecular biology of the cell* 2011, 22, 4380-4389.
202. Bangham, A.; Standish, M. M.; Watkins, J., Diffusion of univalent ions across the lamellae of swollen phospholipids. *Journal of molecular biology* 1965, 13, 238-IN27.
203. Mohan, J.; Morén, B.; Larsson, E.; Holst, M. R.; Lundmark, R., Cavin3 interacts with cavin1 and caveolin1 to increase surface dynamics of caveolae. *J Cell Sci* 2015, 128, 979-991.
204. Wilhelm, C.; Billotey, C.; Roger, J.; Pons, J.; Bacri, J.-C.; Gazeau, F., Intracellular uptake of anionic superparamagnetic nanoparticles as a function of their surface coating. *Biomaterials* 2003, 24, 1001-1011.
205. Schindelin, J.; Arganda-Carreras, I.; Frise, E.; Kaynig, V.; Longair, M.; Pietzsch, T.; Preibisch, S.; Rueden, C.; Saalfeld, S.; Schmid, B., Fiji: an open-source platform for biological-image analysis. *Nature methods* 2012, 9, 676-682.
206. Woods, N.; Niwasabutra, K.; Acevedo, R.; Igoli, J.; Altwaijry, N.; Tusiimire, J.; Gray, A.; Watson, D.; Ferro, V., Natural Vaccine Adjuvants and Immunopotentiators Derived From Plants, Fungi, Marine Organisms, and Insects. In *Immunopotentiators in Modern Vaccines (Second Edition)*, Elsevier: 2017; pp 211-229.
207. Higashi, N.; Sunamoto, J., Endocytosis of poly (ethylene oxide)-modified liposome by human lymphoblastoid cells. *Biochimica et Biophysica Acta (BBA)-General Subjects* 1995, 1243, 386-392.
208. Shen, H.-H.; Crowston, J. G.; Huber, F.; Saubern, S.; McLean, K. M.; Hartley, P. G., The influence of dipalmitoyl phosphatidylserine on phase behaviour of and cellular response to lyotropic liquid crystalline dispersions. *Biomaterials* 2010, 31, 9473-9481.

209. Vranic, S.; Boggetto, N.; Contremoulins, V.; Mornet, S.; Reinhardt, N.; Marano, F.; Baeza-Squiban, A.; Boland, S., Deciphering the mechanisms of cellular uptake of engineered nanoparticles by accurate evaluation of internalization using imaging flow cytometry. *Particle and fibre toxicology* 2013, 10, 2.
210. Albanese, A.; Tang, P. S.; Chan, W. C., The effect of nanoparticle size, shape, and surface chemistry on biological systems. *Annual review of biomedical engineering* 2012, 14, 1-16.
211. Lei, G.; MacDonald, R. C., Lipid bilayer vesicle fusion: intermediates captured by high-speed microfluorescence spectroscopy. *Biophysical journal* 2003, 85, 1585-1599.
212. Kumari, S.; Mg, S.; Mayor, S., Endocytosis unplugged: multiple ways to enter the cell. *Cell research* 2010, 20, 256.
213. Olofsson, A.; Skalman, L. N.; Obi, I.; Lundmark, R.; Arnqvist, A., Uptake of *Helicobacter pylori* vesicles is facilitated by clathrin-dependent and clathrin-independent endocytic pathways. *MBio* 2014, 5, e00979-14.
214. Firdessa, R.; Oelschlaeger, T. A.; Moll, H., Identification of multiple cellular uptake pathways of polystyrene nanoparticles and factors affecting the uptake: Relevance for drug delivery systems. *European journal of cell biology* 2014, 93, 323-337.
215. Sinha, B.; Köster, D.; Ruez, R.; Gonnord, P.; Bastiani, M.; Abankwa, D.; Stan, R. V.; Butler-Browne, G.; Védie, B.; Johannes, L., Cells respond to mechanical stress by rapid disassembly of caveolae. *Cell* 2011, 144, 402-413.
216. Apodaca, G., Modulation of membrane traffic by mechanical stimuli. *American Journal of Physiology-Renal Physiology* 2002, 282, F179-F190.
217. Sens, P.; Plastino, J., Membrane tension and cytoskeleton organization in cell motility. *Journal of Physics: Condensed Matter* 2015, 27, 273103.
218. Papakonstanti, E.; Stournaras, C., Cell responses regulated by early reorganization of actin cytoskeleton. *FEBS letters* 2008, 582, 2120-2127.
219. Kučerka, N.; Tristram-Nagle, S.; Nagle, J. F., Structure of fully hydrated fluid phase lipid bilayers with monounsaturated chains. *The Journal of membrane biology* 2006, 208, 193-202.
220. Alhakamy, N. A.; Kaviratna, A.; Berkland, C. J.; Dhar, P., Dynamic measurements of membrane insertion potential of synthetic cell penetrating peptides. *Langmuir* 2013, 29, 15336-15349.
221. Hovakeemian, S. G.; Liu, R.; Gellman, S. H.; Heerklotz, H., Correlating antimicrobial activity and model membrane leakage induced by nylon-3 polymers and detergents. *Soft matter* 2015, 11, 6840-6851.
222. Patel, H.; Tscheka, C.; Heerklotz, H., Characterizing vesicle leakage by fluorescence lifetime measurements. *Soft Matter* 2009, 5, 2849-2851.
223. Rosoff, M., The Relationship and Interactions Between Lipid Bilayers Vesicles and Lipid Monolayers at the Air/Water Interface. In *Vesicles*, CRC Press: 1996; Vol. 62, pp 3-48.

224. Peetla, C.; Labhasetwar, V., Effect of molecular structure of cationic surfactants on biophysical interactions of surfactant-modified nanoparticles with a model membrane and cellular uptake. *Langmuir* 2009, 25, 2369-2377.
225. Peetla, C.; Stine, A.; Labhasetwar, V., Biophysical interactions with model lipid membranes: applications in drug discovery and drug delivery. *Mol. Pharmaceutics* 2009, 6, 1264-1276.
226. Jablonowska, E. b.; Nazaruk, E.; Matyszewska, D.; Speziale, C.; Mezzenga, R.; Landau, E. M.; Bilewicz, R., Interactions of lipidic cubic phase nanoparticles with lipid membranes. *Langmuir* 2016, 32, 9640-9648.
227. Böttger, S.; Hofmann, K.; Melzig, M. F., Saponins can perturb biologic membranes and reduce the surface tension of aqueous solutions: a correlation? *Bioorganic & medicinal chemistry* 2012, 20, 2822-2828.
228. Walde, P.; Cosentino, K.; Engel, H.; Stano, P., Giant vesicles: preparations and applications. *ChemBioChem* 2010, 11, 848-865.
229. Strobl, F. G.; Seitz, F.; Westerhausen, C.; Reller, A.; Torrano, A. A.; Bräuchle, C.; Wixforth, A.; Schneider, M. F., Intake of silica nanoparticles by giant lipid vesicles: influence of particle size and thermodynamic membrane state. *Beilstein journal of nanotechnology* 2014, 5, 2468.
230. Sagalowicz, L.; Michel, M.; Adrian, M.; Frossard, P.; Rouvet, M.; Watzke, H. J.; Yaghmur, A.; De Campo, L.; Glatter, O.; Leser, M. E., Crystallography of dispersed liquid crystalline phases studied by cryo-transmission electron microscopy. *Journal of microscopy* 2006, 221, 110-121.
231. Deshpande, S.; Singh, N., Influence of Cubosome Surface Architecture on Its Cellular Uptake Mechanism. *Langmuir* 2017, 33, 3509-3516.
232. Guo, C.; Manjili, M. H.; Subjeck, J. R.; Sarkar, D.; Fisher, P. B.; Wang, X.-Y., Therapeutic cancer vaccines: past, present and future. *Adv. Cancer Res.* 2013, 119, 421.
233. McNeela, E. A.; Mills, K. H., Manipulating the immune system: humoral versus cell-mediated immunity. *Adv. Drug Delivery Rev.* 2001, 51, 43-54.
234. Bhowruth, V.; Minnikin, D. E.; Agger, E. M.; Andersen, P.; Bramwell, V. W.; Perrie, Y.; Besra, G. S., Adjuvant properties of a simplified C 32 monomycolyl glycerol analogue. *Bioorg. Med. Chem. Lett.* 2009, 19, 2029-2032.
235. Karlsen, K.; Korsholm, K. S.; Mortensen, R.; Ghiasi, S. M.; Andersen, P.; Foged, C.; Christensen, D., A stable nanoparticulate DDA/MMG formulation acts synergistically with CpG ODN 1826 to enhance the CD4+ T-cell response. *Nanomedicine* 2014, 9, 2625-2638.
236. Mandal, M.; Kawamura, K. S.; Wherry, E. J.; Ahmed, R.; Lee, K.-D., Cytosolic delivery of viral nucleoprotein by listeriolysin O-liposome induces enhanced specific cytotoxic T lymphocyte response and protective immunity. *Mol. Pharmaceutics* 2004, 1, 2-8.

237. Knudsen, N. P. H.; Olsen, A.; Buonsanti, C.; Follmann, F.; Zhang, Y.; Coler, R. N.; Fox, C. B.; Meinke, A.; Casini, D.; Bonci, A., Different human vaccine adjuvants promote distinct antigen-independent immunological signatures tailored to different pathogens. *Sci. Rep.* 2016, 6, 19570.
238. Aravind, U. K.; Mathew, J.; Aravindakumar, C., Transport studies of BSA, lysozyme and ovalbumin through chitosan/polystyrene sulfonate multilayer membrane. *J. Membr. Sci.* 2007, 299, 146-155.
239. Hamborg, M.; Jorgensen, L.; Bojsen, A. R.; Christensen, D.; Foged, C., Protein antigen adsorption to the DDA/TDB liposomal adjuvant: effect on protein structure, stability, and liposome physicochemical characteristics. *Pharm. Res.* 2013, 30, 140-155.
240. Giddam, A. K.; Zaman, M.; Skwarczynski, M.; Toth, I., Liposome-based delivery system for vaccine candidates: constructing an effective formulation. *Nanomedicine* 2012, 7, 1877-1893.
241. Christensen, D.; Agger, E. M.; Andreasen, L. V.; Kirby, D.; Andersen, P.; Perrie, Y., Liposome-based cationic adjuvant formulations (CAF): past, present, and future. *J. Liposome Res.* 2009, 19, 2-11.
242. Kamath, A. T.; Rochat, A.-F.; Christensen, D.; Agger, E. M.; Andersen, P.; Lambert, P.-H.; Siegrist, C.-A., A liposome-based mycobacterial vaccine induces potent adult and neonatal multifunctional T cells through the exquisite targeting of dendritic cells. *PloS One* 2009, 4, e5771.
243. Smith Korsholm, K.; Agger, E. M.; Foged, C.; Christensen, D.; Dietrich, J.; Andersen, C. S.; Geisler, C.; Andersen, P., The adjuvant mechanism of cationic dimethyldioctadecylammonium liposomes. *Immunology* 2007, 121, 216-226.
244. Bhattacharjee, S., DLS and zeta potential-What they are and what they are not? *J. Controlled Release* 2016, 235, 337-351.
245. Tran, N.; Mulet, X.; Hawley, A. M.; Hinton, T. M.; Mudie, S. T.; Muir, B. W.; Giakoumatos, E. C.; Waddington, L. J.; Kirby, N. M.; Drummond, C. J., Nanostructure and cytotoxicity of self-assembled monoolein-capric acid lyotropic liquid crystalline nanoparticles. *Rsc Adv* 2015, 5, 26785-26795.
246. Bakdash, G.; Sittig, S. P.; van Dijk, T.; Figdor, C. G.; de Vries, I. J. M., The nature of activatory and tolerogenic dendritic cell-derived signal II. *Front. Immunol.* 2013, 4, 53.
247. Baaten, B.; Tinoco, R.; Chen, A.; Bradley, L., Regulation of antigen-experienced T cells: lessons from the quintessential memory marker CD44. *Front. Immunol.* 2012, 3, 23.
248. Dooms, H.; Kahn, E.; Knoechel, B.; Abbas, A. K., IL-2 induces a competitive survival advantage in T lymphocytes. *The Journal of immunology* 2004, 172, 5973-5979.
249. Lumsden, J. M.; Schwenk, R. J.; Rein, L. E.; Moris, P.; Janssens, M.; Ofori-Anyinam, O.; Cohen, J.; Kester, K. E.; Heppner, D. G.; Krzych, U., Protective immunity induced with the RTS, S/AS vaccine is associated with IL-2 and TNF- α producing effector and central memory CD4⁺ T cells. *PloS One* 2011, 6, e20775.

250. Seder, R. A.; Darrah, P. A.; Roederer, M., T-cell quality in memory and protection: implications for vaccine design. *Nat. Rev. Immunol.* 2008, 8, 247-258.
251. Lindenstrøm, T.; Agger, E. M.; Korsholm, K. S.; Darrah, P. A.; Aagaard, C.; Seder, R. A.; Rosenkrands, I.; Andersen, P., Tuberculosis subunit vaccination provides long-term protective immunity characterized by multifunctional CD4 memory T cells. *The Journal of Immunology* 2009, 182, 8047-8055.
252. Burgers, W. A.; Chege, G. K.; Müller, T. L.; van Harmelen, J. H.; Khoury, G.; Shephard, E. G.; Gray, C. M.; Williamson, C.; Williamson, A.-L., Broad, high-magnitude and multifunctional CD4+ and CD8+ T-cell responses elicited by a DNA and modified vaccinia Ankara vaccine containing human immunodeficiency virus type 1 subtype C genes in baboons. *J. Gen. Virol.* 2009, 90, 468-480.
253. Darrah, P. A.; Patel, D. T.; De Luca, P. M.; Lindsay, R. W.; Davey, D. F.; Flynn, B. J.; Hoff, S. T.; Andersen, P.; Reed, S. G.; Morris, S. L., Multifunctional TH1 cells define a correlate of vaccine-mediated protection against *Leishmania major*. *Nat. Med.* 2007, 13, 843-850.
254. Huaman, M. C.; Mullen, G. E.; Long, C. A.; Mahanty, S., Plasmodium falciparum apical membrane antigen 1 vaccine elicits multifunctional CD4 cytokine-producing and memory T cells. *Vaccine* 2009, 27, 5239-5246.
255. Millington, K. A.; Innes, J. A.; Hackforth, S.; Hinks, T. S.; Deeks, J. J.; Dosanjh, D. P.; Guyot-Revol, V.; Gunatheesan, R.; Klenerman, P.; Lalvani, A., Dynamic relationship between IFN- γ and IL-2 profile of Mycobacterium tuberculosis-specific T cells and antigen load. *The Journal of Immunology* 2007, 178, 5217-5226.
256. Henriksen-Lacey, M.; Bramwell, V. W.; Christensen, D.; Agger, E.-M.; Andersen, P.; Perrie, Y., Liposomes based on dimethyldioctadecylammonium promote a depot effect and enhance immunogenicity of soluble antigen. *J. Controlled Release* 2010, 142, 180-186.
257. Henriksen-Lacey, M.; Christensen, D.; Bramwell, V. W.; Lindenstrøm, T.; Agger, E. M.; Andersen, P.; Perrie, Y., Liposomal cationic charge and antigen adsorption are important properties for the efficient deposition of antigen at the injection site and ability of the vaccine to induce a CMI response. *J. Controlled Release* 2010, 145, 102-108.
258. Sullivan, K. E.; Cutilli, J.; Piliero, L. M.; Ghavimi-Alagha, D.; Starr, S. E.; Campbell, D. E.; Douglas, S. D., Measurement of cytokine secretion, intracellular protein expression, and mRNA in resting and stimulated peripheral blood mononuclear cells. *Clin. Diagn. Lab. Immunol.* 2000, 7, 920-924.
259. Leung, W. L.; Law, K. L.; Leung, V. S. S.; Yip, C. W.; Leung, C. C.; Tam, C. M.; Kam, K. M., Comparison of intracellular cytokine flow cytometry and an enzyme immunoassay for evaluation of cellular immune response to active tuberculosis. *Clin. Vaccine Immunol.* 2009, 16, 344-351.
260. Nordly, P.; Korsholm, K. S.; Pedersen, E. A.; Khilji, T. S.; Franzyk, H.; Jorgensen, L.; Nielsen, H. M.; Agger, E. M.; Foged, C., Incorporation of a synthetic mycobacterial monomycoloyl glycerol analogue stabilizes dimethyldioctadecylammonium liposomes and potentiates their adjuvant effect in vivo. *Eur. J. Pharm. Biopharm.* 2011, 77, 89-98.

261. Zhuang, Y.; Ma, Y.; Wang, C.; Hai, L.; Yan, C.; Zhang, Y.; Liu, F.; Cai, L., PEGylated cationic liposomes robustly augment vaccine-induced immune responses: Role of lymphatic trafficking and biodistribution. *J. Controlled Release* 2012, 159, 135-142.
262. Pape, K. A.; Catron, D. M.; Itano, A. A.; Jenkins, M. K., The humoral immune response is initiated in lymph nodes by B cells that acquire soluble antigen directly in the follicles. *Immunity* 2007, 26, 491-502.
263. Chiu, M. H.; Prenner, E. J., Differential scanning calorimetry: an invaluable tool for a detailed thermodynamic characterization of macromolecules and their interactions. *Journal of Pharmacy and Bioallied Sciences* 2011, 3, 39.
264. Taylor, K. M.; Morris, R. M., Thermal analysis of phase transition behaviour in liposomes. *Thermochimica Acta* 1995, 248, 289-301.
265. Bunjes, H.; Unruh, T., Characterization of lipid nanoparticles by differential scanning calorimetry, X-ray and neutron scattering. *Adv. Drug Delivery Rev.* 2007, 59, 379-402.
266. van 't Hag, L.; de Campo, L.; Garvey, C. J.; Feast, G. C.; Leung, A. E.; Yepuri, N. R.; Knott, R.; Greaves, T. L.; Tran, N.; Gras, S. L., Using SANS with contrast-matched lipid bicontinuous cubic phases to determine the location of encapsulated peptides, proteins, and other biomolecules. *The journal of physical chemistry letters* 2016, 7, 2862-2866.
267. Kirby, D. J.; Kaur, R.; Agger, E. M.; Andersen, P.; Bramwell, V. W.; Perrie, Y., Developing solid particulate vaccine adjuvants: Surface bound antigen favours a humoral response, whereas entrapped antigen shows a tendency for cell mediated immunity. *Current drug delivery* 2013, 10, 268-278.
268. Yu, H.; Karunakaran, K. P.; Jiang, X.; Shen, C.; Andersen, P.; Brunham, R. C., Chlamydia muridarum T cell antigens and adjuvants that induce protective immunity in mice. *Infection and immunity* 2012, 80, 1510-1518.
269. Sheikh, N.; Rajanathanan, P.; Attard, G.; Morrow, W., Generation of antigen specific CD8+ cytotoxic T cells following immunization with soluble protein formulated with novel glycoside adjuvants. *Vaccine* 1999, 17, 2974-2982.

Curriculum Vitae

Personal Data

Name: Letícia Rodrigues Neibecker (geb. Pires Rodrigues)

Date of Birth: January 16th, 1988

Place of Birth: Montes Claros, Minas Gerais, Brazil

Nationality: Brazilian and Portuguese

Education

- 03/2014 – 07/2017 Ludwig-Maximilians-Universität, Munich, Germany
Department of Pharmacy, Chair of Pharmaceutical Technology and Biopharmaceutics
PhD Studies, supervisor: Prof. Dr. G. Winter
- 10/2011 – 12/2013 Ludwig-Maximilians-Universität, Munich, Germany
Master in Pharmaceutical Sciences / Degree: Master of Science
- 08/2009 – 07/2010 Saarland University, Saarbrücken, Germany
Academic Exchange / Course: Pharmacy
- 08/2006 – 07/2011 Federal University of Minas Gerais, Belo Horizonte, Brazil
Study of Pharmacy / Degree: Pharmacist

Professional & Research Experience

- 12/2017 - present NLO, The Hague, Netherlands - Trainee Patent Attorney
- 10/2016 – 12/2016 Umeå University, Sweden - Visiting PhD Student
- 09/2015 – 12/2015 University of Copenhagen and Statens Serum Institut, Denmark - Visiting PhD Student
- 06/2013 – 12/2013 Helmholtz Zentrum Munich and Chair of Pharmaceutical Technology and Biopharmaceutics, LMU - Master Thesis: „Direct cellular uptake monitoring with ratiometric pH-sensitive gelatin nanoparticles“
- 04/2013 – 05/2013 Institute for Pharmaceutical Biology, LMU - Research Internship
- 09/2012 – 03/2013 Merck KGaA - Drug Delivery Innovation Darmstadt, Germany - Research Internship
- 02/2011 – 08/2011 Fundação Ezequiel Dias (Funed), Belo Horizonte, Brazil
Internship: Tablet manufacture by direct compression
- 04/2010 – 06/2010 Institute for Biopharmacy and Pharmaceutical Technology, Saarland University, Germany - Research Internship
- 03/2007 – 02/2010 Department of Chemistry and Department of Mycology, Federal University of Minas Gerais, Belo Horizonte, Brazil - Research Internship

